INTEGRABLE SYSTEMS RELATED TO SEPARATION OF VARIABLES AND SYMMETRY REDUCTION

Author:
Minh Huyen Nguyen

Supervisor:
Holger Dullin

A Doctoral Thesis submitted in partial fulfilment of the requirements for the degree of Doctor of Philosophy in Mathematics

The School of Mathematics and Statistics
at the University of Sydney

THE UNIVERSITY OF SYDNEY

July 9, 2023

Author Attribution Statement

I certify that the intellectual content of this thesis is the product of my own work and that all the assistance received in preparing this thesis and sources have been acknowledged.

The following chapters contain unaltered manuscripts:

- Chapter 2 of this thesis is published as [DDN21]
  Sections 2.2, 2.3 and the classical aspects of sections 2.5 and 2.6 are researched and written by me. Section 2.4 and the results for the quantum system in sections 2.5 and 2.6 are researched and written by Sean Dawson. Holger Dullin guided the research, edited the paper and wrote section 2.1.
- Chapter 3: of this thesis is published as [NDD23]
  Sean Dawson researched and wrote section 3.1, subsections 3.5.5, 3.6.1, 3.6.2, 3.6.3, 3.6.4, 3.6.5 and helped produce the figures. Holger Dullin guided the research, edited the paper and wrote the conclusion. I researched and wrote the rest of the manuscript.
- Chapter 4 of this thesis is published as [DDN22]
  Sections 4.3, 4.6 are researched and written by me. Sean Dawson produced the figures, researched and wrote sections 4.4 and 4.7. Holger Dullin guided the research, edited the paper and wrote sections 4.1, 4.2, 4.5.

Acknowledgement

I would like to foremost thank my supervisor Prof. Holger Dullin as this thesis would not be possible without his guidance, advice and support. His encouragements and enthusiasm has made this a very enjoyable journey. For being there both in and outside of mathematics, I thank Sean Dawson. Our friendship and research collaboration is an essential part of my candidature and I'm very thankful for all the valuable contributions Sean's made in my studies.

Despite our infrequent gathering due to the pandemic, many fond memories were made in Carslaw and for that I thank my all friends and colleagues, particularly my office-mates Joe, Zach and Tim for our wonderfully humourous banters.

My candidature wasn't without hardship and misadventures. During some of my most difficult times, my yoga teacher Derryn taught me something so simple yet so life-changing: "I am enough". Thinking, feeling, believing and internalising this has allowed me to bring out so much happiness and self-love, and for this I'm grateful for everyone at Yogic State.

Last but not least, I'm indebted to my family for their endless love and support. My two cats Milky and Milly who are like my children to me, I thank them for being my daily dose of serotonin. And of course to my mother Amy, for everything.

Contents

List of Figures

Integrable Systems related to Separation of Variables and Symmetry Reduction

Abstract

This thesis is devoted to studying three families of integrable systems using separation of variables and symmetry reduction. Our aim is to provide concrete examples of integrable systems that fall within and without the scope of the current theory of classification of integrable systems. In this process, we also discovered related systems that have yet to be classified.

The first family of integrable systems originate from the separation of variables of the free particle on $\mathbb{R}^3$ in prolate spheroidal coordinates. The Lie-Poisson reduction of this system by the action of the Euclidean group $E(3)$ gives the prolate spheroidal harmonics integrable system which is symplectically equivalent to the degenerate C. Neumann system on T^*S^2. We will prove the presence of monodromy in the prolate spheroidal harmonics integrable system and show that this system is generalised semi-toric.

Following the same strategy, we perform symmetry reduction after separation of variables of the geodesic flow on S^3 to obtain our second family of integrable systems. Unlike the free particle on $\mathbb{R}^3$, we decided to separate the geodesic flow on S^3 in every orthogonally separable coordinate systems namely: ellipsoidal, prolate, oblate, Lamé, spherical and cylindrical coordinates. This process produces a 2-parameter family of integrable systems on the symplectic manifold $S^2 \times S^2$. We show that the moduli space for this family of integrable system is the Stasheff polytope K^4. In this thesis we will study these systems in detail, presenting the critical points, bifurcation diagram and action map for each system.

In Chapter 4 we consider the Harmonic Lagrange top. This system is obtained by adding a quadratic term to the potential of the Lagrange top. We study the bifurcation diagram of this systems with the help of symmetry reduction and separation of variables in Euler angles.

Chapter 1

Introduction

1.1. Overview

The theory of integrable system has evolved significantly in the past century with many advancements made in classifying systems with certain properties [Del88, Ngọ07, PN09]. However, a complete symplectic classification of integrable systems remains an unsolved problem. Separation of variables and symmetry reduction presents a valuable tool for producing and studying integrable systems. Many physical systems exhibit fascinating and complex behaviours that can be revealed when studied in a different coordinate system. Meanwhile, symmetry reduction produces reduced integrable systems that are of lower dimensions and often simpler than the original. This thesis is devoted to studying three families of integrable systems related to separation of variables and their symmetry reductions.

The first family of integrable systems comes from separating the free particle on $\mathbb{R}^3$ in prolate spheroidal coordinates. The free particle Hamiltonian possess $E(3)$ symmetry. Performing symmetry reduction by the flow of the Hamiltonian gives the reduced system on a co-adjoint orbit of $e^*(3)$ diffeomorphic to T^*S^2. The separation constants obtained from separation of variables descends to commuting integrals on the reduced space, we call this integrable system the prolate spheroidal harmonics integrable system. This system is symplectically equivalent to a degenerate C. Neumann system. The classical spheroidal harmonics integrable system is studied in Chapter 2. We will show that the spheroidal harmonics integrable systems exhibit monodromy and provide explicit parametrisation for the fibre of the focus-focus point which is a doubly pinched torus. The spheroidal harmonics integrable system is a generalised semi-toric system and thus provides a concrete physical example for the current theory of classification [Ngọ07, PN09]. This result is the main focus of chapter 2. Chapter 2 also contains results about the corresponding quantum system studied by Sean Dawson.

The second family originates from the geodesic flow on the sphere S^3. Similar to the free particle in $\mathbb{R}^3$, the geodesic flow on S^3 is a superintegrable system and the Hamilton-Jacobi equation is separable in a large family of orthogonal coordinate systems [KM86, KWMW76, MPW81, KKM18]. The most general orthogonal coordinates on S^3 are the Jacobi ellipsoidal coordinates. The other degenerate coordinates can be obtained as appropriate limits of the ellipsoidal coordinates; they are called: prolate, oblate, Lamé, spherical and cylindrical coordinates. Each of these coordinates produces an integrable system on T^*S^3. Symplectic reduction by the geodesic Hamiltonian using invariants allows us to turn each of these integrable system into a reduced system on the symplectic manifold $S^2 \times S^2$. Since $S^2 \times S^2$ and $\mathbb{C}P^2$ are the only two compact symplectic manifolds of dimension two, integrable systems on $S^2 \times S^2$ have been the subject of active study [ADH19, AH19, FP18, HP17]. Recent works by Schöbel and Veselov [Sch14, SV15, Sch16] showed that the space of orthogonally separable coordinates on S^3 forms an algebraic variety which can be represented by a Stasheff polytope. We show in Chapter 3 that the topology of the space of separable coordinates descents to the family of integrable systems on T^*S^3 and the corresponding family of reduced systems on $S^2 \times S^2$. While this appears intuitive for the integrable systems on T^*S^3, the results for the reduced systems on $S^2 \times S^2$ are new. We will show for this whole family that the image of the action map is the same equilateral triangle. Furthermore, the reduced integrable systems obtained from separating in prolate and cylindrical coordinates are examples of systems that fall under the current theory of classification being (generalised) semi-toric and toric respectively. The Lamé and spherical coordinate systems produce integrable systems with spherical type singularities as studied in [Ker22], with the Lamé system being a new example. Integrable systems originating from the ellipsoidal and oblate coordinates are outside the realm of the current classification due to the presence of both hyperbolic and degenerate singularities. Our hope is to inspire new classification theories that would include these systems since here they appear in one natural big family. The family of integrable systems presented here suggests to consider the rigid triangle of the discrete symmetry reduced system as an analogue of the polygon invariant for toric and semi-toric systems. In particular this carries information about the discrete symmetry reduced symplectic manifold and even perhaps classifies them. The height invariant naturally translates into the position of the singularities in the continuous momentum map given by the discrete symmetry reduced actions. It is to be expected that the analogue of the Taylor series invariant becomes the Taylor series invariant at the hyperbolic-hyperbolic point, plus families of Taylor series invariants along the critical values of hyperbolic type. Whether there are additional global invariants is unclear at the moment.

The free particle on $\mathbb{R}^3$ and the geodesic flow on S^3 are both elementary examples of superintegrable systems. Kalnins, Kress and Miller classified superintegrable systems in two and three degrees of freedom in a series of works [KKM05a, KKM05b, KKM05c, KKM06a, KKM06b], also see their book [KKM18]. It is often the case that a superintegrable system is also multi-separable and this provides a rich source of integrable systems. One feature of a superintegrable system is that the superintegrable Hamiltonian is invariant under a large symmetry group G. This allows for Lie Poisson reduction by the flow of the Hamiltonian giving a co-adjoint orbit of $\mathfrak{g}^*$ as the reduced space. This reduced space is always a symplectic manifold with the Kirillov-Kostant-Souriau symplectic form. Symplectic reduction using invariants in this way is also compatible with separation of variables in the sense that separation constants of the superintegrable system becomes commuting integrals on the reduced space. In the case of the geodesic flow on S^3, we have reduced integrable systems on the compact symplectic manifold $S^2 \times S^2$ which makes a natural starting point for new theories of classification.

Leaving superintegrable systems behind, the last family of systems emerges from rigid body dynamics. We call this system the harmonic Lagrange top. This is the Lagrange top with a quadratic term added to the potential energy, which approximates the Lagrange top on a vibrating suspension [Mar09, Mar12]. The harmonic Lagrange top can also be thought of as a generalisation of the spherical pendulum that combines both the magnetic spherical pendulum [CB95, CB15, Sak02] and the quadratic spherical pendulum [Zou92, Efs05]. The Lagrange top remains integrable after adding the quadratic potential and the harmonic Lagrange top is separable with Euler angles. Our motivation for studying this system is because the quantisation of the harmonic Lagrange top leads to the most general confluent Heun equation.

This dissertation is presented as a "thesis with publications". Chapters 2, 3, and 4 are unaltered publications [DDN21], [NDD23] and [DDN22]. As such, each of these chapters are self-contained with its own literature review, background, motivations, and conclusions. In Chapters 2 and 4, the spheroidal harmonic and harmonic Lagrange top contain detailed analysis of both the classical and quantum systems. We will focus only on the classical systems for both cases in this thesis. The quantum systems are the subject of study for Sean Dawson's PhD thesis and are included here only as part of the unaltered publications. In the remainder of Chapter 1, we will provide a combined literature review introducing basic notions in Hamiltonian mechanics and integrable systems.

1.2. Preliminaries

1.2.1. Hamiltonian Mechanics and Integrable Systems

Hamiltonian mechanics has long been a powerful technique for studying dynamical systems. In this section, we will provide a brief introduction to the symplectic geometry of Hamiltonian integrable systems. Note that Chapters 2, 3, and 4 are all unaltered publications with their own background and preliminaries included. We will only present some elementary definitions and results here. Excellent textbooks in this topic are [BF04, CB15, Arn78, MR94, dS08].

In Hamiltonian mechanics, the phase space of a system is a symplectic manifold.

Definition 1 (Symplectic manifolds). *A smooth manifold M is called symplectic if it is endowed with a differential 2-form ω satisfying the following two properties:*

1) ω is closed so that $d\omega = 0$

2) ω is non-degenerate, that is $\omega(u, \cdot) = 0$ only if $u = 0$.

It follows from this definition that all symplectic manifolds are even-dimensional and orientable.

Theorem 1 (Darboux's Theorem). *In a neighbourhood of each point on (M, ω), there exist coordinates $(q_1, \dots, q_n, p_1, \dots, p_n)$ such that the symplectic from ω takes the form $\omega = \sum_{i=1}^{n} dq_i \wedge dp_i$*

The most prominent example of a symplectic manifold is the cotangent bundle T^*U of a smooth manifold U. Let $(q, p) \in T^*U$ be local coordinates on the cotangent bundle, we have the canonical 1-form $\theta = p \cdot dq$. The canonical symplectic form on T^*U is defined as $\omega = -d(p \cdot dq) = dq \wedge dp$. In many mechanical systems, the phase space is a cotangent bundle with the coordinates q and p representing the positions and momenta, respectively.

Another important class of symplectic manifolds are the coadjoint orbits of a Lie group. Let G be a matrix Lie group with Lie algebra $\mathfrak{g}$. We have the adjoint representation of G and $\mathfrak{g}$ with

$$\mathrm{Ad}_A(g) = A^{-1} g A, \qquad \mathrm{ad}_f(g) = [f, g] = fg - gf \tag{1.1}$$

where $A \in G$ and $f, g \in \mathfrak{g}$. The coadjoint representations $\mathrm{Ad}^* : G \to \mathrm{Aut}(\mathfrak{g}^*)$ and $\mathrm{ad}^* : \mathfrak{g} \to \mathrm{Aut}(\mathfrak{g}^*)$ are defined by

$$\begin{aligned} \mathrm{Ad}^*_A \xi(g) &= \xi(\mathrm{Ad}_{A^{-1}}(g)) = \xi(A g A^{-1}), \\ \mathrm{ad}^*_f \xi(g) &= \xi(-\mathrm{ad}_f(g)) = -\xi([f, g]) \end{aligned} \tag{1.2}$$

with $\xi \in \mathfrak{g}^*$. The orbit of ξ under the coadjoint action is

$$\mathcal{O}_\xi = \{\mathrm{Ad}^*_A \xi \mid A \in G\} \subseteq \mathfrak{g}^*$$

with tangent space

$$T_\mu \mathcal{O}_\xi = \{\mathrm{ad}^*_g \mu \mid g \in \mathfrak{g}\}.$$

The canonical 2-form on a coadjoint orbit $\mathcal{O}_\xi$ is sometimes referred to as the Kirillov-Kostant-Souriau symplectic form and is defined as

$$\omega_\xi(\mathrm{ad}^*_f \xi, \mathrm{ad}^*_g \xi) = \xi([f, g]). \tag{1.3}$$

Given a smooth function $H : M \to \mathbb{R}$ on the symplectic manifold M, we call H a Hamiltonian function.

Definition 2 (Hamiltonian Vector Field). *The Hamiltonian vector field X_H of the Hamiltonian*

H is given by

$$\omega(\cdot, X_H) = dH$$

where dH is the differential of H.

For physical systems, the distinguished Hamiltonian function is the total energy of the system. The equation of motion and conserved quantities can be easily found using the Poisson brackets.

Definition 3 (Poisson Bracket)**.** *The Poisson bracket of two smooth functions f and g on a symplectic manifold M is given as*

$$\{f, g\} = \omega(X_f, X_g) \tag{1.4}$$

On a cotangent bundle T^*U with local coordinates (q, p), Hamilton's equations are neatly written as

$$\dot{q} = \{q, H\}, \qquad \dot{p} = \{p, H\}. \tag{1.5}$$

A function f is a conserved quantity if and only if $\dot{f} = \{f, H\} = 0$, that is f and H Poisson commute.

More general Hamiltonian systems are defined on a Poisson manifold instead of a symplectic manifold.

Definition 4 (Poisson Manifold)**.** *A Poisson manifold is a smooth manifold P endowed with a Poisson bracket $\{\cdot, \cdot\} : C^\infty(P) \times C^\infty(P) \to C^\infty(P)$ satisfying:*

1) $\mathbb{R}$-Bilinearity: $\{\alpha f + \beta g, h\} = \alpha\{f, h\} + \beta\{g, h\}$

2) Skew-symmetry: $\{g, f\} = -\{f, g\}$

3) Jacobi identity:

$$\{f, \{g, h\}\} + \{g, \{h, f\}\} + \{h, \{f, g\}\} = 0$$

4) Leibniz rule:

$$\{fg, h\} = f\{g, h\} + g\{f, h\}$$

In local coordinates $z = (z_i)$ on P, the Poisson bracket can be expressed using a 2-tensor B called the Poisson structure matrix such that

$$\{f, g\}(z) = B^{ij}(z) \frac{\partial f}{\partial z_i} \frac{\partial g}{\partial z_j}. \tag{1.6}$$

It is clear from this definition that a symplectic manifold is a Poisson manifold with the Poisson bracket (1.4). However, a Poisson manifold is only symplectic if the Poisson structure is non-degenerate, that is the Poisson structure matrix B has full rank everywhere. The rank of $\{\cdot,\cdot\}$ at any point on $p \in P$ is the rank of the matrix $B(p)$ and the rank of a Poisson manifold P is the given by $\max\{\mathrm{rk}(B(p)) \mid p \in P\}$. The *Hamiltonian vector field* X_H of a function H on a Poisson manifold P is defined by

$$X_H(f) = \{f, H\}$$

for all $f \in C^\infty(P)$. A function $C \in C^\infty(P)$ that Poisson commutes with every other function $f \in C^\infty(P)$ is called a *Casimir*. A diffeomorphism $\varphi : P_1 \to P_2$ between Poisson manifolds $(P_1, \{\cdot,\cdot\}_1)$ and $(P_2, \{\cdot,\cdot\}_2)$ is called a *Poisson map* if

$$\varphi^*\{f, g\}_2 = \{\varphi^* f, \varphi^* g\}_1$$

for all $f, g \in C^\infty(P_2)$.

An important class of Poisson brackets is the Dirac bracket [CB15]. The Dirac bracket is used to study systems on a submanifold N of a symplectic manifold (M, ω). The submanifold inherits a new Poisson structure via the Dirac bracket that respects the geometry of the constrained system. Suppose the submanifold N is defined by a set of relations $C_i = 0$ and denote canonical Poisson bracket on M, ω as $\{\cdot,\cdot\}$, the Dirac bracket $\{\cdot,\cdot\}_D$ is defined as follows.

Definition 5 (Dirac Bracket)**.** *Let C be the matrix with entries $C_{ij} = \{C_j, C_j\}$, then for all $f, g \in C^\infty(M)$ we have*

$$\{f, g\}_D = \{f, g\} - \{f, C_i\}(C^{-1})_{ij}\{C_j, g\}. \tag{1.7}$$

The Dirac bracket satisfies the conditions of a Poisson bracket in Definition 4 with C_i as Casimirs.

We've now acquired all the tools to formally define an integrable system.

Definition 6 (Liouville Integrable System)**.** *Let (M, ω) be a $2n$-dimensional symplectic manifold. An n-dimensional Liouville integrable system on M is a collection of n smooth functions $\boldsymbol{F} = (F_1, \ldots, F_n) : M \to \mathbb{R}^n$ with the properties:*

1) *the F_i's are in involution, i.e. $\{F_i, F_j\} = 0$ for all $1 \leq i < j \leq n$.*

2) *the F_i's are functionally independent on M so that $dF_1 \wedge dF_2 \wedge \ldots \wedge dF_n \neq 0$ almost everywhere on M*

Note that there is no Hamiltonian H in this definition, however, it is often chosen as F_1 or a function of the F_i's in other definitions. A point $x \in M$ is called a *regular point* of the integrable system $(M, \omega, \boldsymbol{F})$ if $(dF_1 \wedge dF_2 \wedge \ldots \wedge dF_n)(x) \neq 0$, otherwise x is a *critical point*.

Denote the level sets of $\boldsymbol{F}$ as

$$M_{\boldsymbol{c}} = \{x \in M \mid \boldsymbol{F}(x) = \boldsymbol{c}\},$$

then $\boldsymbol{c}$ is a *regular value* of $\boldsymbol{F}$ if $M_{\boldsymbol{c}}$ contains only regular points. The foliation of M in to level sets $M_{\boldsymbol{c}}$ is called the *Liouville foliation*. The mapping $\boldsymbol{F} : M \to \mathbb{R}^n$ is called the *momentum map* of the integrable system $(M, \omega, \boldsymbol{F})$. The *bifurcation diagram* of this system is the image of the critical points under $\boldsymbol{F}$. The momentum map and bifucation diagram are invaluable tools for studying integrable systems.

At a regular value $\boldsymbol{c}$, $M_{\boldsymbol{c}}$ is a smooth manifold that is fully characterised by the Liouville-Arnold theorem.

Theorem 2 (Liouville-Arnold Theorem)**.** *At a regular value* $\mathbf{c}$ *of an* n*-dimensional integrable system* $(M, \omega, \boldsymbol{F})$*, we have:*

1) $M_{\boldsymbol{c}}$ is a smooth manifold which is invariant under the Hamiltonian flow induced by $H = F_1$

2) if $M_{\boldsymbol{c}}$ is compact and connected then it is diffeomorphic to the n-torus T^n

3) there exists local symplectic coordinates $(\phi_1, \ldots, \phi_n, I_1, \ldots, I_n)$ near $M_{\boldsymbol{c}}$ called action-angle coordinates such that the action variables $\boldsymbol{I} = (I_1, \ldots, I_n)$ are functions of F_i and are constant on the level set. The angles ϕ_i satisfies Hamilton's equation $\{\phi_i, H\} = \frac{\partial H}{\partial I_i}$ where H is any function of the $F_i(\boldsymbol{I})$'s. The symplectic form on $M_{\boldsymbol{c}}$ is given by

$$\omega_{\boldsymbol{c}} = \sum_{i=1}^{n} d\phi_i \wedge dI_i.$$

The classical proof of this was given by Arnold in [Arn78].

By the Liouville-Arnold theorem, motion takes place on invariant tori T^n for regular values. There is no general theory for motions at critical values. Some examples of singularities of integrable systems can be found, e.g., in [BF04].

Liouville integrable Hamiltonian systems can also be defined on a Poisson manifold. Let $(P, \{\cdot, \cdot\})$ be an n-dimensional Poisson manifold with rank $2r$, then a Liouville integrable system on P is a collection of smooth functions $\boldsymbol{F} = (F_1, \ldots, F_s)$ with $n = r + s$ where the F_i's are functionally independent and are in involution. General theory on integrable systems on Poisson manifolds can be found in [AMV04, MR94]. An analog of the Liouville-Arnold theorem on Poisson manifolds is given in [LGMV10]. Separation of variables on a Hamiltonian systems is a great tool to generate Liouville integrable systems as the separation constants are in involution and all commute with the Hamiltonian. Some introduction to separation of variables will be given in section 3.2, see [Arn78, KKM18] for a more thorough discussion.

Many integrable Hamiltonian systems possess symmetry that can be described by the action of a Lie group. Suppose that a Lie group G acts smoothly on a Poisson manifold P with $\Phi : G \times P \to P$ where $\Phi_g : P \to P$ is a Poisson map for all $g \in G$, then Φ is called a *Poisson action*. Similarly if M is a symplectic manifold and $\Phi_g : M \to M$ is a symplectic map for all $g \in G$ then we say that G *acts symplectically* on M. For a symplectic group action the standard theory for symmetry reduction is the Marsden-Weinstein reduction [MW74] at a regular point. At a point where the group action is not free we have singular reduction given, e.g., in [CB15]. A comprehensive introduction to symmetry reduction for Poisson manifolds can be found in [MR94].

An alternative approach to reduction that avoids problems with singular reduction uses invariants of the symmetry group action. Given a Hamiltonian H on a Poisson manifold $(P, \{\cdot,\cdot\})$, a function $f \in C^\infty(M)$ is an invariant of H if $\{f, H\} = 0$. A set of invariants I of H is called complete if all other invariants are functions of I. If I is also closed under the Poisson bracket then we can perform symmetry reduction on $(P, \{\cdot,\cdot\}, H)$ by using functions in I as new coordinates on the reduced space. The Poisson brackets on I induces the reduced Poisson structure with bracket $\{\cdot,\cdot\}_I$, and the Casimirs of $\{\cdot,\cdot\}_I$ give explicit equations describing the reduced space. For superintegrable systems, invariants I are often taken as functions that are invariant under the action of G or are symmetry generators in $\mathfrak{g}^*$ for geodesic flows. In the case where the invariants are generators of $\mathfrak{g}^*$, the Poisson structure induced from this reduction is a Lie Poisson bracket that coincides with the canonical bracket on $\mathfrak{g}^*$ obtained from the symplectic form (1.3). The reduced space is a co-adjoint orbit of $\mathfrak{g}^*$ given by fixing the values of the Casimirs, this is called Lie-Poisson reduction [MR94]. The symmetry reduction of free particle on $\mathbb{R}^3$ and the geodesic flow on S^3 are examples of Lie-Poisson reduction by the symmetry groups are $E(3)$ and $SO(4)$ respectively. The invariants are generators of translation and rotations in $e^*(3)$ for the free particle and generators of rotations in $\mathfrak{so}^*(4)$ for the geodesic flow on S^3. Note that reduction by invariants is always compatible with separation variables in the sense that the separation constants give commuting integrals on the reduced space. This is because the set of invariants I is complete and since the separation constants commute with H, they can be written as a function of the invariants in I. Performing separation of variables and symmetry reduction in this way is a very useful tool for both studying integrable systems and for producing new integrable systems. This is evident in the case of the free particle in $\mathbb{R}^3$ giving the prolate spheroidal integrable system on T^*S^2 and the geodesic flow on S^3 giving a large family of integrable systems on $S^2 \times S^2$.

1.2.2. Classification of Integrable Systems

Given two integrable systems $(M, \omega, \boldsymbol{F})$ and $(\tilde{M}, \tilde{\omega}, \tilde{\boldsymbol{F}})$, a natural question to ask is whether or not they are equivalent in some sense. To answer this question, many notions of equivalence of integrable systems have been developed. Suppose there exists a fibre-preserving map

$\Psi : M \to \tilde{M}$ such that the diagram

$$\begin{tikzcd} M \arrow[r, "\Psi"] \arrow[d, "\boldsymbol{F}"'] & \tilde{M} \arrow[d, "\tilde{\boldsymbol{F}}"] \\ \mathrm{im}(\boldsymbol{F}) \arrow[r, "\psi"'] & \mathrm{im}(\tilde{\boldsymbol{F}}) \end{tikzcd}$$

commutes, where ψ is a bijection. If further more:

1) Ψ is a homeomorphism, then $(M, \omega, \boldsymbol{F})$ and $(\tilde{M}, \tilde{\omega}, \tilde{\boldsymbol{F}})$ are *topologically equivalent*.

2) Ψ is a diffeomorphism, then $(M, \omega, \boldsymbol{F})$ and $(\tilde{M}, \tilde{\omega}, \tilde{\boldsymbol{F}})$ are *smoothly equivalent*.

3) Ψ is a symplectomorphism, then $(M, \omega, \boldsymbol{F})$ and $(\tilde{M}, \tilde{\omega}, \tilde{\boldsymbol{F}})$ are *symplectically equivalent*.

Topological analysis of integrable Hamiltonian systems has been an area of active research in the last few decades. Some references are [BF04, CB15, MR94, Zun00, Efs05, BMF90, Osh10]. Finer equivalences and classifications exist between integrable systems satisfying more restrictive properties. The most notable classification is that of toric and semi-toric systems. Sections 2.1 and 3.1 contain a brief introduction and history on these classes of systems.

An example of two symplectically equivalent systems that we will describe in this thesis is the spheroidal harmonics system and the degenerate C. Neumann system in section 2.5 . The general C. Neumann system describes the motion of a particle constrained to move on a unit sphere with a quadratic potential. Let $(\boldsymbol{x}, \boldsymbol{y}) \in T^*\mathbb{R}^{n+1}$ with $\boldsymbol{x} \cdot \boldsymbol{x} = 1$ and $\boldsymbol{x} \cdot \boldsymbol{y} = 0$ be coordinates on T^*S^n, the Hamiltonian of the Neumann system is

$$H_N = \frac{1}{2} \sum_{i=1}^{n} y_i^2 + a_i x_i^2$$

where the a_i's are constants. When some of the a_i are equal we have the degenerate Neumann system. Now consider the free particle on $\mathbb{R}^3$ with position $\boldsymbol{Q}$ and momentum $\boldsymbol{P}$. When separating the free particle in $\mathbb{R}^3$ in prolate spheroidal coordinates we obtain integrals (H, G, L_z) defined in section 2.3. The symmetry group of the free particle Hamiltonian is the Euclidean group $E(3)$ with invariants $(\boldsymbol{P}, \boldsymbol{L})$ where $\boldsymbol{P}$ denotes the vector of linear momenta and $\boldsymbol{L} = \boldsymbol{Q} \times \boldsymbol{P}$ is the vector of angular momenta. Performing symmetry reduction on the free particle after separation of variables on prolate coordinates produces the spheroidal harmonic system (G, L_z) on a coadjoint orbit M_E of $e^*(3)$ with $\boldsymbol{P} \cdot \boldsymbol{P} = 2E$ and $\boldsymbol{P} \cdot \boldsymbol{L} = 0$. The map

$$(\boldsymbol{x}, \boldsymbol{y}) = (\boldsymbol{P}, \boldsymbol{P} \times \boldsymbol{L}|\boldsymbol{P}|^{-2}) \tag{1.8}$$

is a symplectomorphism from M_E to T^*S^2. This gives a symplectic equivalence between the spheroidal harmonics system and the degenerate C. Neumann system with $a_1 = a_2 = -2Ea^2$ and $a_3 = 0$. In fact (1.8) also provides a symplectic equivalence between the reduced free particle when separated in ellipsoidal coordinates on $\mathbb{R}^3$ with semi-major axes (a_1, a_2, a_3) and the general C. Neumann system with parameters $(-a_1, -a_2, -a_3)$.

In general, symmetry reduction of the free particle on $\mathbb{R}^n$ gives a reduced space that is symplectomorphic to a coadjoint orbit M_E of $e^*(n)$ with $\boldsymbol{P} \cdot \boldsymbol{P} = 2E$ and $\boldsymbol{P} \wedge \boldsymbol{L} = 0 = \boldsymbol{L} \wedge \boldsymbol{L}$ where $\boldsymbol{L} = \boldsymbol{Q} \wedge \boldsymbol{P}$. While the cross product does not exist in higher dimensions, we can use geometric algebra to obtain an analog of (1.8). The symplectomorphism between T^*S^n and the coadjoint orbit M_1 with $\boldsymbol{P} \cdot \boldsymbol{P} = 1$ is given by

$$(\boldsymbol{P}, \boldsymbol{L}) = (\boldsymbol{x}, \boldsymbol{x} \wedge \boldsymbol{y})$$

with inverse

$$(\boldsymbol{x}, \boldsymbol{y}) = (\boldsymbol{P}, -\boldsymbol{L} * \boldsymbol{P}^{-1})$$

where $*$ is the geometric product and $\boldsymbol{P}^{-1} = \frac{\boldsymbol{P}}{|\boldsymbol{P}|^2} = \boldsymbol{P}$ on M_1. With this map, we can conjecture that the reduction of the free particle when separated in the ellipsoidal coordinates on $\mathbb{R}^n$ with semi-major axes $(a_1, \ldots, a_n)$ leads to a system that is symplectomorphic to the C. Neumann system on T^*S^n with parameters $(-a_1, \ldots, -a_n)$. Proving this conjecture could be a fruitful future project.

Related to the C. Neumann system is the Jacobi problem, aka the geodesic on an ellipsoid. It was first shown by Knörrer [Kn2] that the trajectories for the solutions to the C. Neumann system can be obtained from the geodesics on a ellipsoid with semi-major axes $(a_1, \ldots, a_n)$ via Gauss's map. Both the C. Neumann system on S^3 and the geodesic flow on a 3-dimensional ellipsoid are intimately connected to the geodesic flow on the sphere S^3. Since the geodesic flow on T^*S^3 is simply the C. Neumann system with zero potential energy, one might expect that most of the interesting features of the C. Neumann system may vanish together with the potential energy. However, as we will show in Chapter 3, many topological aspects of the C. Neumann system still linger in the geodesic flow on T^*S^3. The key to this connection is separation of variables. While the geodesic flow on T^*S^3 is separable in a large family of coordinates, the C. Neumann system on S^3 with fixed parameters (a_1, a_2, a_3, a_4) is only separable in the ellipsoidal coordinates on S^3 with semi-major axes equal to (a_1, a_2, a_3, a_4). Similarly, the geodesic on an ellipsoid with semi-major axes (a_1, a_2, a_3, a_4) is separable in the Jacobi ellipsoidal coordinates on $\mathbb{R}^4$. There are clear similarities between the first integrals, action integrals and even the bifurcation diagrams of these three systems. The geodesic flow on degenerate ellipsoids was studied in details in Chris Davison's thesis [DD06]. The bifurcation diagram and the topological analysis of the singularies of the geodesics of a generic ellipsoid in [DD06] is remarkably similar to that of the ellipsoidal integrable system in section 3.5. On top of that, this connection is also seen between the geodesics of a degenerate ellipsoid (one with some equal semi-major axes) and the geodesic on the sphere when separated in one of the degenerate coordinates. A similar correlation is observed for the degenerate C. Neumann system. Unlike the the geodesic flow on S^3 where we have a projective variety of separable coordinates parametrised by the projective parameters (e_1, e_2, e_3, e_4), the parameters (a_1, a_2, a_3, a_4) for the C. Neumann system and the Jacobi problem do not have this projective property. We'll show in Chapter 3, that the degenerate coordinates as well as the corresponding integrable/reduced integrable systems can be obtained from the general ellipsoidal coordinates and the ellipsoidal integrable/reduced integrable system by taking appropriate projective limits of the parameters (e_1, e_2, e_3, e_4). In particular the Lamé system is obtained using the projective limit $e_4 \to \infty$, there are no obvious analogs of this system for the degenerate C. Neumann system or the geodesic flow on an ellipsoid. Another related system is the Manakov top on $SO(4)$. It was noted in [SZ07b] that the bifurcation diagrams of the geodesic flow on ellipsoids in [DD06] correlate to that of a special case of the Manakov top. In Chapter 3, we show that the reduced ellipsoidal integrable system on $S^2 \times S^2$ coincides with the subclass of the Manakov top studied in [SZ07b].

Chapter 2

Monodromy in Prolate Spheroidal Harmonics

Abstract

We show that spheroidal wave functions viewed as the essential part of the joint eigenfunction of two commuting operators of $L_2(S^2)$ has a defect in the joint spectrum that makes a global labelling of the joint eigenfunctions by quantum numbers impossible. To our knowledge this is the first explicit demonstration that quantum monodromy exists in a class of classically known special functions. Using an analogue of the Laplace-Runge-Lenz vector we show that the corresponding classical Liouville integrable system is symplectically equivalent to the C. Neumann system. To prove the existence of this defect we construct a classical integrable system that is the semi-classical limit of the quantum integrable system of commuting operators. We show that this is a generalised semi-toric system with a non-degenerate focus-focus point, such that there is monodromy in the classical and the quantum system.

2.1. Introduction

Prolate spheroidal wave functions are important and well known special functions that appear when separating variables in problems that have the symmetry of prolate ellipsoids. Classical references on spheroidal wave functions are [WW65, MS54, Fla57, SMC$^+$59, Ars64]. One inspiration for our work is the general theory of separation of variables developed in [MJ77, BKM76, KKM18]. There spheroidal harmonics appear as the joint eigenfunctions of two commuting operators on the Hilbert space $L_2(S^2)$. The two operators are constructed from separation of variables in spheroidal coordinates. In the spherical limit the spheroidal harmonics reduce to the well known spherical harmonics. In this paper we study the joint spectrum of these two commuting operators and show that the lattice of joint eigenvalues has a global defect. Even though prolate spheroidal wave functions are very well studied special functions this observation about the joint spectrum seems to be new.

Another inspiration for our work is the study of quantum and Hamiltonian monodromy in integrable systems, specifically so-called semi-toric integrable systems. The global study of Liouville integrable systems was initiated by Duistermaat in [Dui80]. In a subsequent paper with Cushman [CD88] it was shown that classically and quantum mechanically the spherical pendulum has Hamiltonian and quantum monodromy, respectively. It was realised that classically [Mat96, Zun97] and quantum mechanically [VN99] monodromy is caused by a so-called focus-focus equilibrium point of the classical system. More recently a global classification of semi-toric integrable systems has been achieved [PN09]. By definition [Ngọ07], semi-toric systems have two degrees of freedom and one proper global integral which induces an S^1 action. Furthermore, no critical points can be of hyperbolic or degenerate type. The condition of properness is rather restrictive, such that, e.g., the spherical pendulum and the integrable system studied in this paper are not semi-toric system in this strict sense. They are, however, *generalised* semi-toric systems [PR$^+$17], for which only the combined moment map needs to be proper. In general integrable systems that come from separation of variables of the free particle in $\mathbb{R}^3$ do not possess a global S^1 action. If we restrict to those coordinate systems that have rotational symmetry we do have a global S^1-action: rotation about the symmetry axis. As we will show, separation in spheroidal coordinates provides an example of a generalised semi-toric system.

In two recent papers [DW18] and [CDEW19] we have used separation in spheroidal coordinates for the Kepler problem in space and the harmonic oscillator in space, respectively, and shown that both problems – when considered in prolate spheroidal variables – have Hamiltonian and quantum monodromy. The present paper grew out of the realisation that an even simpler problem, namely the free particle, can be studied in a similar way, and leads to similar results, namely monodromy in the joint spectrum. As in the two previous works it is crucial for this approach that the system under consideration is superintegrable. In the Kepler problem and the harmonic oscillator superintegrability implies that the flow of the Hamiltonian is periodic with constant period, and hence it is possible to consider symplectic reduction with respect to this flow, viewed as an action of the group S^1. The reduced system inherits two constants of motion which are the separation constants from the separation of variables. In the present example of the free particle the orbits of the Hamiltonian are not periodic orbits, but instead straight lines. Thus we need to consider reduction not with respect to a compact group S^1 but with respect to the non-compact group $\mathbb{R}^1$. Even though there are no general theorems about reduction in this case it turns out that the reduction can be performed nicely and elegantly using the invariants of the Hamiltonian flow. This leads to the classical analogue of the commuting operators described by Kalnins and Miller [BKM76], and we then show using singular reduction with respect to the global S^1 action (the angular momentum about the z-axis) that the system is generalised semi-toric and has a non-degenerate focus-focus point and hence monodromy.

The fact that the free particle when treated in this way has monodromy was first observed in [MDEW19, Mar18] as a special limit of Euler's two-centre problem in which the masses of both centres vanish. The main point of [MDEW19, Mar18] was the investigation of scattering monodromy, and in [Mar18] it was shown that after reduction by the free flow the degenerate C. Neumann system aka the quadratic spherical pendulum is obtained. The presence of monodromy in the quadratic spherical pendulum is well known [BZ93, Efs05], and the interpretation as a degeneration of the C. Neumann system was elucidated in [DH12]. The reduction using invariants we perform in this paper leads to the classical analogue of the work of Kalnins and Miller [KKM18], and gives rise to a generalised semi-toric system with Lie-Poisson structure $e^*(3)$, see Theorem 1. From [Mar18] we know that this system must be equivalent to the degenerate C. Neumann system on T^*S^2, and in Theorem 5 we give the explicit symplectomorphism that establishes this equivalence. Thus Theorem 6 is already known indirectly, because using Theorem 5 the monodromy in the degenerate C. Neumann system applies. Nevertheless, we give a direct proof of monodromy in Theorem 6, and illustrate it following an idea from [CIAD14].

The third inspiration for our work is to connect the two threads described above: separation of variables including the corresponding special functions on the one hand and the global theory of integrable systems on the other hand. Special functions related to (confluent) Fuchsian equation beyond the (confluent) hypergeometric equation are for example discussed in [Ars64, SL00]. The spheroidal wave equation is a particular case of the confluent Heun equation, see [RA95] and the references therein. In our setting spheroidal harmonics are joint eigenfunctions of two commuting operators, and we show that a defect in the joint spectrum of these operators can be understood from the analysis of the corresponding Liouville integrable system. This is more than a WKB analysis of the solutions, since it takes into account global information about the action variables of the integrable system. Nevertheless, we remark that the essence of the defect could have been observed by analysing well known asymptotic expansions [AS92] for the eigenvalues of the spheroidal wave equation; but to our knowledge such an analysis has not been presented before.

The solutions of the Helmholtz equation inside the prolate ellipsoid (aka the quantum billiard in the prolate ellipsoid) have been studied in [WD02], and monodromy was found in the joint spectrum. Since this is a system with three commuting operators (as opposed to two in the current paper) the radial equation has to be included and this leads to two coupled boundary value problems that were numerically solved in [WD02]. In the present problem we only study the angular wave equation and find monodromy also in this simpler setting.

The plan of the paper is as follows. In section 2 we describe a reduction of the free particle in $\mathbb{R}^3$ that leads to a reduced system with a Lie-Poisson structure of the algebra $e^*(3)$ of the Eulidean group of translations and rotations $E(3)$. To obtain an integrable system on the reduced space separation of variables in prolate spheroidal coordinates is employed in the next section. The centrepiece of the paper is the description of monodromy in the corresponding quantum system, which is obtained from separation of variables of the Helmholtz equation in $\mathbb{R}^3$. We show that the joint spectrum of the two commuting operators has quantum monodromy. In particular this can be seen from the analysis of the classical asymptotic series for the eigenvalues in two distinct limits. Then we show that the spheroidal harmonics integrable system is in fact symplectically equivalent to the integrable C. Neumann system of a particle constrained to move on a sphere with an added harmonic potential, which in this case has rotational symmetry. The analysis of monodromy using well known asymptotic formulas is somewhat heuristic, and to prove monodromy we show that the underlying classically integrable spheroidal harmonics system is generalised semi-toric with a non-degenerate focus-focus point corresponding to a doubly pinched torus.

2.2. The Free Particle

The free particle in $\mathbb{R}^3$ lives on the phase space $T^*\mathbb{R}^3 \cong \mathbb{R}^6$ with global coordinates $\boldsymbol{Q} := (x, y, z)^T$ and $\boldsymbol{P} := (p_x, p_y, p_z)^T$. The Hamiltonian is simply $H = \frac{1}{2}\left(p_x^2 + p_y^2 + p_z^2\right)$ and the equations of motion are $\dot{\boldsymbol{Q}} = \boldsymbol{P}$ and $\dot{\boldsymbol{P}} = \boldsymbol{0}$. The trajectories or geodesics are

$$\boldsymbol{Q} = \boldsymbol{P}t + \boldsymbol{Q}_0, \quad \boldsymbol{P} = \boldsymbol{P}_0$$

where $\boldsymbol{Q}_0, \boldsymbol{P}_0$ are the intitial position and momentum vectors, respectively, and t is time. In position space, the geodesics are oriented lines through $\boldsymbol{Q}_0$ in the direction of $\boldsymbol{P} = \boldsymbol{P}_0$. We can perform a symplectic reduction that identifies the oriented straight lines of the flow of H to points and so lowers the dimensionality of the phase space from 6 to 4. We will see that this reduction also produces a compact configuration space, which is the space of oriented lines through the origin, which is a sphere. The conserved quantities are the linear momenta $\boldsymbol{P} = (p_x, p_y, p_z)$ and the angular momenta $\boldsymbol{L} := \boldsymbol{Q} \times \boldsymbol{P} = (l_x, l_y, l_z)^T$, since

$$\boldsymbol{L}(t) = (\boldsymbol{Q}_0 + t\boldsymbol{P}_0) \times \boldsymbol{P}_0 = \boldsymbol{Q}_0 \times \boldsymbol{P}_0 = \text{constant}.$$

By construction we have $\boldsymbol{P} \cdot \boldsymbol{L} = \boldsymbol{0}$.

The six invariants $\boldsymbol{P}$, $\boldsymbol{L}$ are closed under the standard Poisson bracket in $T^*\mathbb{R}^3$. For example $\{p_x, l_y\} = p_z$, and $\{l_x, l_y\} = l_z$, etc. Assembling all such identities into a 6×6 matrix B gives[1]

$$B = -\begin{pmatrix} \boldsymbol{0} & \hat{\boldsymbol{P}} \\ \hat{\boldsymbol{P}} & \hat{\boldsymbol{L}} \end{pmatrix}. \tag{2.1}$$

The matrix B is the matrix of a Lie-Poisson structure on $\mathbb{R}^6$ with coordinates $\boldsymbol{P}$ and $\boldsymbol{L}$. This

[1] For a vector $\boldsymbol{v} \in \mathbb{R}^3$ the corresponding antisymmetric hat matrix $\hat{\boldsymbol{v}}$ is defined by

$$\hat{\boldsymbol{v}}\boldsymbol{u} = \boldsymbol{v} \times \boldsymbol{u} \quad \forall \boldsymbol{u} \in \mathbb{R}^3.$$

Later we also use hat to denote the quantum operator corresponding to a classical observable; from the context it should be clear which one is meant.

Lie-Poisson structure is the algebra $e^*(3)$ corresponding to the Euclidean group $E(3)$, the group of isometries of Euclidean space $\mathbb{R}^3$. In particular the components of $\boldsymbol{P}$ are generators of translations, while the components of $\boldsymbol{L}$ are generators of rotations. Given a Hamiltonian G the time evolution of any function $f(\boldsymbol{P}, \boldsymbol{L})$ is given by $\dot{f} = \{f, G\} = \nabla f^t B \nabla G$ and thus

$$\dot{\boldsymbol{P}} = -\boldsymbol{P} \times \nabla_L G, \quad \dot{\boldsymbol{L}} = -\boldsymbol{P} \times \nabla_P G - \boldsymbol{L} \times \nabla_L G \,. \tag{2.2}$$

The Poisson structure B has rank 4 with two Casimirs $C_1 = \boldsymbol{P} \cdot \boldsymbol{P} = 2E$ and $C_2 = \boldsymbol{P} \cdot \boldsymbol{L} = 0$, such that $B \nabla C_i = 0$. The first Casimir $C_1 = 2E$ is often set to 1 by normalisation of the speed of the particle, whereas the second Casimir C_2 is an identity that states that $\boldsymbol{L}$ is orthogonal to $\boldsymbol{P}$. In addition to these 6 basic invariants an analogue of the Laplac-Runge-Lenz (LRL) vector can be defined and we will discuss this in more detail in section 2.5.

Fixing the two Casimirs defines the reduced phase space of T^*S^2 as a subset of $\mathbb{R}^6$ with coordinates $\boldsymbol{P}$ and $\boldsymbol{L}$. Here the sphere is defined in momentum space, and reflects the constancy of the kinetic energy of the particle, while the tangent space to the sphere is the set of planes with normal vectors $\boldsymbol{P}$ in $\boldsymbol{L}$ space, hence $C_2 = 0$. Every point on T^*S^2 represents a line (geodesic) in the original $T^*\mathbb{R}^3$ with direction $\boldsymbol{P}$ (the point on the sphere) and angular momentum $\boldsymbol{L}$ (the vector in the tangent space of the sphere). Note that $\boldsymbol{L}$ is a normal vector to the plane that contains the geodesic and the origin, and the length of $\boldsymbol{L}$ is the distance of the geodesic to the origin divided by the value of C_1. There are four oriented lines with direction $\pm\boldsymbol{P}$ in a given plane with normal vector $\pm\boldsymbol{L}$. Changing the orientation of the geodesic amounts to changing the sign of $\boldsymbol{P}$ and $\boldsymbol{L}$. Changing the sign of $\boldsymbol{L}$ but not of $\boldsymbol{P}$ represents a parallel line with the same orientation in the same plane that is passing on the other side of the origin. Lastly, changing the sign of $\boldsymbol{P}$ but not of $\boldsymbol{L}$ represents a parallel line with the opposite orientation that is passing on the other side of the origin. Later we will identify any two such geodesics, which will lead to $T^*\mathbb{RP}^2$ instead of T^*S^2.

Since we have reduced by the dynamics of H there are no dynamics defined on T^*S^2 at the moment. In the next section we are going to define an integrable system on T^*S^2 by separating the free particle in spheroidal coordinates. The separation constant and the angular momentum will induce an integrable system on T^*S^2.

2.3. The Spheroidal Harmonics Integrable System

Prolate ellipsoids are formed by rotating an ellipse around its focal axis. Let the foci of the resulting ellipsoid be located at $(0, 0, \pm a)$. Prolate spheroidal coordinates are then defined by

$$\begin{aligned} x &= a\sqrt{(\xi^2-1)(1-\eta^2)}\cos(\phi), \\ y &= a\sqrt{(\xi^2-1)(1-\eta^2)}\sin(\phi), \\ z &= a\xi\eta \,, \end{aligned} \tag{2.3}$$

where $\eta \in [-1, 1]$, $\xi \in [1, \infty)$ and $\phi \in [0, 2\pi) = S^1$. Each point of $\mathbb{R}^3$ is associated with the intersection of the ellipsoid described by (2.3), a confocal hyperboloid and a plane. These surfaces correspond to fixed ξ, η and ϕ respectively. The Hamiltonian of the free particle in prolate spheroidal coordinates is

$$H = \frac{1}{2a^2}\left(\frac{(1-\eta^2)p_\eta^2 + (\xi^2-1)p_\xi^2}{(\xi^2-\eta^2)} + \frac{p_\phi^2}{(1-\eta^2)(\xi^2-1)}\right) \tag{2.4}$$

where p_η, p_ξ and p_ϕ are the momenta conjugate to η, ξ, ϕ, respectively. Clearly p_ϕ is a constant angular momentum, since H is independent of ϕ. To separate the variables observe that

$$0 = (H-E)2a^2(\xi^2-\eta^2) = G(\eta, p_\eta) - G(\xi, p_\xi),$$

where

$$G(q,p) = (1-q^2)(p^2 - 2a^2E) + \frac{p_\phi^2}{1-q^2} \tag{2.5}$$

such that $G(\xi, p_\xi) = g = G(\eta, p_\eta)$ where g is the separation constant. Substituting $E = H$ into G gives

$$G = \frac{p_\eta^2 - p_\xi^2}{\xi^2-\eta^2}(1-\eta^2)(\xi^2-1) + p_\phi^2\frac{\xi^2-\eta^2}{(\xi^2-1)(1-\eta^2)}\,.$$

To convert this to the original variables observe that

$$|\boldsymbol{L}|^2 = \frac{(\xi^2-1)(1-\eta^2)}{(\xi^2-\eta^2)^2}(p_\xi\eta - p_\eta\xi)^2 + p_\phi^2\left(\frac{1+\xi^2-\eta^2}{(\xi^2-1)(1-\eta^2)}\right)$$

and

$$a^2(p_x^2+p_y^2) = \frac{(\xi^2-1)(1-\eta^2)}{(\xi^2-\eta^2)^2}(p_\xi\xi - p_\eta\eta)^2 + p_\phi^2\frac{1}{(\xi^2-1)(1-\eta^2)}$$

such that

$$G = |\boldsymbol{L}|^2 - a^2(p_x^2+p_y^2)\,. \tag{2.6}$$

This is a smooth function on T^*S^2, as is $p_\phi = L_z$, and it is easy to check that they have vanishing Poisson bracket. This can be computed in the original variables $(\boldsymbol{Q}, \boldsymbol{P})$ with respect to the canonical bracket on $T^*\mathbb{R}^3$, or in the variables $(\boldsymbol{P}, \boldsymbol{L})$ after reduction to T^*S^2 with respect to the induced bracket with Poisson tensor B. In both cases $\{|\boldsymbol{L}|^2, L_z\} = 0$ and also $\{p_x^2+p_y^2, L_z\} = 0$ and hence $\{G, L_z\} = 0$. We write L_z for the function that maps a point $(\boldsymbol{P}, \boldsymbol{L})$ to the coordinate l_z. Thus we arrive at the main classical object of this paper:

Theorem 7 (Spheroidal harmonics integrable system)**.** *Consider $\mathbb{R}^6$ with coordinates $(\boldsymbol{P}, \boldsymbol{L})$ and Lie-Poisson structure of $e^*(3)$ with Poisson tensor B given by (2.1) and Casimirs $\boldsymbol{P}\cdot\boldsymbol{P} = 2E$ and $\boldsymbol{P}\cdot\boldsymbol{L} = 0$. The functions $(L_z, G) = (l_z, l_x^2+l_y^2+l_z^2 - a^2(p_x^2+p_y^2))$ define a Liouville integrable system on T^*S^2.*

The values of (L_z, G) will be denoted by (m, g). We call this integrable system the (prolate) *spheroidal harmonics integrable system*, since it arises from separation of variables in spheroidal coordinates. It is the classical analogue of the compact part of the spheroidal wave equation, whose solutions are known as spheroidal harmonics.[2] In this work we are only interested in the prolate spheroidal harmonics. Formally the oblate case can be found by flipping the sign of a^2, and this system is also Liouville integrable. However, the dynamics in the oblate case are quite different and in particular does not exhibit monodromy, so we do not consider this case in the present work. Repeating this procedure for any of the 11 separating coordinate systems on $\mathbb{R}^3$ gives rise to an integrable system on $e^*(3)$. The list of the resulting smooth commuting integrals is given in [MPW81]. For example, for Euclidean coordinates the integrals are the components of $\boldsymbol{P}$, and the dynamics produces straight lines in $\boldsymbol{L}$. This is an integrable system, but all the dynamics is unbounded. Separation in ellipsoidal coordinates leads to an integrable system on $e^*(3)$ with two quadratic commuting functions and with two parameters. Under the mapping described in Theorem 5 this integrable system is equivalent to the (non-degenerate) C. Neumann system. It is an interesting research project to study these integrable Hamiltonian systems alongside the corresponding special functions. In this paper we restrict our attention to spheroidal coordinates, because, as we will show, it leads to a generalised semi-toric system that exhibits Hamiltonian monodromy. The related quantum system has quantum monodromy. In other words, the eigenvalues of the spheroidal wave equation exhibit monodromy. Before we describe the spheroidal wave equation and its quantum monodromy in the next section, here we are going to describe some aspects of the dynamics of the spheroidal harmonics integrable system. A detailed analysis including the proof that it is a generalised semi-toric system with Hamiltonian monodromy is postponed to a later section.

The vector field that is generated by the Hamiltonian L_z is given by $B\nabla L_z$ which gives

$$\dot{\boldsymbol{P}} = -\boldsymbol{P} \times \boldsymbol{e}_z, \quad \dot{\boldsymbol{L}} = -\boldsymbol{L} \times \boldsymbol{e}_z \,. \tag{2.7}$$

The solution is a rotation of the first two components of $\boldsymbol{P}$ and $\boldsymbol{L}$ by the same amount; the third components are unchanged. Thus the point $\boldsymbol{P}$ on S^2 is rotated about the p_z-axis, while $\boldsymbol{L}$ in the tangent space is rotated in the same way. The north- and the south-poles of S^2 are fixed by this rotation, but then $\boldsymbol{L} = (l_x, l_y, 0)^T$ is not fixed, unless it vanishes. A vector $\boldsymbol{L} = (0, 0, l_z)^T$ that is in the tangent space of a point $\boldsymbol{P} = (\cos\phi, \sin\phi, 0)$ on the equator of the sphere is fixed by this rotation, but the corresponding $\boldsymbol{P}$ is not. This shows that the only fixed points of this S^1 action are $\boldsymbol{P} = (0, 0, \pm 1)^T$, $\boldsymbol{L} = (0, 0, 0)^T$. They correspond to geodesics along the z-axis, i.e., lines through the two foci of the ellipsoid of the spheroidal

[2]The term spheroidal harmonics is used in different ways in the literature. The strict use of "harmonics" refers to solutions of the Laplace equation. When considering the Laplacian in $\mathbb{R}^3$ separated in spheroidal coordinates the eigenfunctions are products of associated Legendre functions, however, one of them is evaluated outside the usual range $|z| < 1$, and is thus sometimes referred to as a spheroidal harmonic [DLMF, 14.3]. Our use of the term spheroidal harmonic is different and serves as a "reminder of the kinship with the spherical harmonics" [PFTV88, 17.4].

coordinates.

The vector field that is generated by the Hamiltonian G is

$$\dot{\boldsymbol{P}} = -2\boldsymbol{P} \times \boldsymbol{L}, \quad \dot{\boldsymbol{L}} = a^2 \boldsymbol{P} \times (\boldsymbol{P} - \boldsymbol{e}_z p_z) = -a^2 p_z \boldsymbol{P} \times \boldsymbol{e}_z \,. \tag{2.8}$$

Clearly $\boldsymbol{L} = \boldsymbol{0}$ and $\boldsymbol{P} = \boldsymbol{e}_z p_z$ is an equilibrium point. Moreover, for $\boldsymbol{P} = (p_x, p_y, 0)^T$ and $\boldsymbol{L} = (0, 0, l_z)^T$ we have $\boldsymbol{L} = const$, $p_z = 0 = const$ and $\dot{p}_x = -2l_z p_y$ and $\dot{p}_y = 2l_z p_x$, a periodic solution along the equator with orientation depending on the sign of l_z. For $l_z = 0$ the equator is a circle of non-isolated equilibrium points of the flow of G.

In the limiting case $a \to 0$ the integral G becomes the angular momentum squared. In this limit the equations of motion can be solved explicitly in terms of trigonometric functions. Since $\dot{\boldsymbol{L}} = 0$ the equation for $\dot{\boldsymbol{P}}$ is that of a rotation about the fixed axis $\boldsymbol{L}$. The period of these rotation is given by $\sqrt{|\boldsymbol{L}|}$. If instead of $G = |\boldsymbol{L}|^2$ we consider $|\boldsymbol{L}|$ as a Hamiltonian then the period is 2π, and hence $|\boldsymbol{L}|$ is an action variable. To see this just integrate $\dot{\boldsymbol{P}} = -\boldsymbol{P} \times \boldsymbol{L}/|\boldsymbol{L}|$ for constant non-zero $\boldsymbol{L}$. The solution is a rotation of $\boldsymbol{P}$ about the fixed normal vector in the direction of $\boldsymbol{L}$. The only problem with the flow of $|\boldsymbol{L}|$ is that the vector field is not defined when $\boldsymbol{L} = \boldsymbol{0}$ and hence the flow does not define a global S^1 action. When instead the flow of $G = |\boldsymbol{L}|^2$ (for $a = 0$) is considered the vector field simply vanishes when $\boldsymbol{L} = \boldsymbol{0}$, and so the whole sphere $|\boldsymbol{P}| = 2E$ is a sphere of fixed points.

The spheroidal harmonics integrable system has a number of discrete symmetries. We restrict our attention to discrete symmetries that are canonical transformations.

Proposition 8 (Discrete symmetries)**.** *The group of linear discrete canonical symmetries of the spherical harmonics integrable system is $\mathbb{Z}_2 \times \mathbb{Z}_2$. For $s_i = \pm 1$, $i = 1, 2, 3$ define $S = \mathrm{diag}(s_1, s_2, s_3)$ and $\tilde{S} = \mathrm{diag}(s_2 s_3, s_1 s_3, s_1 s_2)$ so that a linear map of $(\boldsymbol{P}, \boldsymbol{L})$ is given by $(S\boldsymbol{P}, \tilde{S}\boldsymbol{L})$. The non-trivial elements of $\mathbb{Z}_2 \times \mathbb{Z}_2$ are obtained from $S_1 = \mathrm{diag}(+,+,-)$, $S_2 = \mathrm{diag}(-,-,-)$ and $S_3 = \mathrm{diag}(-,-,+)$.*

Proof. Since $S^{-1} = S^t$ the map $\boldsymbol{Q} \mapsto S\boldsymbol{Q}$ extends to a symplectic map as $(\boldsymbol{Q}, \boldsymbol{P}) \mapsto (S\boldsymbol{Q}, S\boldsymbol{P})$. The induced sign flip on the angular momentum is $\boldsymbol{L} \mapsto \tilde{S}\boldsymbol{L}$ where $\hat{S} = \mathrm{diag}(s_2 s_3, s_1 s_3, s_1 s_2)$ is found by computing the cross product $\boldsymbol{Q} \times \boldsymbol{P}$. The integral G is invariant under all such sign flips, since it is quadratic in components of $\boldsymbol{P}$ and $\boldsymbol{L}$. In addition $L_z = xp_y - yp_x$ should be invariant under the discrete symmetry which requires $s_1 s_2 = +1$. Thus the discrete symmetries of the spheroidal harmonics system are $S_1 = \mathrm{diag}(++-)$, $S_2 = \mathrm{diag}(---)$ and $S_3 = \mathrm{diag}(--+)$ together with the corresponding induced map $\tilde{S}_i$ on $\boldsymbol{L}$. Together with the identity they form the group $\mathbb{Z}^2 \times \mathbb{Z}^2$.

∎

In prolate spheroidal coordinates (2.3) the symmetry operations are realised as follows. Changing the sign of η changes the sign of z but leaves x and y unchanged, so that $\eta \mapsto -\eta$ corresponds to the symmetry S_1. Adding π to ϕ changes the signs of x and y while z is unchanged, so that $\phi \mapsto \phi + \pi$ corresponds to the symmetry S_3. The composition of both gives S_2.

2.4. Quantum monodromy in prolate spheroidal harmonics

Separation of variables of the Laplace equation or the Helmholtz equation in $\mathbb{R}^3$ in spheroidal coordinates leads to spheroidal harmonics. The classical references on spheroidal harmonics are [SMC+59, MS54, Fla57], and a few more modern ones are [PFTV88, FAW03, Vol03, DLMF, Zha17]. We would like to mention that prolate spheroidal wave functions have found applications as band-limited functions [Sle83], also see [XRY01, Boy04] and the references therein. Here we will derive the spheroidal wave equation in the traditional way from the Schrödinger equation of the free particle separated in spheroidal coordinates. This will allow us to connect to the spheroidal harmonics integrable system by way of semi-classical quantisation, a connection we need later to prove the existence of quantum monodromy.

The stationary Schrödinger equation for the free particle is $-\frac{1}{2}\hbar^2\Delta\Psi = E\Psi$, or we can think of it as Helmholtz's wave equation $\Delta\Psi + k^2\psi = 0$. Writing the Laplacian Δ in spheroidal coordinates (2.3) gives

$$\frac{1}{(\xi^2-\eta^2)}\left(\frac{\partial}{\partial\xi}\left((\xi^2-1)\frac{\partial\Psi}{\partial\xi}\right)+\frac{\partial}{\partial\eta}\left((1-\eta^2)\frac{\partial\Psi}{\partial\eta}\right)\right)+\frac{1}{(1-\eta^2)(\xi^2-1)}\frac{\partial^2\Psi}{\partial\phi^2} = -\frac{2Ea^2}{\hbar^2}\Psi\,. \tag{2.9}$$

Separation into product form $\Psi(\eta,\xi,\phi) = \psi_\eta(\eta)\psi_\xi(\xi)\psi_\phi(\phi)$ yields the simple equation

$$\frac{\partial^2\psi_\phi}{\partial\phi^2} + m^2\psi_\phi = 0 \tag{2.10}$$

and the (prolate angular) spheroidal wave equation

$$\hat{G}\psi_\eta = g\psi_\eta, \quad \hat{G} = -\frac{d}{d\eta}\left((1-\eta^2)\frac{d}{d\eta}\right) + \frac{m^2}{1-\eta^2} - \gamma^2(1-\eta^2), \quad \gamma^2 = \frac{2Ea^2}{\hbar^2} \tag{2.11}$$

with separation constants m and g. The third separated equation is found by replacing η by ξ. The difference is in the domain $\eta \in [-1,1]$ while $\xi \geq 1$.

For general values of γ the equation (2.11) is a singular Sturm-Liouville equation. It can be transformed into an equation with periodic (but still singular) coefficients, see, e.g. [Ars64]. Viewed as a polynomial differential equation in the complex plane it can be transformed into the confluent Heun equation [RA95]. The general Heun equation is the second order ordinary differential equation of Fuchsian type with four regular singular points. Letting two of the regular singular points coalesce leads to an irregular singular point. The result is the confluent Heun equation.

The quantum integrable system (QIS) on the reduced space consists of two self-adjoint operators $\hat{L}_z$ and $\hat{G}$ acting on functions on the sphere S^2. The eigenvalues g_l^m of G are those values of g in (2.11) for which the solution of the spheroidal wave equation for η leads to a smooth function $\psi_\eta \psi_\phi$ on the sphere. In our treatment we ignore the equation for ξ.

The solution ψ_ϕ to the angular equation is proportional to linear combinations of $e^{\pm im\phi}$ and 2π-periodicity in ϕ implies $e^{\pm im2\pi} = 1$, and hence m must be an integer. This integer m is the quantum number for the z-component of the angular momentum $l_z = m\hbar$.

When g is an eigenvalue g_l^m of the singular Sturm-Liouville problem (2.11) the corresponding eigenfunction bounded on $(-1, 1)$ is called the (prolate angular) spheroidal wave function of the first kind, which we denote by $S_l^m(\gamma, \eta)$.[3] In the limit $\gamma \to 0$ these solutions degenerate to the associated Legendre polynomials of the first kind $P_l^m(\eta)$. For $\gamma \neq 0$ the spheroidal wave functions can be written as a (generally infinite) series of associated Legendre polynomials

$$S_l^m(\gamma, \eta) = {\sum_{k=0,1}^{\infty}}' \, d_k^{lm}(\gamma) P_{m+k}^m(\eta) \tag{2.12}$$

where d_k^{lm} are the expansion coefficients and the prime on the summation indicates to sum over odd k if $l - m$ is odd and over even k if $l - m$ is even. Expressions for the resulting three term recursion relation that determines d_k^{lm} can be found, e.g., in [AS92, 21.7.3].

The product of the eigenfunctions of (2.10) and (2.11) gives the spheroidal harmonics

$$Z_l^m(\gamma, \eta, \phi) := \frac{1}{\sqrt{2\pi}} S_l^m(\gamma, \eta) e^{im\phi} = \sum_k d_k^{lm} Y_{m+k}^m(\eta, \phi) \tag{2.13}$$

expressed as a series of spherical harmonics Y_l^m. In the limit $\gamma \to 0$ we have $Z_l^m = Y_l^m$. Normalisation on the sphere requires

$$\int_0^{2\pi} \int_0^{\pi} Z_l^m \, (Z_l^m)^* \sin\theta d\theta d\phi = 1.$$

and the d_k^{lm} are chosen such that this holds, see, e.g., [AS92]. An example of the spheroidal wave function $S_l^m(\gamma, \eta)$ is shown in Fig. 2.7 and a comparision of $Z_l^m(\theta, \phi)$ with the corresponding spherical harmonic $Y_l^m(\theta, \phi)$ is presented in Fig. 2.8.

[3] The notation for the angular spheroidal wave function varies, see [AS92] for a table comparing various common notations. Our notation loosely follows [AS92], but we prefer to write l instead of n as in [SMC+59, MF53], and we write the indices ${}^m_l$ as in the associated Legendre polynomials.

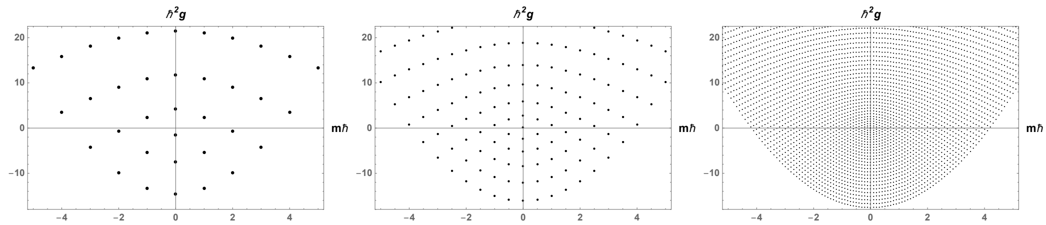

Figure 2.1: Joint spectrum $(\hbar m, \hbar^2 g_l^m)$ of the spheroidal harmonics with $2Ea^2 = 18$ for $\hbar = 1.0, 0.5, 0.1$ illustrating the semi-classical limit $\hbar \to 0$.

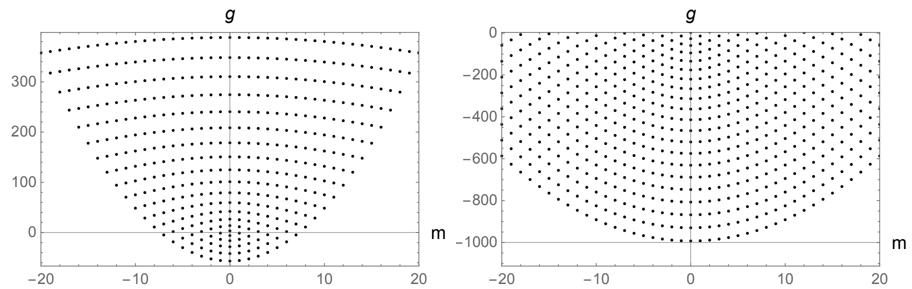

Figure 2.2: Joint spectrum (m, g_l^m) of the spheroidal harmonics for $\gamma = 8, 32$. The asymptotic expansion for g_l^m (2.14) is valid in the top part of the left figure, while (2.15) is valid in the bottom part of the right figure.

We now consider the joint spectrum of the QIS $(\hat{L}_z, \hat{G})$. The joint spectrum of a QIS $(\hat{H}_1, \ldots, \hat{H}_n)$ is the set of $(\lambda_1, \ldots \lambda_n) \in \mathbb{R}^n$ where $\hat{H}_i\psi = \lambda_i\psi$ for $i = 1, \ldots, n$ and ψ is a joint eigenfunction. For periodicity in ϕ we need to require that the eigenvalue of $\hat{L}_z$ is $\hbar$ times an integer m. The eigenvalues g_l^m of $\hat{G}$ can in general only be computed numerically. The Mathematica [Res] function `SpheroidalEigenvalue[`l, m, γ`]` gives the spheroidal eigenvalue g_l^m of (2.11). From general results in microlocal analysis, see, e.g., [PPN14], we know that in the semiclassical limit $\hbar \to 0$ the joint spectrum $(\hbar m, \hbar^2 g_l^m)$ is locally a lattice $\mathbb{Z}^2$. For a fixed spheroidal coordinate system, i.e., a fixed value of a decreasing $\hbar$ makes this local lattice finer and finer, see Fig. 2.1.

In the following we prefer to absorb $\hbar$ in the definition of the single parameter $\gamma = 2Ea^2/\hbar^2$ and present the scaled joint spectrum (m, g_l^m). When changing γ the values and the distribution of the joint eigenvalues changes. We are going to explain the structure of the joint spectrum and its dependence on γ in the course of the paper. Two examples of the joint spectrum are shown in Fig. 2.2 for $\gamma = 8, 32$. Note that this lattice is bounded below by a parabola (given by the critical values of the energy-momentum map, see below) but unbounded from above. We can observe that, locally the lattice is isomorphic to $\mathbb{Z}^2$ thus allowing local assignments of quantum numbers. However, there is a lattice defect at the origin, and thus we do not have a global $\mathbb{Z}^2$ lattice, indicating the presence of quantum monodromy.

The spectrum of the spheroidal wave equation is well understood, and asymptotic expansions for the eigenvalues g_l^m are well known [MS54, AS92, DLMF, Ars64]. Here we are going to use these formulas to describe the quantum monodromy in the joint spectrum.

When $a \to 0$ the constant $\gamma \to 0$ and the operator $\hat{G} \to |\boldsymbol{L}|^2$ becomes that of the associated Legendre equation with spectrum $g_l^m = l(l+1)$ and corresponding eigenfunction the associated Legendre polynomial $P_l^m(\eta)$ for $-l \leq m \leq l$. The spectrum is degenerate since g_l^m is independent of m. The labelling of eigenvalues in the spheroidal wave equation is continued from this limit for non-zero a. This means that in the Sturm-Liouville problem of the operator $\hat{G}$ for given fixed integer m the eigenvalue g_l^m of the ground state is labelled by $l = |m|$. The degeneracy is split for non-zero γ and

$$\hat{g}_l^m = l(l+1) - \frac{1}{2}\left(1 + \frac{(2m-1)(2m+1)}{(2l-1)(2l+3)}\right)\gamma^2 + O(\gamma^4/l^2), \tag{2.14}$$

see, e.g., [MS54, AS92, DLMF, Ars64]. This expansion converges when $\gamma^2 < \rho_l^m$ where $\rho_l^m > 4l+6$ for $l-|m| = 0, 1$ and $\rho_l^m > 4l-2$ for $l-|m| \geq 2$, see [MS54, 3.22]. This means that for fixed γ one can always choose l large enough so that the series converges. For fixed γ this approximation can be understood as a semi-classical limit with fixed a but large quantum number l or correspondingly large values of the eigenvalue g_l^m.

When $\gamma \to \infty$ the spectrum also becomes simpler, but in this limit we are only aware of an asymptotic series expansion for the eigenvalues. The leading order of the operator $\hat{G}$ is $-a^2(\hat{p}_x^2 + \hat{p}_y^2)$. The eigenvalues satisfy

$$\breve{g}_l^m = -\gamma^2 + (2(l-|m|)+1)\gamma - \tfrac{3}{4} + m^2 - \tfrac{1}{2}(l-|m|)(l-|m|+1) + O(1/\gamma), \tag{2.15}$$

see [MS54, AS92, DLMF, Ars64, Mül63]. Thus eigenvalues with the same value of $l-|m|$ and small $|m|$ are degenerate at leading order. The limit of large γ can be understood as the semiclassical limit where $\hbar \to 0$ for fixed value of a for quantum numbers l close to the ground state with $l = |m|$.

Fig. 2.3 illustrates the monodromy about the origin. A unit cell is parallel transported along a path that encloses the origin. As the basis vectors (say v_1 is the vertical vector and v_2 is the horizontal one) are fully transported around the loop, we observe that v_1 stays constant whilst v_2 becomes $v_2 + 2v_1$. This implies that we have a basis transformation according to

$$\begin{pmatrix} v_1' \\ v_2' \end{pmatrix} = \begin{pmatrix} 1 & 0 \\ k & 1 \end{pmatrix} \begin{pmatrix} v_1 \\ v_2 \end{pmatrix} \tag{2.16}$$

where $k = 2$. This integer is called the monodromy index. In the figure the full loop is broken up into two symmetric half-loops. At each of the two points where the two half-loops meet a basis transformation with $k = 1$ occurs, and their product gives the monodromy with $k = 2$. In the next section we will prove monodromy by showing that

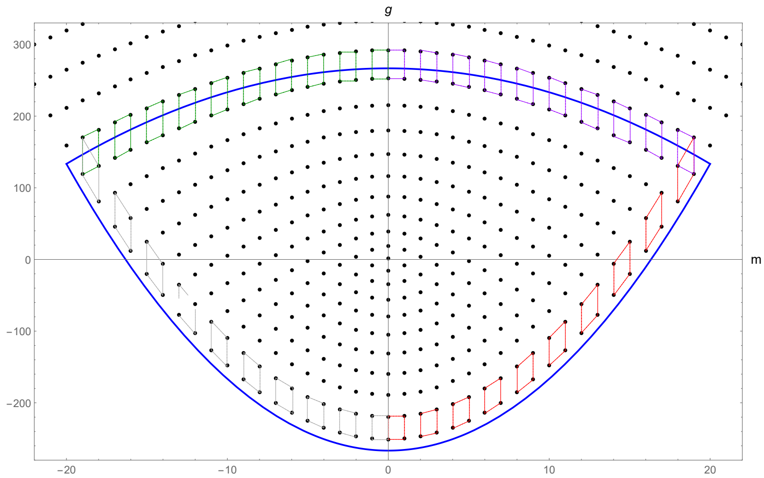

Figure 2.3: Joint spectrum (m, g_l^m) of the spheroidal harmonics for $\gamma = 16$. A lattice unit cell is transported around the origin. The lower blue parabola is $g = -\gamma^2 + m^2$ and the upper blue parabola is $2g = 2l^2 - \gamma^2 - m^2(\gamma/l)^2$ for $l = l^*$. The red and purple cells are transports of the bottom cell B_l^m and the top cell T_l^m, respectively, for positive m. The grey and green cells are those for negative m.

in the classical phase space there are isolated critical points of focus-focus type and the pre-image of the corresponding critical value is a doubly pinched torus. Here we give a direct quantum mechanical interpretation of monodromy that is based on discrete symmetries and the well known asymptotic formulas (2.14) and (2.15). We should emphasise that the following discussion is a heuristic analysis of monodromy. While (2.14) can be extended to a convergent series, we are not aware of a a convergent extension of the asymptotic formula (2.15). Because of this it is not easy to make the following argument rigorous.

The monodromy along a loop in the joint spectrum around the origin can be analysed by transporting a unit cell, see Fig. 2.3. Transporting a unit cell only makes sense where there are at least two negative eigenvalues in the sequence g_l^0, $l = 0, 1, \ldots$. The ground state g_0^0 is always non-positive. For $\gamma = \pi$ we have $g_1^0 < 0 < g_2^0$ and hence we require $\gamma \geq \pi$. The transport is done along the lower parabola where $l^2 - m^2 = 0$ in the joint spectrum and near a particular "upper" parabola where $l = l^* = \lceil \kappa\gamma \rceil$ is constant in the joint spectrum. The factor κ needs to satisfy $\kappa > 1/\sqrt{2}$ so that $g_{l^*}^0(\gamma) > 0$. In Fig. 2.3 we choose $\kappa = \sqrt{2/3}$ and in Fig. 2.4 we choose $\kappa = 3/4$. To see that these are indeed parabolas in (m, g)-space a truncation of (2.14) gives $g = -\gamma^2 + m^2$ and a truncation of (2.15) gives $g = (l^*)^2 - \gamma^2/2 - \frac{1}{2}m^2(\gamma/l^*)^2$. Note that it is neither required nor necessary that these parabolas go through points in the spectrum. They merely serve as an approximate guide to where the lattice structure of the joint spectrum is going to be analysed.

A unit cell in the joint spectrum is defined at $l = m = 0$ and moved along the lower parabola. Another unit cell in the joint spectrum is defined at $l = l^*$, $m = 0$ and transported along the upper parabola. The two parabolas meet where $m = l^*$. A unit cell near the

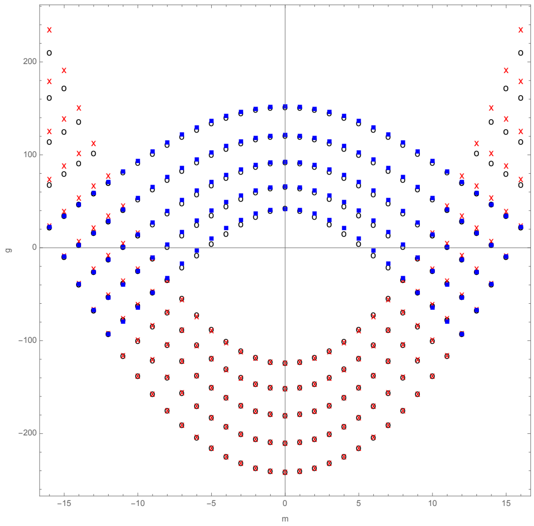

Figure 2.4: Joint spectrum (m, g_l^m) (black dots) compared to the asymptotic formulas $(m, \hat{g}_l^m)$ (blue dots) and $(m, \check{g}_l^m)$ (red dots) for $\gamma = 16$. The two asymptotic formulas approximately agree near the lattice point $l = |m| = l^* = 12$.

bottom parabola is defined by its four corners as $B_l^m = (g_l^m, g_{l+1}^{m+1}, g_{l+2}^{m+1}, g_{l+1}^m)$ moving counterclockwise around the unit cell. A unit cell near the top parabola is defined by its four corners as $T_l^m = (g_l^m, g_l^{m+1}, g_{l+1}^{m+1}, g_{l+1}^m)$ moving counterclockwise around the unit cell. For negative m cells are obtained by reflection about $m = 0$. The cell at the top has a natural labelling, which is inherited from the spherical harmonics limit. Now the cells are moved together to the point where the parabolas meet. There $B_{l^*-1}^{l^*-1}$ is compared with $T_{l^*}^{l^*-1}$. The 2nd and 3rd state in the two unit cells agree, and the last of B with the first of T. Thus a basis transformation will add 1 unit to l. A mirror symmetric situation occurs for negative m, and hence the total monodromy around the loop is 2.

When repeating this process with the asymptotic formulae (2.14) and (2.15) instead of with the (numerically computed) exact spectrum, the cell B_l^m is defined using $\check{g}_l^m$ in (2.14) and T_l^m is defined using $\hat{g}_l^m$ in (2.15). Approximate eigenvalues in these cells will only approximately agree near $l = l^* = |m|$. In Fig. 2.4 the exact eigenvalues are shown as black dots, approximations from (2.14) (using $\check{g}_l^m$ up to including terms of order γ^4) are shown as blue dots for $l - l^* = 0, \ldots, 4$, $\pm m = 0, \ldots, l$ and approximations from (2.15) (using $\hat{g}_l^m$ up to including terms of order γ^{-2}) are shown as red dots for $l - |m| = 0, \ldots, 4$, $\pm m = 0, 1, \ldots, l^* + 4$. The blue dots sit nearly on top of the black dots for larger l, while the red dots sit nearly on top of the black dots for small $l - |m|$. The choice of κ and hence l^* is selecting the region near $(l, m) = (l^*, l^*)$ where both formulas work. To make this quantitative we introduce a measure for the quality of the asymptotic formulas as the relative error

$$e(l, m) = \frac{\hat{g}_l^m - \check{g}_l^m}{\hat{g}_{l+1}^m - \hat{g}_l^m}$$

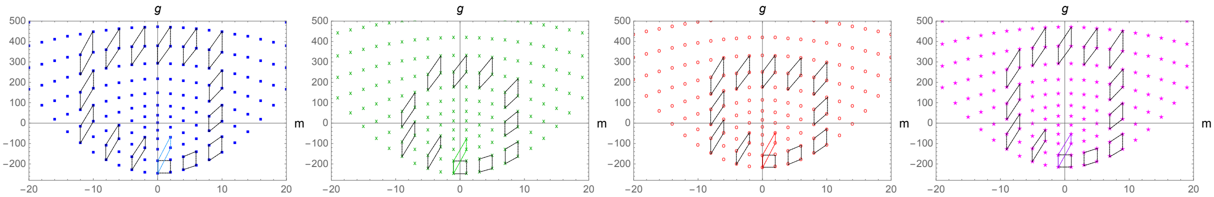

Figure 2.5: a) and b) Joint spectrum where $l-m$ is even and m is even/odd respectively. c) and d) where $l-m$ is odd and m is even/odd respectively. a) is invariant under the whole discrete symmetry group, b), c), d) are invariant under S_1, S_3, S_2, respectively.

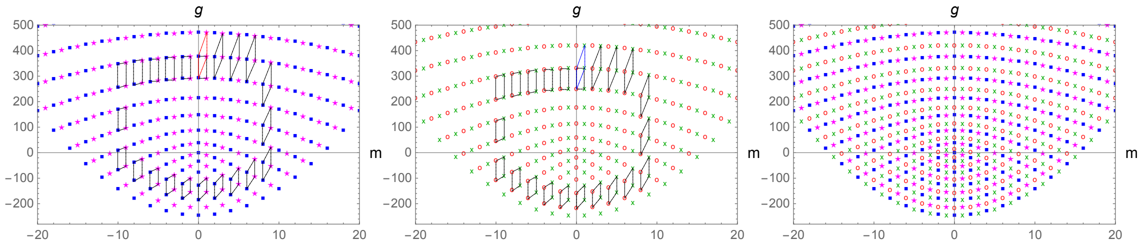

Figure 2.6: Parts of the joint spectrum whose eigenfunctions are a) even under S_2, b) odd under S_2 and c) the complete joint spectrum. The spectra shown in a) and b) both have monodromy index 1.

evaluated at lattice points (l,m) where both hold approximately. Evaluated with $\kappa = 3/4$ this gives $|e(l^*,l^*)| < 0.07$, $|e(l^*+1,l^*+1)| < 0.07$ for the two lower states near (l^*,l^*) and $|e(l^*+1,l^*)| < 0.19$, $|e(l^*,l^*-1)| < 0.19$ for the two higher states. These estimates hold for any $\gamma > \pi$. This implies that even though there is a considerable error, it is still possible to identify the unit cells, since the error is less than 20% for all four corners relative to the size of the cell. Thus it is possible to define quantum monodromy using the asymptotic formulas alone.

The joint spectrum can be divided into symmetry classes. Since (2.11) is even in η the eigenfunctions S_l^m are even or odd. They inherit the symmetry of P_l^m so that S_l^m is even when $l-m$ is even and odd when $l-m$ is odd. Accordingly $S_l^m \circ S_1 = (-1)^{l-m} S_l^m$. Similarly for $\psi_\phi = e^{im\phi}$ it holds that $\psi_\phi \circ S_3 = (-1)^m \psi_\phi$. Thus every point in the joint spectrum can be classified according to the parity of $l-m$ and m. This is illustrated in Fig. 2.5 a) through d), where each subfigure contains one quarter of the number of points the full spectrum possesses. Despite this, the unit cell is still deformed in the same way as in Fig. 2.3 and the monodromy index is 2.

It is interesting to note that when selecting states according to their symmetry under $S_2 = S_1 \circ S_3$ the monodromy index changes to 1. Since Z_l^m is the product of ψ_ϕ and S_l^m it is invariant under S_2 if $l-m$ and m are either both even or both odd. The corresponding joint eigenvalues are shown in Fig. 2.6 left and middle, and for this selection of joint eigenstates the monodromy is 1.

The most striking effect of the monodromy is a change in what the symmetry of horizontally neighbouring states near the line $m = 0$ is. Consider Fig. 2.6 left and middle. When $g \ll 0$ the horizontally neighbouring states have the same symmetry type, while for $g \gg 0$ the symmetry type changes. Not only does the symmetry type change, but also the location of states comparing $m = 0$ and $m = 1$. For $g \gg 0$ horizontally neighbouring states with $m = 0$ and $m = 1$ have nearly the same eigenvalue. By contrast, for $g \ll 0$ consider a state with $m = 0$. Now there is no horizontally neighbouring state with $m = 1$. Instead the eigenvalue for a state with $m = 1$ is approximately half way between the nearby states with $m = 0$.

We are now going to make these observations precise using (2.14) and (2.15). Consider states invariant under S_2, hence with even $l - m$ and even m, see Fig. 2.6, left. Observe the upper end of the figure where $g \gg 0$ with $m = 0$ and $l \gg 0$. These states are described by (2.15), the asymptotics for large γ or small $\hbar$. Horizontally neighbouring states with $m = 0$ and $m = 1$ have nearly the same eigenvalue. Using (2.15) we find

$$g^1_{l+1} - g^0_l = 1 + O(1/\gamma), \quad \text{for } g^0_l \gg 0.$$

The same analysis holds for Fig. 2.6, where l in the above formula is odd, while in the left figure it is even. Note that the separation of states in the vertical direction $g^0_{l+2} - g^0_l = 4\gamma + (2l + 3) + O(1/\gamma)$ is of order γ, and hence we perceive the neighbour in the horizontal direction as nearly the same. If we were to present eigenvalues with dimensions then the difference in eigenvalue of two horizontally neighbouring states would be of order $\hbar^2$, while those of two vertically neighbouring states would be $\hbar$.

Now compare this to the situation with $g \ll 0$ and hence small l near the line $m = 0$. There the state with $m = 1$ is approximately equal to the average of neighbouring states with $m = 0$. Using (2.14) we find

$$\frac{g^0_l + g^0_{l+2}}{2} - g^1_{l+1} = 1 + O(\gamma^2), \quad \text{for } g^0_l \ll 0$$

in the horizontal direction, while in the vertical direction the separation is $g^1_{l+1} - g^0_l = 2(l + 1) + O(\gamma^2)$. A comment similar to the previous case about the scaling with $\hbar$ applies here.

The previous discussing of neighbouring states was done separately for states that are either invariant under S_2 or not. The reason is that for these subsets the monodromy index is 1. When considering all states the monodromy index is 2, and its manifestation on the symmetry and labelling of states is different. In the set of all states in both limits, large positive and large negative g^0_l, there is always a horizontally neighbouring state with almost the same eigenvalue, see Fig. 2.6, right. A direct consequence of monodromy is the following observation: for large l such that $g^0_l \gg 0$ for horizontally neighbouring states $g_l^0 - g_l^1 = O(\gamma^2)$. For small l such that $g_l^0 \ll 0$ however this difference is not small, $g_l^0 - g_l^1 = 2\gamma + O(1)$. This means that states with the same l are not horizontal neighbours, instead the index l needs to be increased by 1 when going to the right, then $g_l^0 - g_{l+1}^1 = 1 + O(1/\gamma)$ is small. This means that when comparing the labelling of states along the line $m = 0$ with the line $m = 1$ there is a mismatch that occurs for small l (negative g), while for large l (positive g) states are labelled in the natural way. As already mentioned the fact that this labelling is "natural" in the latter case is a choice that was made in order to have continuity with the labelling in the spherical harmonics limit $a \to 0$. One could redefine the labelling to be "natural" with respect to the Sturm-Liouville problems for fixed m, then each ground state for fixed m would have the same quantum number. Then the mismatch in the labelling of horizontal neighbours would appear for states with large eigenvalues g_l^m. The fact that this mismatch cannot be avoided is an expression of the quantum monodromy in the system.

The discussion of monodromy using the asymptotic expansions (2.14) and (2.15) is enlightning, but it is somewhat heuristic, since we don't know about the convergence of (2.15). If we stay near the line $m = 0$ and observe the change in lattice for small and large g (as we did in the discussion of neighbours above) we cannot complete a loop around the focus-focus point, because neither formula is valid there. If we do complete the loop along the parabolas as indicated in Fig. 2.3 we are stretching the asymptotic expansions to the limit of their validity. For this reason we are going to prove existence of monodromy in the semi-classical limit by a detailed analysis of the corresponding classically integrable system in section 2.6, and by appealing to the general theory of quantum monodromy [VN99]. It is interesting to note that the general theory only makes sense in the semi-classical limit; when explicit approximate formulas for the quantum eigenvalues like (2.14) and (2.15) are known, quantum monodromy makes sense as long as there are at least a few eigenvalues $g_l^0 < 0$, so down to say $\gamma = \pi$.

2.5. Laplace-Runge-Lenz and C. Neumann

In this section we will show that the spheroidal harmonics system is symplectomorphic to the degenerate C. Neumann system. The C. Neumann system is a famous integrable system that was studied by Jacobi's student Carl Neumann [Neu59], as a prime example of separation of variables. It consists of a particle constrained to move on the unit sphere (in any dimension) under influence of an additional harmonic potential [Mos80a, Mos80b, Ves80, Raţ81]. The degenerate case has been studied in [Vuk08, DH12], and the action variables in the general case were analysed in [DRVW01], also see [DS07]. For the quantisation of the C. Neumann system (in the non-degenerate case) see [BT92, Tot93, Gur95].

The invariants $\boldsymbol{P}$ and $\boldsymbol{L} = \boldsymbol{Q} \times \boldsymbol{P}$ of the free particle are of degree 1 and 2 in the original phase space variables. Invariant degree 3 polynomials can be formed from them using an analogue of the Laplace-Runge-Lenz vector $\boldsymbol{A} = \boldsymbol{P} \times \boldsymbol{L}$. As in the Kepler problem it is useful to scale with the energy: $\boldsymbol{K} = \boldsymbol{A}|\boldsymbol{P}|^{-\alpha}$. The Poisson tensor in $\mathbb{R}^9$ with coordinates $(\boldsymbol{P}, \boldsymbol{L}, \boldsymbol{K})$ then is

$$B_\alpha = \begin{pmatrix} \boldsymbol{0} & -\hat{\boldsymbol{P}} & \hat{\boldsymbol{P}}^2|\boldsymbol{P}|^{-\alpha} \\ -\hat{\boldsymbol{P}} & -\hat{\boldsymbol{L}} & -\hat{\boldsymbol{K}} \\ -\hat{\boldsymbol{P}}^2|\boldsymbol{P}|^{-\alpha} & -\hat{\boldsymbol{K}} & \hat{\boldsymbol{L}}|\boldsymbol{P}|^{2(1-\alpha)} \end{pmatrix}. \tag{2.17}$$

In the Kepler problem the idea is to have the bracket between $\boldsymbol{L}$ and $\boldsymbol{K}$ close, so there the choice is $\alpha = 1$ so that $|\boldsymbol{P}|$ drops out in the lower right corner and the algebra is $so(4)$. In our case the choice $\alpha = 1$ leads to a realisation of the spheroidal harmonic system on $so(3,1)$, but the Hamiltonian G is not smooth when written in terms of $\boldsymbol{L}$ and $\boldsymbol{K}$, so we do not investigate this further. Instead we are interested to make the bracket between $\boldsymbol{P}$ and $\boldsymbol{K}$ close. To achieve this we need to eliminate $\boldsymbol{L}$. Using standard cross product identities we find $\boldsymbol{P}\times\boldsymbol{A} = -|\boldsymbol{P}|^2\boldsymbol{L}+\boldsymbol{P}(\boldsymbol{P}\cdot\boldsymbol{L})$. Choosing $\alpha = 2$ thus gives $\boldsymbol{P}\times\boldsymbol{K} = -\boldsymbol{L}+\boldsymbol{P}(\boldsymbol{P}\cdot\boldsymbol{L})|\boldsymbol{P}|^{-2}$. Now fixing the Casimir $\boldsymbol{P}\cdot\boldsymbol{L} = b$ of B_α allows us to eliminate $\boldsymbol{L}$ and the resulting Poisson structure on $\mathbb{R}^6$ with coordinates $(\boldsymbol{P}, \boldsymbol{K})$ is

$$B_{P,K} = |\boldsymbol{P}|^{-2}\begin{pmatrix} \boldsymbol{0} & \hat{\boldsymbol{P}}^2 \\ -\hat{\boldsymbol{P}}^2 & -\hat{\boldsymbol{U}} \end{pmatrix}, \quad \text{where} \quad \boldsymbol{U} = \boldsymbol{P}\times\boldsymbol{K} - b\boldsymbol{P}|\boldsymbol{P}|^{-2} \tag{2.18}$$

with Casimirs $\boldsymbol{P}\cdot\boldsymbol{P}$ and $\boldsymbol{P}\cdot\boldsymbol{K}$. Setting the magnetic term $b = 0$ and using the identity $\boldsymbol{P}\boldsymbol{P}^t - \hat{\boldsymbol{P}}^2 = id\boldsymbol{P}\cdot\boldsymbol{P}$ we see that this is the Dirac structure of T^*S^2 embedded in $\mathbb{R}^6$ as, e.g., derived in [DH12]. When considering the Dirac structure of T^*S^2 in $\mathbb{R}^6$ we use coordinates $\boldsymbol{x} = (x_1, x_2, x_3)^t \in S^2$ and momenta $\boldsymbol{y} = (y_1, y_2, y_3)^t$ in the tangent space of the sphere so that $\boldsymbol{x}\cdot\boldsymbol{y} = 0$. Thus define the Dirac structure B_D of T^*S^2 in $\mathbb{R}^6$ as

$$B_D = \begin{pmatrix} \boldsymbol{0} & -id + \boldsymbol{x}\boldsymbol{x}^t|\boldsymbol{x}|^{-2} \\ id - \boldsymbol{x}\boldsymbol{x}^t|\boldsymbol{x}|^{-2} & -\widehat{\boldsymbol{x}\times\boldsymbol{y}}|\boldsymbol{x}|^{-2} \end{pmatrix} \tag{2.19}$$

with Casimirs $\boldsymbol{x}\cdot\boldsymbol{x}$ and $\boldsymbol{x}\cdot\boldsymbol{y} = 0$. Note that the lower left block is the projector to the subspace orthogonal to $\boldsymbol{x}$.

Lemma 9. *Consider the manifold $M_r = \{(\boldsymbol{x}, \boldsymbol{y}) \in \mathbb{R}^6 \mid \boldsymbol{x}\cdot\boldsymbol{x} = r^2, \boldsymbol{x}\cdot\boldsymbol{y} = 0\}$ for $r > 0$. The map $\mu : M_r \to M_r$, $(\boldsymbol{x}, \boldsymbol{y}) \mapsto (\boldsymbol{x}, -\boldsymbol{x}\times\boldsymbol{y})$ is a diffeomorphism with inverse $(\boldsymbol{x}, \boldsymbol{y}) \mapsto (\boldsymbol{x}, \boldsymbol{x}\times\boldsymbol{y}/r^2)$.*

Proof. Composing μ with μ^{-1} and using the vector triple product expansion formula gives $-\boldsymbol{x}\times(\boldsymbol{x}\times\boldsymbol{y})/r^2 = \boldsymbol{y}(\boldsymbol{x}\cdot\boldsymbol{x})/r^2 - \boldsymbol{x}(\boldsymbol{x}\cdot\boldsymbol{y})/r^2 = \boldsymbol{y}$.

■

Note that for $r = 1$ the map μ of M_1 has order 3. If we think of a curve $\boldsymbol{x}(t)$ on the sphere such that $\boldsymbol{y}$ is the tangent vector to the curve then μ maps the tangent vector to the normal vector. When applied a second time μ maps the normal vector to the binormal vector. When applied a third time μ maps the binormal vector back to the tangent vector.

Proposition 10. *The map $(\boldsymbol{P}, \boldsymbol{L}) \mapsto (\boldsymbol{x}, \boldsymbol{y}) = (\boldsymbol{P}, \boldsymbol{P} \times \boldsymbol{L}|\boldsymbol{P}|^{-2})$ is a symplectomorphism between the co-adjoint orbit of the Lie-Poisson structure of $e^*(3)$ in $\mathbb{R}^6$ with variables $\boldsymbol{P}, \boldsymbol{L}$ given by (2.1) to T^*S^2 embedded in $\mathbb{R}^6$ with variables $\boldsymbol{x}, \boldsymbol{y}$ with Dirac structure given by (2.19).*

Proof. The Jacobian of the mapping is

$$M = \begin{pmatrix} id & 0 \\ -\hat{\boldsymbol{L}}|\boldsymbol{P}|^{-2} - 2(\boldsymbol{P} \times \boldsymbol{L})\boldsymbol{P}^t|\boldsymbol{P}|^{-4} & \hat{\boldsymbol{P}}|\boldsymbol{P}|^{-2} \end{pmatrix}.$$

Computing MBM^t gives all blocks but the lower right block of $B_{P,K}$ immediately. For this block notice the identity $\hat{\boldsymbol{L}}\hat{\boldsymbol{P}}^2 + \hat{\boldsymbol{P}}^2\hat{\boldsymbol{L}} - \hat{\boldsymbol{P}}\hat{\boldsymbol{L}}\hat{\boldsymbol{P}} = -\hat{\boldsymbol{L}}|\boldsymbol{P}|^2$ (or in cross-product terms $\boldsymbol{L} \times (\boldsymbol{P} \times (\boldsymbol{P} \times \boldsymbol{v})) + \boldsymbol{P} \times (\boldsymbol{P} \times (\boldsymbol{L} \times \boldsymbol{v})) - \boldsymbol{P} \times (\boldsymbol{L} \times (\boldsymbol{P} \times \boldsymbol{v})) = \boldsymbol{L} \times \boldsymbol{v}|\boldsymbol{P}|^2$ for all $\boldsymbol{v} \in \mathbb{R}^3$) while all other terms vanish because $\boldsymbol{P}$ is in the kernel of $\hat{\boldsymbol{P}}$. Now using the map μ from the Lemma we see that $\boldsymbol{P} = \boldsymbol{x}$ and $\boldsymbol{L} = -\boldsymbol{x} \times \boldsymbol{y}$ and this gives the result.

■

Having established the equivalence of the Lie-Poisson structure of $e^*(3)$ of the spheroidal harmonics system with the Dirac structure of T^*S^2 the question is what the Hamiltonian G becomes when interpreted in these terms.

Theorem 11. *The integrable spheroidal harmonics system of Theorem 7 with energy $|\boldsymbol{P}| = \sqrt{2E}$ is symplectomorphic to the integrable C. Neumann system of a particle constrained to move on the unit sphere $|\boldsymbol{x}| = 1$ with a harmonic potential. In the coordinates $(\boldsymbol{x}, \boldsymbol{y})$ on $T^*S^2 \in \mathbb{R}^6$ with the Dirac structure (2.19) the Hamiltonian of the Neumann system is*

$$G_N = \frac{1}{2}(y_1^2 + y_2^2 + y_3^2) - Ea^2(x_1^2 + x_2^2)$$

with second integral $L_N = -x_1y_2 + x_2y_1$.

Proof. We start with an $\boldsymbol{x}$ that is not yet restricted to the unit sphere. The map from Proposition 10 gives $|\boldsymbol{L}| = |\boldsymbol{x}||\boldsymbol{y}|$, so that the the term $|\boldsymbol{L}|^2$ in G becomes $|\boldsymbol{x}|^2|\boldsymbol{y}|^2$. Finally we do a symplectic scaling to the unit sphere, namely $\boldsymbol{x} = c\tilde{\boldsymbol{x}}$ and $\boldsymbol{y} = \tilde{\boldsymbol{y}}/c$ where $c = \sqrt{2E}$. Dropping the tildes and dividing by 2 gives G_N.

■

Theorem 11 has been proved in [Mar18] in the context of scattering problems. Here we prove the result by explicitly constructing the symplectomorphism. In its usual form the

C. Neumann system has a positive attractive potential. This can be adjusted by shifting the potential by the constant term $Ea^2|\boldsymbol{x}|^2$, such that the shifted potential is $Ea^2x_3^2$. To keep the analogy with the spheroidal harmonics integrable system we choose not to do this shift.

Note that while in the spheroidal harmonics system L_z is a coordinate after reduction, and this coordinate is a constant of motion, in the Neumann system the corresponding integral is again the angular momentum $x_1y_2 - x_2y_1$ about the third axis but here this is a function of the coordinates $\boldsymbol{x}$ and $\boldsymbol{y}$. Even when interpreting L_z as a function of the original coordinates $\boldsymbol{Q}$ and $\boldsymbol{P}$ before reduction the difference is that then $\boldsymbol{P}$ was the momentum, while now after renaming $\boldsymbol{P}$ as $\boldsymbol{x}$ this is the coordinate in configuration space. When considering the units of the quantities defined we see, however, that $\boldsymbol{x} = \boldsymbol{P}$ does have units of momentum while $\boldsymbol{y} = \boldsymbol{P} \times (\boldsymbol{Q} \times \boldsymbol{P})|\boldsymbol{P}|^{-2}$ has units of length, so that $\boldsymbol{x} \times \boldsymbol{y}$ does have units of angular momentum, except it has the opposite sign: $\boldsymbol{x}\times\boldsymbol{y} = \boldsymbol{P}\times(\boldsymbol{P}\times(\boldsymbol{Q}\times\boldsymbol{P})|\boldsymbol{P}|^{-2} = -\boldsymbol{Q}\times\boldsymbol{P}$.

We can introduce spherical coordinates on the unit sphere by

$$x_1 = \sin\theta\cos\phi, \quad x_2 = \sin\theta\sin\phi, \quad x_3 = \cos\theta$$

which transforms the Hamiltonian G_N to

$$G_N(\theta, \phi, p_\theta, p_\phi) = \frac{1}{2}\left(p_\theta^2 + \frac{p_\phi^2}{\sin^2\theta}\right) - Ea^2\sin^2\theta \tag{2.20}$$

where $p_\theta^2 = \frac{y_3^2}{\sqrt{1-x_3^2}}$ and $p_\phi = x_1y_2 - x_2y_1$ are canonically conjugate momenta to θ and ϕ, respectively.

Thus we see that separation of the (rotationally symmetric) Neumann system in spherical coordinates leads to the same Hamiltonian as the prolate spheroidal harmonics system obtained from separation in $\mathbb{R}^3$ in prolate spheroidal coordinates. A corresponding statement holds for the quantum systems. Since the phase space T^*S^2 is a cotangent bundle, Weyl quantization maps the coordinate variables (x_i, y_i) to the operators $(x_i, \frac{\hbar}{i}\frac{\partial}{\partial x_i})$. The operator corresponding to the Hamiltonian G_N is

$$2\hat{G}_N = -\hbar^2\nabla_{S^2} - 2Ea^2\sin^2\theta$$

which for $\hbar = 1$ can be seen to be the same as (2.11) by making the substitution $\eta = \cos\theta$. We close this section by showing the graph of a spheroidal wave function for $m = 2, l = 4$ and a contour plot of the real part of the corresponding spheroidal harmonic Z_l^m on the sphere, along with the spherical harmonic Y_l^m for comparison. Since the potential has its maximum at the poles (and its minimum along the equator) the wave function is "repelled" from the poles.

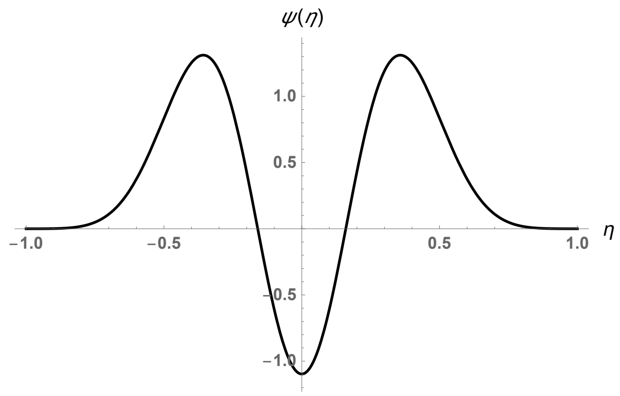

Figure 2.7: Spheroidal wave function with $(n, m, \gamma) = (4, 2, 20)$.

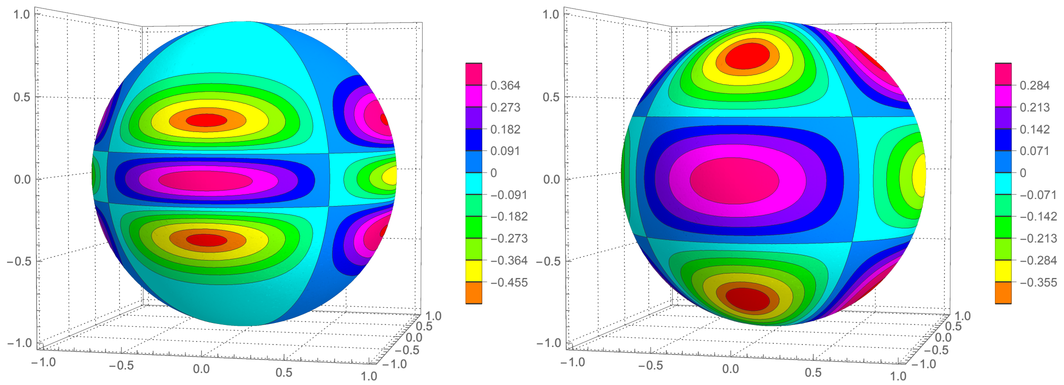

Figure 2.8: a) The spheroidal harmonic $Z_4^2(\theta, \phi)$ with $\gamma = 20$. b) The spherical harmonic $Y_4^2(\theta, \phi)$ for comparison.

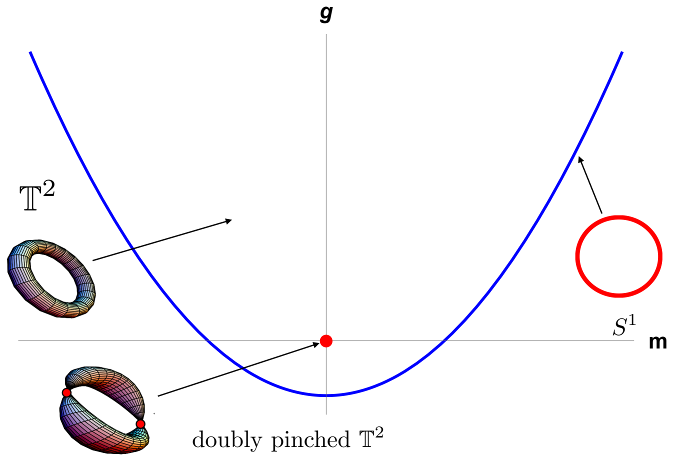

Figure 2.9: Bifurcation diagram of the spheroidal harmonics integrable system.

2.6. Momentum map of the spheroidal harmonics systems

We are now going to analyse the global geometry of the singular Liouville foliation of the integrable spheroidal harmonics system. In a number of steps we will prove

Theorem 12. *The spheroidal harmonics integrable system is a generalised semi-toric system with global S^1 action L_z. The momentum map $F = (L_z, G) : T^*S^2 \to \mathbb{R}^2$ has two isolated co-rank 2 critical points $\boldsymbol{P} = \pm \boldsymbol{e}_z\sqrt{2E}$, $\boldsymbol{L} = \boldsymbol{0}$ and a family of co-rank 1 critical points $\boldsymbol{P} = \sqrt{2E}(\cos\phi, \sin\phi, 0)^t$, $\boldsymbol{L} = \boldsymbol{e}_z m$, $\phi \in S^1$, $m \in \mathbb{R}$. The image of the co-rank 2 critical points is the critical value $(0,0)$, which is a non-degenerate focus-focus value and $F^{-1}(0,0)$ is a doubly pinched torus. The image of the co-rank 1 critical points is the parabola $(m, m^2 - 2Ea^2)$, points on which are of elliptic-transversal type and $F^{-1}(m, m^2 - 2Ea^2)$ is a periodic orbit consisting of co-rank 1 critical points parametrised by ϕ. The pre-image of each regular value of F is a single torus $\mathbb{T}^2$.*

As already mentioned in the introduction, the results of Theorem 12 have been established in [BZ93, Efs05] in the context of the quadratic spherical pendulum on T^*S^2. Using the equivalence given by Theorem 11 these results also hold for the spheroidal harmonics integrable system on $e^*(3)$. Here we prove these results directly on $e^*(3)$ so that the connection to the spheroidal wave functions is more transparent. The system will be analysed using singular reduction (using invariants), regular reduction (using global but singular canonical coordinates) and reconstruction to understand the fibres of the momentum map. In particular we will show that the focus-focus critical value is non-degenerate and hence there is Hamiltonian monodromy in the classical system invoking [Mat96, Zun97]. In particular this also implies the existence of quantum monodromy in the semiclassical limit as shown in general by San Vũ Ngọc in [VN99].

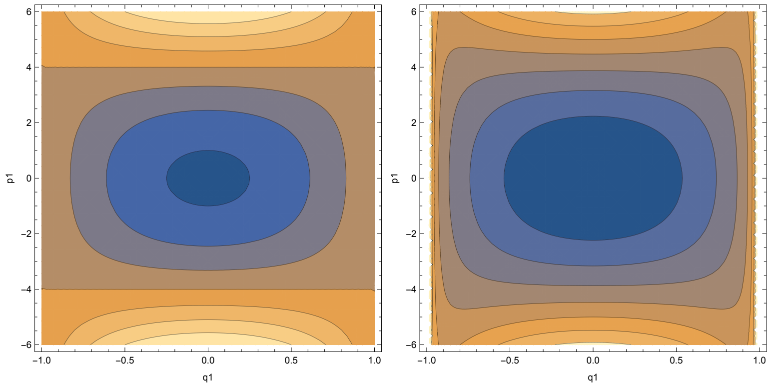

Figure 2.10: Level lines of $G(q,p)$ for $m = 0$ (left) and $m = 1$ (right), $\gamma = 4$.

We already know a symmetry reduced description (2.5) from separation of variables, albeit in singular coordinates. Eqn. (2.5) is connected to the Neumann system (2.20) via the transformation $\eta = \cos\theta$. Setting $\hbar = 1$ we have $l_z = m$ and arrive at the one degree of freedom Hamiltonian

$$G(q,p) = (1-q^2)(p^2-\gamma^2) + \frac{m^2}{1-q^2}\,. \tag{2.21}$$

There is a coordinate singularity at $|q| = 1$. The phase portrait of this reduced Hamiltonian is shown in Fig. 2.10. Away from the singularity there is an equilibrium at the origin with critical value $G(0,0) = m^2 - \gamma^2$. This gives the line of critical values $g = m^2 - \gamma^2$ in the bifurcation diagram Fig. 2.9. The corresponding motion in the original system in Euclidean coordinates is a periodic orbit along the equator of the sphere, as already discussed in section 2.3. The parabola of critical values $g = m^2 - \gamma^2$ is also the lower boundary of the joint spectrum and is hence shown in Fig. 2.3.

Since the coordinate system from the separation of variables is singular along the z-axis we now use singular reduction starting from the global Euclidean description in $(\boldsymbol{P}, \boldsymbol{L}) \in \mathbb{R}^6$ to understand the global dynamics.

Lemma 13. *Reduction of the spheroidal harmonics system of Theorem 7 by the global S^1 symmetry leads to a Poisson structure in $\mathbb{R}^3$ with coordinates (b_1, b_2, b_3). The reduction map $T^*S^2 \to \mathbb{R}^3$ for $|\boldsymbol{P}| = \sqrt{2E}$ is given by*

$$b_1 = \frac{p_z}{\sqrt{2E}}, \qquad b_2 = l_x^2 + l_y^2, \qquad b_3 = \frac{l_x p_y - l_y p_x}{\sqrt{2E}}\,.$$

with syzygy

$$C_3(b_1, b_2, b_3) = (1 - b_1^2)b_2 - b_1^2 m^2 - b_3^2 = 0\,.$$

The Poisson tensor is $\widehat{\nabla C_3}$.

Proof. The global S^1 action L_z as a Hamiltonian with respect to the Poisson structure B

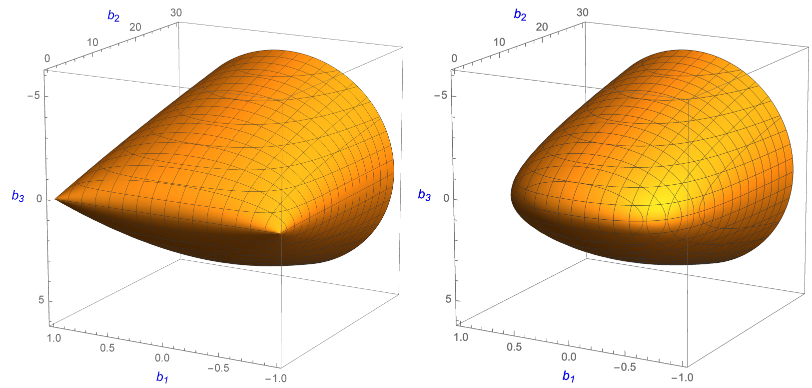

Figure 2.11: a) The singular reduced phase space $P_{m=0}$ with two singular points at $(b_1, b_2, b_3) = (\pm 1, 0, 0)$; b) A regular reduced phase space $P_{m=2}$ with non zero m.

generates a rotation in the first two components of $\boldsymbol{P}$ and $\boldsymbol{L}$ and fixes the third component, see (2.7). Thus p_z and l_z are invariant under this symmetry. Introducing $p_w = p_x + ip_y$ and $l_w = l_x + il_y$ the S^1 action is multiplication of p_w and l_w by $e^{i\phi}$. Any polynomial of p_z and l_z is also invariant. Additional quadratic polynomial invariants are $|p_w|^2$, $|l_w|^2$ and the real and imaginary part of $p_w \bar{l}_w$. All other polynomial invariants are functions of these 6 invariants, 2 linear and 4 quadratic. The Casimirs of the Poisson structure B expressed in these invariants read $|p_w|^2 + p_z^2 = 2E$ and $\Re(p_w \bar{l}_w) + p_z l_z = 0$ and can be used to eliminate $|p_w|^2$ and $\Re(p_w \bar{l}_w)$ wherever they appear. As before we set $l_z = m$ where m is now considered as a parameter. In addition we scale the momentum with $\sqrt{2E}$ as for the transformation to the Neumann system. The remaining invariants are denoted by b_i where $b_2 = |l_w|^2$ and $b_3 = \frac{\Im(p_w \bar{l}_w)}{\sqrt{2E}}$. This gives the stated reduction map. The invariants satisfy $|b_1| \leq 1$ and $b_2 \geq 0$ by construction. The identity $\Re(p_w \bar{l}_w)^2 + \Im(p_w \bar{l}_w)^2 = |p_w \bar{l}_w|^2 = |p_w|^2 |l_w|^2$ rewritten in terms of the invariants gives $C_3 = 0$. A fundamental property of invariants is that their Poisson bracket is again an invariant. By using the original Poisson structure B in the original variables $(\boldsymbol{P}, \boldsymbol{L})$ one can verify that

$$\{b_1, b_2\} = 2b_3, \quad \{b_1, b_3\} = 1 - b_1^2, \quad \{b_2, b_3\} = 2b_1 m^2 + 2b_1 b_2 \,.$$

The right hand sides are given by the derivatives $\partial C_3 / \partial b_i$, such that the reduced Poisson structure is $\widehat{\nabla C_3}$ as claimed. By construction then C_3 is a Casimir of the reduced Poisson structure. Since this encodes an identity between invariants (a so-called syzygy) the value of C_3 must be zero.

■

The invariants can of course also be written in the coordinates $(\boldsymbol{x}, \boldsymbol{y})$ of the Neumann system on the unit sphere where they look more natural as

$$b_1 = x_3, \qquad b_2 = y_1^2 + y_2^2, \qquad b_3 = y_1 x_2 - y_2 x_1 \,.$$

The points $\boldsymbol{P} = (0, 0, \pm\sqrt{2E})$ and $\boldsymbol{L} = (0, 0, 0)$ are fixed under rotations about the third axis. Hence the global S^1 action has fixed points and the symmetry reduced phase space is not in general a smooth manifold. This is the reason that we are using singular reduction. This fixed point occurs for $l_z = m = 0$ and its image under the reduction map is $(\pm 1, 0, 0)$. We now verify that these are exactly the singular points of the reduced phase space.

Lemma 14. *The reduced phase space* $P_m = \{(b_1, b_2, b_3) \mid C_3 = 0, b_2 \geq 0, b_1^2 \leq 1\}$ *is a smooth surface for* $m \neq 0$ *and a singular semi-algebraic variety with two conical singularities at* $(b_1, b_2, b_3) = (\pm 1, 0, 0)$ *for* $m = 0$.

Proof. The reduced phase space is the subset of $\mathbb{R}^3$ with coordinates b_1, b_2, b_3 for which the syzygy Casimir is satisfied, $C_3 = 0$, and in addition the inequalities $b_2 \geq 0$ and $b_1^2 \leq 1$ hold. Singular points occur when $\partial C_3 / \partial b_i = 0$ which implies $b_3 = 0$, $b_1 = \pm 1$ and $b_2 = -m^2$, which is only possible for $m = b_2 = 0$. Thus for $m = 0$ the variety $\{C_3 = 0\}$ is not a smooth manifold, but has two singular points at $(\pm 1, 0, 0)$, see Fig. 2.11. For $m \neq 0$ it is a smooth manifold. The inequalities select one connected component.

■

The next step is the analysis of the dynamics of the reduced system. We write the Hamiltonian G of (2.6) in terms of invariants as

$$G(b_1, b_2, b_3) = b_2 + m^2 - \gamma^2 (1 - b_1^2) \tag{2.22}$$

using $l_z = m$ and $\gamma = 2Ea^2$ with $\hbar = 1$. The trajectories of the reduced system are given by the intersection of the reduced “energy surface" $\{G = g\}$ with reduced phase space P_m. This leads to the description of the image of the momentum map (L_z, G), see Fig. 2.9.

Lemma 15. *The set of critical values of the energy-momentum map* (L_z, G) *consists of an isolated point at the origin* $(0, 0)$ *and the parabola* $g = m^2 - \gamma^2$. *The corresponding critical points are* $(\pm 1, 0, 0)$ *and* $(0, 0, 0)$, *respectively. The sepatratrices connecting* $(\pm 1, 0, 0)$ *are the parabolic arcs* $(b_1, b_2, b_3) = \big(b_1, \gamma^2 (1 - b_1^2), \pm\gamma (1 - b_1^2)\big)$.

Proof. In general a tangency between the reduced phase space P_m and the parabolic cylinder $\{G = g\}$ occurs when their gradients are parallel, which implies $b_3 = 0$ and either $b_1 = 0$ or $b_2 = -m^2 - \gamma^2 (1 - b_1^2)$. Since $b_2 \geq 0$ the latter implies $b_1 = \pm 1$ and $m = 0$. These are two isolated critical points at $(\pm 1, 0, 0)$ both with isolated critical value $(m, g) = (0, 0)$. The preimage of this critical value in the reduced system is given by the intersection of

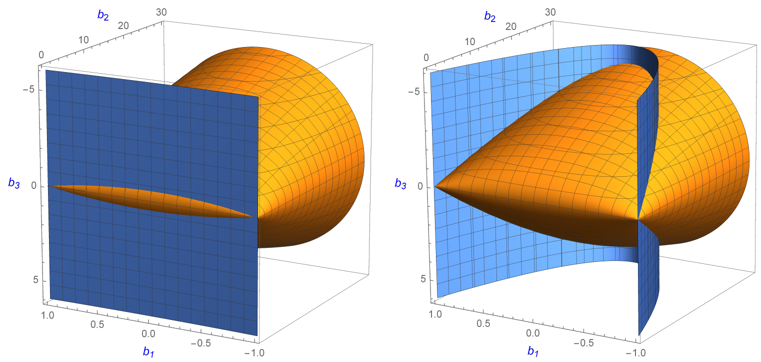

Figure 2.12: Separatrix connecting the singular points. It is given by the intersection of the singular reduced phase space P_0 (yellow) with the energy surface $\{G = 0\}$ (blue) for $\gamma = 0.5$ (left) and $\gamma = 5$ (right).

the singular reduced phase space P_0 with the reduced energy surface $\{G(b_1, b_2, b_3) = 0\}$. Solving $G = 0$ with $m = 0$ gives the equation for b_2. Inserting into $C_3 = 0$ and extracting a square root gives the equation for b_3. See Fig. 2.12

In the other case of parallel gradients with $b_1 = 0$ the Casimir $C_3 = 0$ implies $b_2 = 0$ as well, so that the critical point is $(0, 0, 0)$ with corresponding family of critical values $(m, g) = (m, m^2 - \gamma^2)$. All points in the (m, g) plane above the parabola $g = m^2 - \gamma^2$ with the exception of the origin are regular values. For each regular value the intersection of P_m and $\{G = 0\}$ is a single curve diffeomorphic to S^1. These intersections can also be seen as the level lines of $G(q, p)$ as shown in Fig. 2.10 (right).

■

The final step in the analysis of the classical dynamics is the reconstruction, which leads to a description of the invariant sets of the dynamics in the original coordinates $(\boldsymbol{P}, \boldsymbol{L})$. The reduction map of Lemma 13 is a projection from the 4-dimensional space $T^*S^2 \subset \mathbb{R}^6$ to $\mathbb{R}^3$.

Lemma 16. *For given b_1, b_2, b_3 points in the preimage of the reduction map are given by*

$$\boldsymbol{P} = \sqrt{2E}\left(\sqrt{1 - b_1^2}\cos u, \sqrt{1 - b_1^2}\sin u, b_1\right), \quad \boldsymbol{L} = \left(\sqrt{b_2}\cos v, \sqrt{b_2}\sin v, m\right)$$

where $u - v = \arg(-b_1 m + i b_3)$. The S^1 action increases both u and v by ϕ and leaves the difference $u - v$ invariant.

Proof. In Lemma 13 we already noted that the S^1 action is most easily described by multiplication with $e^{i\phi}$ after introducing the complex variables $p_w = p_x + i p_y$ and $l_w = l_x + i l_y$. By definition b_2 is the modulus squared of l_w and b_1 is the normalised size of p_z, such that $|p_w|^2 = 2E - p_z^2 = 2E(1 - b_1^2)$. Thus there are angles u and v such $e^{i\phi} p_w = \sqrt{2E(1 - b_1^2)} e^{iu}$

and $e^{i\phi}l_w = \sqrt{b_2}e^{iv}$. For given b_1, b_2, b_3 the arguments u and v are related. On the one hand from Lemma 13 we have $\Re(p_w\bar{l}_w) = -p_z l_z$ and $\Im(p_w\bar{l}_w) = \sqrt{2E}b_3$, such that $p_w\bar{l}_w = \sqrt{2E}(b_1 m + b_3)$. On the other hand $p_w\bar{l}_w = \sqrt{2E}\sqrt{1-b_1^2}\sqrt{b_2}e^{i(u-v)}$, and hence the result. At the singular point $(\pm 1, 0, 0)$ the angles u and v are undefined, but this is the fixed point of the S^1 action, so the preimage of each of these points is just a single point each, instead of a circle each.

■

It is interesting to note that these formulas can be directly expressed in terms of the original separating variables. In particular both, p_w and l_w when expressed in terms of $(\xi, \eta, \phi, p_\xi, p_\eta, p_\phi)$ after cotangent lift of the definition (2.3) of spheroidal coordinates can be written as $p_w = e^{i\phi}p_{w0}$ and $l_w = e^{i\phi}l_{w0}$ where p_{w0} and l_{w0} are independent of ϕ. This leads to formulas for b_1, b_2, b_3 in terms of the separating variables. One subtlety here is that in such formulae the value of E is not fixed, but is determined by the values of ξ, η, p_ξ, p_η, while $l_z = p_\phi = m$, as always. The difference in the reconstruction formula is that there ξ and p_ξ have been eliminated.

Symplectic coordinates on the reduced phase space can be introduced by

$$(q, p) = \left(b_1, \frac{b_3}{1-b_1^2} \right) .$$

It is easy to check that these functions satisfy $\{q, p\} = 1$, and that they reduce the Poisson structure $\widehat{\nabla C_3}$ in $\mathbb{R}^3$ to the standard symplectic structure in $\mathbb{R}^2$. Using the Casimir to express b_2 as a function of (q, p) the Hamiltonian G in (2.22) can be turned into the form (2.21). Of course reintroducing symplectic coordinates also reintroduces the coordinate singularity.

However, notice that through the chain of transformations we have arrived again at the separated Hamiltonian function G albeit evaluated in different coordinates. Originally the separation gave a function $G(q, p)$ where either $(q, p) = (\eta, p_\eta)$ or $(q, p) = (\xi, p_\xi)$. The variables (q, p) just introduced as a function of b_i however set $q = p_z/\sqrt{2E}$ and $p = \sqrt{2E}(\boldsymbol{P} \times \boldsymbol{L})_z/(p_x^2 + p_y^2)$.

In order to classify the critical point corresponding to the critical values the dynamics needs to be analysed in full phase space. First we show that the preimage of the isolated critical value $(0, 0)$ of the momentum map (L_z, G) is a doubly pinched torus, and then we will show that it is a non-degenerate focus-focus critical value.

Lemma 17. *The preimage of the critical value $(0, 0)$ of the prolate spheroidal harmonics system is a* *doubly pinched torus with $l_z = 0$ in the phase space T^*S^2 parametrised by p_z and ϕ as*

$$\begin{pmatrix} p_x \\ p_y \\ l_x \\ l_y \end{pmatrix} = \sqrt{2E - p_z^2} \begin{pmatrix} 1 & 0 \\ 0 & 1 \\ 0 & \pm a \\ \mp a & 0 \end{pmatrix} \begin{pmatrix} \cos\phi \\ \sin\phi \end{pmatrix}.$$

Proof. Combining the parabolic arcs from Lemma 15 with the reconstruction formula Lemma 16 for the case $g = m = 0$ gives the result. We have $\Re(p_w \bar{l}_w) = 0$ since $m = 0$ and hence $u - v = \pm\pi/2$ where the plus sign correspond to the upper parabolic arc with $b_3 \geq 0$ and the minus sign to the lower arc with $b_3 \leq 0$.

∎

This Lemma gives a parametrisation of the doubly pinched torus in phase space. For the spheroidal harmonics system it is even possible to describe the dynamics on this doubly pinched torus in terms of simple formulas. Consider the local symplectic coordinates $G(q,p)$. When $m = 0$ then $G = 0$ implies either $q = \pm 1$ or $p = \pm\gamma$. We choose the second condition to stay away from the critical point. Hamilton's equations then say that $p = \pm\gamma$ is constant, as can be seen in Fig. 2.10. The remaining ODE for q can be solved to give $q(t) = \tanh(\pm 2t\gamma - c)$, which is the connection from the north-pole to the south-pole of the sphere, or vice versa, depending on the sign of $p = \pm\gamma$. The dynamics of ϕ is trivial, since $\dot{\phi} = -\partial G(q,p)/\partial m = 0$ for $m = 0$.

Lemma 18. *The critical value $(0,0)$ of the momentum map $(L_z, G) : T^*S^2 \to \mathbb{R}^2$ is a non-degenerate focus-focus value. The critical values $(m, m^2 - \gamma^2)$ are non-degenerate values of elliptic-transversal type.*

Proof. At a critical point of the map (L_z, G) the flows (in the original coordinates) generated by G and L_z are parallel:

$$\alpha B\nabla G + \beta B\nabla L_z = \mathbf{0}, \quad \beta \in \mathbb{R}\setminus\{0\}\,. \tag{2.23}$$

The vector fields are given by (2.8) and (2.7), and since the the former is non-vanishing for $E > 0$ we can set $\alpha = 1$.

Critical points of the form $\boldsymbol{P} = (0,0,p_z)$ and $\boldsymbol{L} = (0,0,0)$ with β arbitrary have the critical values $(0,0)$. Critical points of the form $\boldsymbol{P} = (p_x, p_y, 0)$ and $\boldsymbol{L} = (0,0,m)$ with $\beta = m$ have the critical value $(m, m^2 - \gamma^2)$.

The essential object for the classification of critical values and non-degeneracy are the eigenvalues of the Jacobian $\partial_{\boldsymbol{P},\boldsymbol{L}}\,(B\nabla G + \beta B\nabla L_z)$ at these critical points. Two of the six eigenvalues are always zero; corresponding to the two Casimirs of the Poisson structure B.

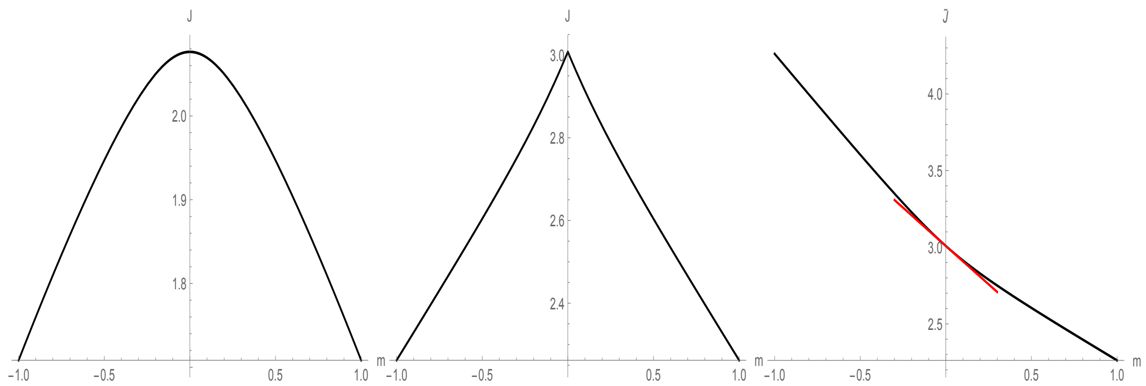

Figure 2.13: Plot of J versus m for a) $g < 0$ and b) $g > 0$. c) Plot of $J + 2\,|m|$ versus m when $g > 0$.

At the north and south poles of the $\boldsymbol{P}$ sphere the eigenvalues are $\lambda = \pm a p_z \pm i\beta$ where $\beta \in \mathbb{R} \backslash \{0\}$ is an arbitrary parameter and $p_z = \pm\sqrt{2E}$. This implies that the poles of the $\boldsymbol{P}$-sphere are non-degenerate focus-focus points, with corresponding non-degenerate focus-focus value $(0, 0)$.

At the equator of the $\boldsymbol{P}$ sphere the eigenvalues are $\lambda = 0, 0, \pm i\sqrt{m^2 + \gamma^2}$. Thus, all points on the equator of the $\boldsymbol{P}$ sphere are elliptic-transversal critical points.

■

Note that for the elliptic-transversal points the vector field of G is $\dot{\boldsymbol{P}} = 2m\,(-p_y, p_x, 0)$ and $\dot{\boldsymbol{L}} = \boldsymbol{0}$. Thus for $m \neq 0$ the set of critical points in the preimage of $(m, m^2 - \gamma^2)$ is a periodic orbit along the equator of the $\boldsymbol{P}$-sphere. For $m = 0$ this periodic orbit degenerates into a circle of fixed points, but from the point of view of the momentum map (L_z, G) they are still non-degenerate.

The classical monodromy of the spheroidal harmonics system can also be understood from the non-trivial action variable J. Recall that L_z is already an action variable. The second action is given by $J = \frac{1}{2\pi}\oint_\beta p\,dq$ where p is obtained from solving (2.5). The β-cycle encloses the interval $[-r_1, r_1]$ where $\pm r_1$ are the two middle roots of $p^2 = 0$ and $|r_1| \leq 1$. In Fig. 2.13 we show J as a function of m for positive (a) and negative (b) values of g. Observe that J is a symmetric but non-smooth function of m for $g > 0$ at $m = 0$. The action J is a smooth function of (m, g) on the image of the momentum map with the slit $m = 0$, $g \geq 0$ removed. However, $m = 0$, $g > 0$ is not a critical value of the momentum map. Thus, there is an alternate definition of action $\tilde{J}$ that is the smooth continuation of J across the slit. This is shown in (c) and defined by $\tilde{J} = J$ for $m \geq 0$ and by $\tilde{J} = J + 2|m|$ for $m < 0$. The alternate action $\tilde{J}$ defines a smooth action function on the image of the momentum map with the slit $m = 0$, $g < 0$ removed. The action $\tilde{J}$ is a function of the values (m, g). Considering $m = L_z$ and $g = G$ as functions on phase space the action $\tilde{J}$ becomes a function on phase space, and

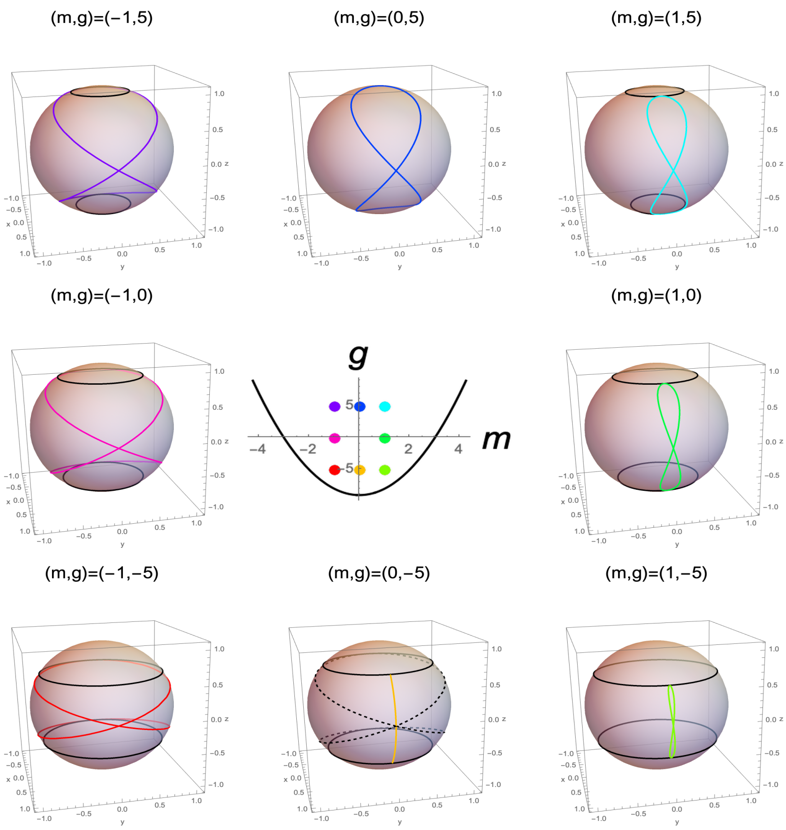

Figure 2.14: Evolution of an angle-variable on the projected torus when a loop around the focus-focus point is completed. The initial loop (orange) and the final loop (dashed) differ by 2 rotations (monodromy index 2).

hence has a Hamiltonian vector field $X_{\tilde{J}}$. From the chain rule we obtain

$$X_{\tilde{J}} = \frac{\partial \tilde{J}}{\partial g} X_G + \frac{\partial \tilde{J}}{\partial m} X_{L_z}\,.$$

Note that $\frac{\partial \tilde{J}}{\partial g}$ is the reduced period and $\frac{\partial \tilde{J}}{\partial m}$ is the rotation number. They constitute part of the so-called period lattice, see, e.g., [Dui80]. By definition the flow of an action is 2π-periodic, so that integrating $X_{\tilde{J}}$ gives a closed curve. The two vector fields $X_{\tilde{J}}$ and X_{L_z} can be used to generate the coordinate lines of the angle coordinates on a torus. This grid of coordinate lines has been computed in [CIAD14] in order to better understand classical monodromy, and we have done the same here for the spheroidal harmonics system. Instead of showing a whole grid we simply show a single curve, see Fig. 2.14. The reason for that is that in our case all other curves of the grid are obtained by rotation about the z-axis. The angle coordinate lines corresponding to the global action L_z are simply lines of constant latitude, and we only show the two extremal such curves which mark the caustic of the torus. We begin the loop at $m = 0$ and $g < 0$ (orange). Moving in a counter-clockwise direction around the focus-focus point we see the caustics shrink to the poles when $m = 0$, $g > 0$ (blue loop). Moving into the region where $m < 0$ we see the loop flip to the other side of the sphere. Finally, as we arrive back at the initial point on the bifurcation diagram, we see that the original loop has two cycles in the ϕ direction added, and so the monodromy index is 2.

The spheroidal harmonics system has a discrete symmetry that can be reduced such that the doubly pinched torus becomes a reduced singly pinched torus. In particular the two focus-focus critical points are identified with each other. When reducing by the full symmetry group the quotient is not a smooth manifold. Consequently, we quotient by symmetry S_2 that flips $\boldsymbol{P}$ to $-\boldsymbol{P}$ only.

Lemma 19. *After discrete symmetry reduction by S_2, the reduced phase space is $T^*\left(\mathbb{RP}^2\right)$.*

Proof. The reduced $\boldsymbol{P}$-space is $\mathbb{RP}^2$ because discrete symmetry S_2 identifies antipodal points of the sphere S^2. A possible fundamental region is the northern hemisphere with $p_z \geq 0$. Since S_2 does not act on $\boldsymbol{L}$, the reduced phase space is therefore $T^*\left(\mathbb{RP}^2\right)$. There is only one focus-focus point in the reduced phase space since S_2 maps the north-pole and the south-pole of the sphere S^2 into each other.

■

Note that the S_2 reduced system (L_z, G) on $T^*\left(\mathbb{RP}^2\right)$ has an S^1 action that is not effective. The reason is that the equator is halved by the symmetry reduction, so that the action is not free for all values (m, g) on the parabola in Fig. 2.9. Hence the symmetry reduced system is not even generalised semi-toric in the sense of [PR+17].

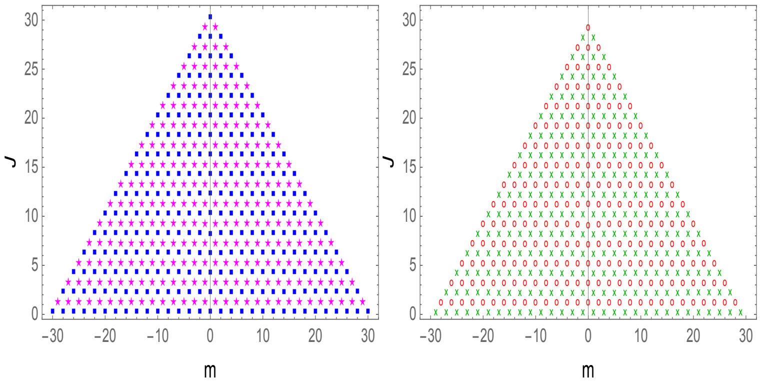

Figure 2.15: Action lattice $(m, J(m, g_l^m))$ for points in the joint spectrum that are a) invariant under S_2 b) flip sign under S_2.

The even/odd spectra in Fig. 2.6 correspond to the same classical integrable system (L_z, G) on $T^*(\mathbb{RP}^2)$ obtained in the previous Lemma. Quantum mechanically the two spectra correspond to different systems since they have different boundary conditions. Thus the semi-classical quantisation of these system will quantise the same action variables, but with different Maslov indices. This is illustrated in Fig. 2.15 which shows the action lattice $(m, J(m, g_l^m))$ for states invariant under S_2 (left) or odd under S_2 (right). Shifting all points in the right figure up by 1 unit will make them coincide (in the semi-classical approximation) with the points in the left figure, except for the line of ground states.

An interesting observation that can be made from Fig. 2.10 (left) for $m = 0$ is that because $p = const$ on the critical level the action of the critical level is simply equal to the area of the rectangle with side lentghs 2γ and 2 divided by 2π, so that $I_\eta(0,0) = 2\gamma/\pi$. By Weyl's law this tells us that in the semiclassical limit (i.e. for large γ) the number of negative eigenvalues g_l^0 is to leading order $2\gamma/\pi$, which for $\gamma = 16$ gives approximately 10, which can be observed in Fig. 2.3.

Chapter 3

Classical Integrable Systems Arising from Separation of Variables on S^3

Abstract

We show that the space of orthogonally separable coordinates on the sphere S^3 induces a natural family of integrable systems, which after symplectic reduction leads to a family of integrable systems on $S^2 \times S^2$. The generic member of the family corresponds to ellipsoidal coordinates. We use the theory of compatible Poisson structures to study the critical points and critical values of the momentum map. Interesting structure arises because the ellipsoidal coordinate system can degenerate in a variety of ways, and all possible orthogonally separable coordinate systems on S^3 (including degenerations) have the topology of the Stasheff polytope K^4, which is a pentagon. We describe how the generic integrable system degenerates, and how the appearance of global $SO(2)$ and $SO(3)$ symmetries is the main feature that organises the various degenerate systems. For the whole family we show that there is an action map whose image is an equilateral triangle. When higher symmetry is present, this triangle "unfolds" into a semi-toric polygon (when there is one global S^1-action) or a Delzant polygon (when there are two global S^1-actions). We believe that this family of integrable systems is a natural playground for theories of global symplectic classification of integrable systems.

3.1. Introduction

Classifying and cataloguing integrable systems is an important unsolved problem. Only for particular classes of systems does a classification exist. It was shown by Atiyah-Guillemin-Sternberg [Ati82, GS82] that the image of the momentum map of a toric system is a convex polytope, called the momentum polytope. This polytope completely classifies the toric system up to an equivariant symplectomorphism. Delzant [Del88] gave an explicit construction of toric manifolds based on their momentum polytopes. Topological classification of Liouville foliations has been extensively studied by Bolsinov and Fomenko [BF04] and extended towards the orbital classification of integrable systems. Vũ Ngọc and Pelayo have extended the toric classification to semi-toric systems [Ngọ07, PN09]. While a complete theory of classification is still far out of reach, we'd like to investigate the possibility of extending the current theory to broader classes of integrable systems.

A very well studied class of integrable systems are superintegrable systems, see, e.g., [Fas05]. A classification of superintegrable systems in two and three degrees of freedom has been achieved by Kalnins, Kress and Miller in a series of works [KKM05a, KKM05b, KKM05c, KKM06a, KKM06b]. In their book [KKM18] they highlight the link between superintegrability and separation of variables. Superintegrable systems that are separable in multiple coordinate systems provide a rich source of integrable systems. This is because each distinct separable coordinate system gives rise to a Stäckel integrable system [Ben89]. Separable coordinates on conformally flat spaces has been extensively studied by Kalnins and Miller in [KM86, KWMW76, MPW81]. More recently, Schöbel studied the space of separable coordinates on the n-sphere as an algebraic variety [Sch14, SV15, Sch16]. While it is known [KKM18] that all separable coordinates on the sphere can be obtained as appropriate limits of the general Jacobi ellipsoidal coordinates, Schöbel's work formalises this by giving a topology to this space in the form of the Stasheff polytope. The inspiration for this paper was to establish a similar topology in the space of integrable systems that arise from separating the geodesic flow on S^3 in this family of coordinates. It is likely that similar constructions can be done for any superintegrable and multi-separable systems. In fact, the idea to use multi-separability to define interesting fibrations has been used in [DH12, DW18] for the most fundamental systems of classical mechanics, the harmonic oscillator and the Kepler problem. To then use the periodic flow of the superintegrable system for reduction was first done in [DDN22] and this paper is the natural continuation of that work where instead of a superintegrable system on $\mathbb{R}^3$ a superintegrable system on S^3 is the starting point.

Another motivation for our work are the recent studies [ADH19, AH19, FP18, HP17] of various integrable systems on the compact symplectic manifold $S^2 \times S^2$. We will show that the symplectic reduction of the geodesic flow on S^3 results in a reduced system on a compact symplectic leaf of $\mathfrak{so}^*(4)$ that is diffeomorphic to $S^2 \times S^2$. The 3-degrees of freedom integrable systems on T^*S^3 obtained from separation of variables descend to 2-degrees of freedom systems on $S^2 \times S^2$ through this quotient. We will employ more recent techniques in the theory of compatible Poisson structures and bi-Hamiltonian systems [BB02, BO09] to study these systems in detail. This will allow us to realise these systems as special restricted cases of the Manakov top [KK91, SZ07b].

A somewhat related question is the study of separable systems depending on parameters, foremost the geodesic flow on an ellipsoid [Mos81]. In [DDB07, DD07] the geodesic flow on 3-dimensional ellipsoids with various sets of equal semi-major axes has been studied. It is astonishing how similar these systems – degenerate or not – are to the ones studied in this paper. However, the fundamental difference is that there a constant energy slice of a 3-degree of freedom system is studied, while here we reduce and study the resulting 2-degree of freedom system. As a result, here we obtain a system on a compact symplectic manifold, which is better suited as a playground for symplectic classification. Similar degenerations have also been studied for the Neumann system [DH12] and again there are many similarities.

The paper is structured as follows. Section 3.2 introduces the basic theory of separation of variables. We focus on the separation of variables in the ellipsoidal coordinate system in Section 3.3. Section 3.4 discusses the symplectic reduction of the geodesic flow on S^3 with emphasis on establishing the reduced ellipsoidal integrable system on $S^2 \times S^2$. The theory of compatible Poisson structures is applied to study the reduced ellipsoidal integrable system in Section 3.5. In Section 3.6, we combine the techniques and results of Sections 3.3, 3.4, and 3.5 to study the integrable systems obtained from separation of variables in the degenerate coordinate systems, namely prolate, oblate, Lamé, spherical and cylindrical coordinates.

3.2. Orthogonally Separable Coordinate Systems on S^3

In this section, we introduce some basic concepts from the theory of separation of variables. For more details, see [KKM18, Ben89]. Let (s_i, p_i) be local canonical coordinates on T^*M where M is an $n-$dimensional differentiable manifold with metric g. Define $\mathcal{S}^k(M)$ to be the space of smooth contravariant symmetric tensors of order k on M, in particular $k = 1$ is the space of vector fields on the manifold. Each $\boldsymbol{K} \in \mathcal{S}^k(M)$ can be associated with a C^∞ real function $E_{\boldsymbol{K}}$ on T^*M locally expressed in the momenta as

$$E_{\boldsymbol{K}} = \sum_i \frac{1}{k!} \boldsymbol{K}^{i_1 \dots i_k} p_{i_1} \dots p_{i_k}. \tag{3.1}$$

The Lie bracket between two tensors $\boldsymbol{K} \in \mathcal{S}^k(M)$ and $\boldsymbol{R} \in \mathcal{S}^r(M)$, denoted by $[\boldsymbol{K}, \boldsymbol{R}] \in \mathcal{S}^{k+r-1}(M)$, is defined by

$$E_{[\boldsymbol{K},\boldsymbol{L}]} = \{E_{\boldsymbol{K}}, E_{\boldsymbol{L}}\}_{(s_i,p_i)} \tag{3.2}$$

where $\{\cdot,\cdot\}_{(s_i,p_i)}$ denotes the canonical Poisson bracket in the curvilinear coordinates.

Definition 1. *On a Riemannian manifold (M, g), a symmetric tensor $\boldsymbol{K}$ is a Killing tensor if it commutes with the metric $[\boldsymbol{K}, g] = 0$.*

There is a natural identification of Killing tensors with first integrals of the geodesic flow: A function $E_{\boldsymbol{K}}$ is a first integral of the geodesic flow if and only if $\boldsymbol{K}$ is a Killing tensor, see, e.g [Ben89]. Similarly to how a set of n integrals in involution on a manifold form a Liouville-integrable system, a collection of n Killing tensors defines a Stäckel system.

Definition 2. *A Stäckel system on an $n-$dimensional Riemannian manifold (M, g) is a set of n*

Killing tensors $\boldsymbol{K}_i$ of order 2 that commute under the commutator in (3.2) and are simultaneously diagonalisable with g.

Eisenhart proved in [Eis34] that there is a bijective correspondence between equivalence classes of Stäckel systems and equivalence classes of orthogonal separable coordinate systems. Given an orthogonal coordinate system s_i on an n-dimensional manifold M, we can define a Stäckel system by constructing a Stäckel matrix.

Definition 3. *A Stäckel matrix Φ for a given metric g is any $n \times n$ matrix where each row depends on only one of the curvilinear coordinates s_i, and*

$$\frac{1}{g_{ii}} = \frac{\det(\Omega_i)}{\det(\Phi)}, \tag{3.3}$$

where Ω_i is the minor formed by deleting the i^{th} row and first column of Φ and g_{ii} is the (i, i) element of the metric tensor.

The functional value of the Hamiltonian H will be denoted by h. Let $W := W(\boldsymbol{s}, \boldsymbol{\eta})$ where $\boldsymbol{s} = (s_1, \ldots, s_n)$ are the separable curvilinear coordinates and $\boldsymbol{\eta} = (\eta_0, \ldots, \eta_{n-1})$ are parameters. The Hamilton Jacobi equation is given by

$$\sum_i \frac{1}{2}(g^{-1})_{ii} \left(\frac{\partial W}{\partial s_i}\right)^2 = h. \tag{3.4}$$

This can be separated by computing

$$\Phi^{-1}\mathfrak{p} = \boldsymbol{\eta}, \tag{3.5}$$

where $\mathfrak{p} = \left(p_1^2, \ldots, p_n^2\right)^t$ is the vector of squared canonical curvilinear momenta and the parameters $\boldsymbol{\eta}$ are the separation constants. Comparing (3.5) and (3.1), we see that rows of Φ^{-1} encode the diagonal entries of the Killing tensors for separable orthogonal coordinates s_i. The first row of (3.5) gives (3.4) and so we have $\eta_0 = h$.

The work of Kalnins and Miller [KM86] gave a graphical algorithm for constructing all orthogonally separable coordinates on constant curvature manifolds. Recent results by Schöbel and Veselov extended this by giving an algebraic geometric classification of separable coordinate systems on S^n [SV15, Sch14]. In particular, they showed that the variety of Stäckel systems on S^n is given by the Stasheff polytope K_{n+1} which is a convex polytope of dimension $n-1$. In this paper we work only with S^3; the relevant Stasheff polytope K_4 is shown in Figure 3.1.

The codimension 0 face of a Stasheff polytope represents the family of ellipsoidal coordinates s_i. These are defined as the roots of $T(s) = \sum_{i=1}^{n+1} \frac{x_i^2}{s-e_i} = 0$ where x_i are Cartesian coordinates on $\mathbb{R}^{n+1}$, $e_j \leq s_j \leq e_{j+1}$ for all $j = 1, \dots, n$, the $e_i \geq 0$ are all distinct and are called the semi-major axes. Note that when using a similar coordinate system to separate the geodesic flow on an ellipsoid these parameters actually are semi-major axes (hence the name), while here they describe a separating coordinate system but *not* the underlying manifold. Solving $T(s_j) = 0$ together with $\sum_{i=1}^{n+1} x_i^2 = 1$ gives

$$x_i^2 = \frac{\prod_{j=1}^{n}(s_j - e_i)}{\prod_{k \neq i}(e_k - e_i)}. \tag{3.6}$$

Note that for S^3, despite the ellipsoidal coordinates being parametrised by the 4 parameters $e_1 < e_2 < e_3 < e_4$, the Stasheff polytope is only 2-dimensional. Affine transformation of the parameters of the form $e_i \mapsto \alpha e_i + \beta$ for $\alpha \neq 0$ gives a equivalent coordinate system up to scaling. Thus each ellipsoidal coordinate system on S^3 with parameters $e_1 < e_2 < e_3 < e_4$ can be transformed to an equivalent system with parameters $0 < 1 < a < b$, see [KKM18] for details.

Higher codimension faces represent families of degenerate coordinate systems on the sphere. Degenerate coordinate systems on S^n are constructed by gluing ellipsoidal coordinates on lower dimensional spheres together. Let $\boldsymbol{w}_\alpha$ and $\boldsymbol{z}$ be Cartesian coordinates expressed in terms of local ellipsoidal coordinates on $S^{k_\alpha - 1}$ and S^m respectively where $\alpha = 1, \dots, m+1$ and $n = k_1 + \dots k_{m+1} - 1$. Then any degenerate coordinate system on S^n is found by recursively applying composition [SV15]

$$\begin{aligned}\circ : S^m \times S^{k_1 - 1} \times \cdots \times S^{k_{m+1}-1} &\to S^{k_1 + \cdots + k_{m+1} - 1}\\ (\boldsymbol{z}, \boldsymbol{w}_1, \dots, \boldsymbol{w}_{m+1}) &\to (z_1 \boldsymbol{w}_1, \dots, z_{m+1}\boldsymbol{w}_{m+1})\end{aligned}$$

where $z_\beta \boldsymbol{w}_\beta$ are Cartesian coordinates on $\mathbb{R}^{n+1}$ expressed in the new degenerate coordinate system.

In this paper we have chosen to adopt the notation of Schöbel [Sch14]. The general ellipsoidal coordinates on S^n are represented as $(1\ 2\ \dots\ n{+}1)$. If one attaches an S^j to the m^{th} Cartesian coordinate, then we enclose brackets around all numbers m to $m+j$. For instance, attaching S^1 to the the x_2 coordinate on S^2 is written as $(1\ (2\ 3)\ 4)$. Symmetric bracketing results in systems with similar behaviour, i.e. (1 2 (3 4)) and ((1 2) 3 4) describe equivalent coordinate systems as we will discuss in more detail below, also see [KKM18, Sch16, SV15, Sch14]. For the various degenerate coordinate systems we are going to use shorthand names as indicated in Figure 3.1.

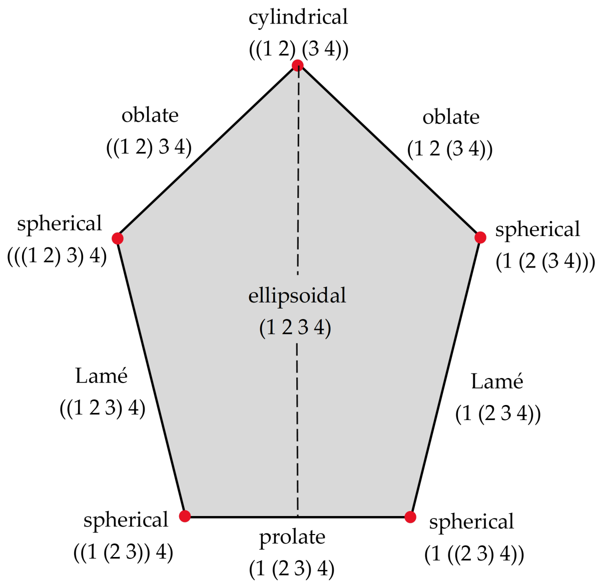

Figure 3.1: Stasheff polytope K^4 of separating coordinate systems on S^3 with corresponding names and bracket notation.

3.3. Separation of variables of the Geodesic Flow on S^3 and Ellipsoidal Coordinates

Consider the geodesic flow on the $3-$sphere as a constrained system on $T^*\mathbb{R}^4$ with Cartesian coordinates $(\boldsymbol{x},\boldsymbol{y})$ where $\boldsymbol{x}\cdot\boldsymbol{x}=1$ and $\boldsymbol{x}\cdot\boldsymbol{y}=0$. We define the Poisson bracket on T^*S^3 to be the Dirac bracket $\{\cdot,\cdot\}$ enforcing these two constraints. Let $\{\cdot,\cdot\}_{T^*\mathbb{R}^4}$ be the canonical Poisson bracket on $T^*\mathbb{R}^4$. Set $c_1=\boldsymbol{x}\cdot\boldsymbol{x}$, $c_2=\boldsymbol{x}\cdot\boldsymbol{y}$ and define the matrix

$$C_{ij}=\{c_i,c_j\}_{T^*\mathbb{R}^4}.$$

The Dirac bracket on T^*S^3 is given by

$$\{f,g\}=\{f,g\}_{T^*\mathbb{R}^4}+\{f,c_i\}_{T^*\mathbb{R}^4}(C^{-1})_{ij}\{c_j,g\}_{T^*\mathbb{R}^4}$$

with structure matrix

$$B_{(\boldsymbol{x},\boldsymbol{y})}=\begin{pmatrix}\boldsymbol{0} & id-\boldsymbol{x}\boldsymbol{x}^t\,|\boldsymbol{x}|^{-2}\\ -id+\boldsymbol{x}\boldsymbol{x}^t\,|\boldsymbol{x}|^{-2} & -(\boldsymbol{x}\boldsymbol{y}^t-\boldsymbol{y}\boldsymbol{x}^t)\,|\boldsymbol{x}|^{-2}\end{pmatrix}. \tag{3.7}$$

From (3.7), the Poisson bracket between two functions f and g on T^*S^3 is

$$\{f,g\}:=(\nabla f)^T\,B_{(\boldsymbol{x},\boldsymbol{y})}\nabla g \tag{3.8}$$

where ∇ denotes the gradient with respect to the Cartesian coordinates $(\boldsymbol{x},\boldsymbol{y})$.

Let $H = \frac{1}{2}\boldsymbol{y} \cdot \boldsymbol{y}$ be the Hamiltonian of the geodesic flow on S^3. It is well known that this system is superintegrable and separates in multiple coordinate systems [Sch14]. The Hamilton Jacobi equation can be separated in general ellipsoidal coordinates (s_1, s_2, s_3) given by (3.6) for $n = 3$ as

$$x_j^2 = \frac{(s_1 - e_j)(s_2 - e_j)(s_3 - e_j)}{\Pi_{i \neq j}(e_i - e_j)}, \quad j = 1, \dots, 4 \tag{3.9}$$

where $0 \le e_1 \le s_1 \le e_2 \le s_2 \le e_3 \le s_3 \le e_4$ and the e_i's are all distinct. In these coordinates, the geodesic Hamiltonian is (see e.g. [DDB07, KKM18])

$$H = -2 \sum_{i=1}^{3} \frac{\prod_{j=1}^{4}(s_i - e_j)}{\prod_{k \neq i}(s_i - s_k)} p_i^2. \tag{3.10}$$

This system is Liouville integrable. To separate the Hamilton Jacobi equation we use the following Stäckel matrix

$$\Phi_{el} = \frac{1}{4} \begin{pmatrix} -\frac{s_1^2}{A(s_1)} & -\frac{s_1}{A(s_1)} & -\frac{1}{A(s_1)} \\ -\frac{s_2^2}{A(s_2)} & -\frac{s_2}{A(s_2)} & -\frac{1}{A(s_2)} \\ -\frac{s_2^2}{A(s_3)} & -\frac{s_1}{A(s_3)} & -\frac{1}{A(s_3)} \end{pmatrix}. \tag{3.11}$$

where $A(z) = \prod_{k=1}^{4}(z - e_k)$. From (3.5), we compute $\Phi_{el}^{-1}\mathfrak{p} = (\eta_0, -\eta_1, \eta_2)^T$ where

$$\eta_0 = -4 \sum_{i=1}^{3} \frac{A(s_i)}{D(s_i)} p_i^2, \qquad \eta_1 = -4 \sum_{i=1}^{3} \left(\frac{A(s_i)}{D(s_i)} p_i^2 \sum_{k \neq i} s_k \right), \qquad \eta_2 = -4 \sum_{i=1}^{3} \left(\frac{A(s_i)}{D(s_i)} p_i^2 \prod_{k \neq i} s_k \right), \tag{3.12}$$

and $D(s_i) = \prod_{k \neq i}(s_i - s_k)$. To express (3.12) in terms of the angular momenta $\ell_{ij} \coloneqq x_i y_j - x_j y_i$, we note that

$$\ell_{ij}^2 = \frac{x_i^2 x_j^2}{4} \left(\sum_{k=1}^{3} \left(-\frac{1}{s_k - e_i} + \frac{1}{s_k - e_j} \right) p_k \right)^2$$

with x_i given by (3.9). Let $\boldsymbol{L} \coloneqq (\ell_{12}, \ell_{13}, \ell_{14}, \ell_{23}, \ell_{24}, \ell_{34})$, it can be verified that

$$\eta_0(\boldsymbol{L}) = \sum_{i<j} \ell_{ij}^2 = 2H, \qquad \eta_1(\boldsymbol{L}) = \sum_{i<j} \left(\ell_{ij}^2 \sum_{k \neq i,j} e_k \right), \qquad \eta_2(\boldsymbol{L}) = \sum_{i<j} \left(\ell_{ij}^2 \prod_{k \neq i,j} e_k \right). \tag{3.13}$$

The separated equations are obtained by multiplying both sides of (3.5) by Φ_{el}. This gives

$$p_i^2 = \frac{-R(s_i)}{4A(s_i)} \tag{3.14}$$

where $R(z) = 2hz^2 - \eta_1^* z + \eta_2^*$ and (η_1^*, η_2^*) are the values of the integrals (η_1, η_2). Thus, the geodesic flow is separable on the hyperelliptic curve $w^2 = -R(z)A(z)$ which has genus

3.

It is known [Mos81] that a set of global polynomial integrals for the geodesic flow are given by

$$F_i = \sum_{j=1, j\neq i}^{4} \frac{\ell_{ij}^2}{e_i - e_j}, \tag{3.15}$$

where $i \in \{1, 2, 3, 4\}$. The F_i are known as the Uhlenbeck integrals and satisfy $\sum_{i=1}^{4} F_i = 0$. The separation constants η_1 and η_2 are related to the F_i via the identity

$$\sum_{i=1}^{4} \frac{F_i}{z - e_i} = \frac{2Hz^2 - \eta_1 z + \eta_2}{\prod_{k=1}^{4}(z - e_k)}. \tag{3.16}$$

Since all integrals are polynomial, we can easily show that η_1, η_2 and H are functionally independent almost everywhere and $\{\eta_1, H\} = \{\eta_2, H\} = \{\eta_1, \eta_2\} = 0$. This establishes that the triple (H, η_1, η_2) is an integrable system on T^*S^3. We call this the ellipsoidal integrable system on T^*S^3. This is a reformulation of the underlying Stäckel system, whose commuting Killing tensors lead to quadratic (in momenta) integrals, which are also quadratic in angular momenta.

Since H is a global S^1 action on the energy surface where $2h = 1$ we can use it to perform symplectic reduction. Doing so, we obtain a reduced system on the symplectic manifold $S^2 \times S^2$. The integrals (η_1, η_2) descend to form an integrable system on this quotient space.

3.4. Reduction by Geodesic Flow

The orbits of H are oriented great circles on S^3. Since each great circle is the intersection of a two dimensional plane through the origin with S^3, the orbit space of H is given by

$$T^*S^3/S^1|_{H=h} = U^*S^3/S^1 \cong \widetilde{Gr}(2,4)$$

where the oriented Grassmanian $\widetilde{Gr}(2,4)$ is the set of oriented two dimensional planes in $\mathbb{R}^4$ and U^*S^3 is the unit cotangent bundle of S^3. One way to see that $\widetilde{Gr}(2,4) \cong S^2 \times S^2$ is using the Plücker embedding (for more details on this, see Appendix A.1). For our purposes, the reduction will be performed with invariants of the geodesic Hamiltonian.

Invariants of H are the six angular momenta $\boldsymbol{L} := (\ell_{12}, \ell_{13}, \ell_{14}, \ell_{23}, \ell_{24}, \ell_{34})$. These form a closed set of invariants under the Dirac bracket $\{\cdot, \cdot\}$ from (3.8). The Poisson algebra of these invariants has the structure matrix

$$B_{\boldsymbol{L}} = \begin{pmatrix} 0 & \ell_{23} & \ell_{24} & -\ell_{13} & -\ell_{14} & 0 \\ -\ell_{23} & 0 & \ell_{34} & \ell_{12} & 0 & -\ell_{14} \\ -\ell_{24} & -\ell_{34} & 0 & 0 & \ell_{12} & \ell_{13} \\ \ell_{13} & -\ell_{12} & 0 & 0 & \ell_{34} & -\ell_{24} \\ \ell_{14} & 0 & -\ell_{12} & -\ell_{34} & 0 & \ell_{23} \\ 0 & \ell_{14} & -\ell_{13} & \ell_{24} & -\ell_{23} & 0 \end{pmatrix} \tag{3.17}$$

with 2 Casimirs: $\mathcal{C}_1 = 2H = \sum_{j>i} \ell_{ij}^2$ and $\mathcal{C}_2 = \ell_{12}\ell_{34} - \ell_{13}\ell_{24} + \ell_{14}\ell_{23}$. The first is the energy of the geodesic flow which we have the freedom to set to an arbitrary value $2h$. The second Casimir is the Plücker relation and must be zero since the angular momenta $\boldsymbol{L} = \boldsymbol{x} \wedge \boldsymbol{y}$ where $\wedge$ is the wedge operator. This means that $\boldsymbol{L}$ is a totally decomposable bivector and so must satisfy $C_2 = |\boldsymbol{L} \wedge \boldsymbol{L}| = 0$. The Lie Poisson algebra of the ℓ_{ij}'s is isomorphic to the Lie algebra $\mathfrak{so}(4)$.

Using the ℓ_{ij} as new coordinates, we obtain an explicit realisation of $S^2 \times S^2$ as

$$\begin{aligned} \mathscr{C}_1 &= \mathcal{C}_1 + 2\mathcal{C}_2 = (\ell_{12} + \ell_{34})^2 + (\ell_{13} - \ell_{24})^2 + (\ell_{14} + \ell_{23})^2 = 2h, \\ \mathscr{C}_2 &= \mathcal{C}_1 - 2\mathcal{C}_2 = (\ell_{12} - \ell_{34})^2 + (\ell_{13} + \ell_{24})^2 + (\ell_{14} - \ell_{23})^2 = 2h. \end{aligned} \tag{3.18}$$

The Poisson bracket of functions on $S^2 \times S^2$, denoted by $\{\cdot, \cdot\}_{\boldsymbol{L}}$ is

$$\{f, g\}_{\boldsymbol{L}} = (\nabla f)^T B_{\boldsymbol{L}} \nabla g \tag{3.19}$$

where ∇ denotes the gradient with respect to $\boldsymbol{L}$.

A sometimes more convenient set of coordinates on $S^2 \times S^2$ is obtained by applying the linear transformation $T : \boldsymbol{L} \mapsto (\boldsymbol{X}, \boldsymbol{Y}) = (X_1, X_2, X_3, Y_1, Y_2, Y_3)$ with

$$\begin{aligned} X_1 &= \frac{1}{2}(\ell_{12} + \ell_{34}), & Y_1 &= \frac{1}{2}(\ell_{12} - \ell_{34}), \\ X_2 &= \frac{1}{2}(\ell_{13} - \ell_{24}), & Y_2 &= -\frac{1}{2}(\ell_{13} + \ell_{24}), \\ X_3 &= \frac{1}{2}(\ell_{14} + \ell_{23}), & Y_3 &= \frac{1}{2}(\ell_{14} - \ell_{23}). \end{aligned} \tag{3.20}$$

In these variables we can rewrite (3.18) as $\mathscr{C}_1 = 4\,|\boldsymbol{X}|^2$ and $\mathscr{C}_2 = 4\,|\boldsymbol{Y}|^2$ which both have functional value $2h$. The Poisson structure (3.7) becomes block diagonal

$$B_{\boldsymbol{X},\boldsymbol{Y}} = \begin{pmatrix} \hat{\boldsymbol{X}} & \boldsymbol{0} \\ \boldsymbol{0} & \hat{\boldsymbol{Y}} \end{pmatrix} \tag{3.21}$$

and is isomorphic to $\mathfrak{so}(3) \times \mathfrak{so}(3)$. The notation in (3.21) is such that for a vector $\boldsymbol{v} \in \mathbb{R}^3$ the corresponding antisymmetric hat matrix $\hat{\boldsymbol{v}}$ is defined by

$$\hat{\boldsymbol{v}}\boldsymbol{u} = \boldsymbol{v} \times \boldsymbol{u} \quad \forall \boldsymbol{u} \in \mathbb{R}^3.$$

This reduction gives an integrable system on the reduced manifold $S^2 \times S^2$. While the integrals (η_1, η_2) can be easily rewritten in terms of the $(\boldsymbol{X}, \boldsymbol{Y})$ variables using (3.20), they are simplest and most symmetric as functions of the ℓ_{ij}'s as in (3.13).

Under (3.19), (η_1, η_2) are commuting quadratic functions on $S^2 \times S^2$ and so we arrive at the following result.

Theorem 20. *The integrable sytem (H, η_1, η_2) on T^*S^3 descends to an integrable system $(\eta_1(\boldsymbol{L}), \eta_2(\boldsymbol{L}), \{\cdot,\cdot\}_{\boldsymbol{L}})$ on $S^2 \times S^2$ with two degrees of freedom and integrals quadratic in ℓ_{ij}.*

We call this integrable system the reduced ellipsoidal integrable system. The symplectic reduction performed in this section also applies to integrable systems obtained from separating the geodesic flow in the degenerate coordinate systems shown in Figure 3.1.

Separating coordinate systems on S^3 are invariant under affine transformations $e_i \mapsto \alpha e_i + \beta$ for $\alpha \neq 0$. This allows us to normalise the ordered distinct parameters (e_1, e_2, e_3, e_4) to $(0, 1, a, b)$ by a shift by $\beta = -e_1$ and a scaling by $\alpha = e_2 - e_1$. Thus the inside of Figure 3.1 can be thought of as the region $1 < a < b$. The affine transformations when applied to the family of corresponding integrable systems on T^*S^3 gives topologically equivalent integrable systems. This property can be observed directly in the reduced systems on $S^2 \times S^2$.

Lemma 21. *Affine transformation of the parameters $e_i \mapsto \alpha e_i + \beta$ for $\alpha \neq 0$ when applied to the reduced system $(\eta_1(\boldsymbol{L}), \eta_2(\boldsymbol{L}))$ gives a topologically equivalent integrable system.*

Proof. Applying $e_i \mapsto \alpha e_i + \beta$ to $(\eta_1(\boldsymbol{L}), \eta_2(\boldsymbol{L}))$ induces the map

$$(\eta_1, \eta_2) \mapsto (\alpha\eta_1 + 4\beta h, \alpha^2\eta_2 + \alpha\beta\eta_1 + 2\beta^2 h)$$

which gives a topologically equivalent system, because it is a linear map of the original integrals, plus affine terms that add the Casimir h.

∎

This result illustrates nicely how the equivalence of separating coordinates leads to an equivalence of reduced integrable systems. It highlights the fact that the reduced system does not have a Hamiltonian (since we reduced by the flow of H) and hence it is natural to consider quadratic integrals up to linear transformations.

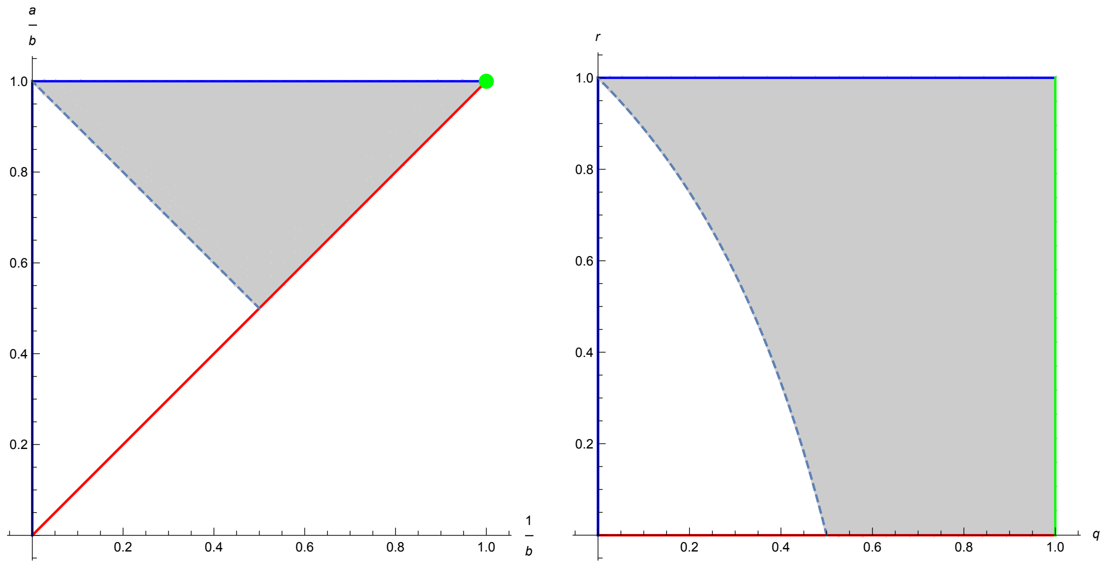

Figure 3.2: a) Parameter space of ellipsoidal coordinates $1 < a < b$ (red: prolate, blue: oblate, dashed: fixed set). b) Blown up parameter space giving half the Stasheff polytope (green: Lamé).

There is another equivalence between separating coordinates which maps an ordered quadruple (e_1, e_2, e_3, e_4) to an ordered quadruple $(-e_4, -e_3, -e_2, -e_1)$. After normalisation this maps $(0, 1, a, b)$ to $(0, 1, a', b')$ where $a' = (b-1)/(b-a)$ and $b' = b/(b-a)$. This map is an involution that can be written as

$$\frac{1}{b'} = 1 - \frac{a}{b}, \quad \frac{a'}{b'} = 1 - \frac{1}{b}\,. \tag{3.22}$$

The line of fixed points of the involution is $1/b+a/b = 1$. This suggests to map the parameter region $1 < a < b$ to the triangle $0 < a/b < 1/b < 1$ which is cut in half by the line of fixed points, see Figure 3.2 a). The prolate case $a = 1$ and the oblate case $a = b$ correspond to two edges of this triangle. To see the whole parameter space the e_i need to be considered projectively. In particular the point $1 = a = b$ representing the Lamé family needs to be blown up.

Lemma 22. *Define $q = 1/b, r = (a-1)/(b-1)$. There is a one-to-one correspondence between equivalence classes of reduced integrable system on $S^2 \times S^2$ and points in the region $0 \le q \le 1$, $0 \le r \le 1$, $q \ge (1-r)/(2-r)$.*

Proof. The map $r = (a-1)/(b-1)$ blows up the point $1 = a = b$ to a line. The parameter r is the inverse of the slope of a straight line in ab-space through the point $a = b = 1$. Due to $1 \le a \le b$ we have $0 \le r \le 1$. Consider the images of the edges of the triangle $0 < a/b < 1/b < 1$. The prolate line segment is mapped to $r = 0$, $1/2 < q < 1$. The oblate line segment is mapped to $r = 1$, $0 < q < 1$. The line of fixed points is mapped to $q = (1-r)/(2-r)$. This establishes the claimed boundaries of the region. The corners of the region are:

- $(q, r) = (0, 1/2)$: symmetric prolate coordinates.
- $(q, r) = (0, 1)$: spherical coordinates.
- $(q, r) = (1, 1)$: spherical coordinates.
- $(q, r) = (0, 1)$: cylindrical coordinates.

■

The region described in the Lemma in (r, q) space is shown in Figure 3.2 b). It represents half of the Stasheff polytope Figure 3.1.

In the next section, we study the reduced ellipsoidal system in depth. We find the momentum map, compute the critical points and critical values. The integrable systems arising from the degenerate coordinate systems will be covered in detail in section 3.6.

3.5. The Reduced Ellipsoidal Integrable System

To construct and study the bifurcation diagram for the ellipsoidal integrable system we will employ techniques from [BB02] and [BO09] using compatible Poisson structures.

3.5.1. Compatible Poisson Structures

In this section, we will be closely following Example B in [BO09]. Let us consider the reduced system on a symplectic leaf of $\mathfrak{so}^*(4)$ defined by $\mathcal{C}_1 = \boldsymbol{L} \cdot \boldsymbol{L} = 2h$ and $\mathcal{C}_2 = \ell_{12}\ell_{34} - \ell_{13}\ell_{24} + \ell_{14}\ell_{23} = 0$. On $\mathfrak{so}(4)$ we have the standard bracket $[X, Y] = XY - YX$ and we can identify elements $X \in \mathfrak{so}(4)$ with elements $X^* \in \mathfrak{so}^*(4)$ via

$$K(X, \cdot) = X^*.$$

Here K is the Killing form defined as

$$K(X, Y) = \mathrm{Tr}(\mathrm{ad}_X \circ \mathrm{ad}_Y) \in \mathbb{R}$$

where $\mathrm{ad}_X = [X, \cdot]$. Explicitly, let us define X_{ij} to be the 4×4 matrix with 1 in the ij^{th} position, -1 in the ji^{th} position and 0 everywhere else. This gives us a basis of $\mathfrak{so}(4)$. An element $X \in \mathfrak{so}(4)$ of the form

$$X = \begin{pmatrix} 0 & \ell_{12} & \ell_{13} & \ell_{14} \\ -\ell_{12} & 0 & \ell_{23} & \ell_{24} \\ -\ell_{13} & -\ell_{23} & 0 & \ell_{34} \\ -\ell_{14} & -\ell_{24} & \ell_{34} & 0 \end{pmatrix}$$

can be written as $X = \sum_{j>i} \ell_{ij} X_{ij}$. This allows for the further identification of $T(\mathfrak{so}^*(4)) \equiv \mathfrak{so}(4)$ with $\nabla_{\boldsymbol{L}} f \leftrightarrow \sum_{i<j} \frac{\partial f}{\partial \ell_{ij}} X_{ij}$. We can now express the integrals η_1 and η_2 as functions on $\mathfrak{so}(4)$ as

$$\eta_1 = \mathrm{Tr}(X^t \nabla_{\boldsymbol{L}} \eta_1) \qquad \eta_2 = \mathrm{Tr}(X^t \nabla_{\boldsymbol{L}} \eta_2)$$

with $\nabla_{\boldsymbol{L}} \eta_1 \coloneqq A_1 = \sum_{i<j} (e_m + e_n) \ell_{ij} X_{ij}$ and $\nabla_{\boldsymbol{L}} \eta_2 \coloneqq A_2 = \sum_{i<j} e_m e_n \ell_{ij} X_{ij}$ where i, j, m, n are all distinct. Dynamics on $\mathfrak{so}^*(4)$ with Hamiltonian η_1 or η_2 can be rewritten in Lax form as $\dot{X} = [A_1, X]$ or $\dot{X} = [A_2, X]$. The trace of X^2 and X^4 recover the Casimirs $-2\mathcal{C}_1$ and $-4\mathcal{C}_2^2 + 2\mathcal{C}_1^2$, respectively.

Let C be a symmetric matrix and define the Lie bracket $[X, Y]_C \coloneqq XCY - YCX$. This lifts to the Poisson bracket $\{\cdot, \cdot\}_C$ on $\mathfrak{so}^*(4)$. We can WOLG assume that C is diagonal of the form $C = \mathrm{diag}(c_1, c_2, c_3, c_4)$. If C is invertible, then there exists an isomorphism α from $\mathfrak{so}(4, \mathbb{C})$ to $\mathfrak{so}(4, [\cdot, \cdot]_C)$ defined by $\alpha : X \mapsto C^{1/2} X C^{1/2}$. This lifts to a linear map

$$\begin{aligned} \gamma_C : \mathfrak{so}^*(4, \mathbb{C}) &\to \mathfrak{so}^*(4, \{\cdot, \cdot\}_C) \\ \boldsymbol{L} &\mapsto M_C \boldsymbol{L} \end{aligned} \tag{3.23}$$

where $M_C = \mathrm{diag}(\sqrt{c_1 c_2}, \sqrt{c_1 c_3}, \sqrt{c_1 c_4}, \sqrt{c_2 c_3}, \sqrt{c_2 c_4}, \sqrt{c_3 c_4})$.

The Poisson matrix for $\mathfrak{so}^*(4, \{\cdot, \cdot\}_C)$ in the basis of $(\ell_{12}, \ell_{13}, \ell_{14}, \ell_{23}, \ell_{24}, \ell_{34})$ is given by

$$B_C = \begin{pmatrix} 0 & -c_1\ell_{23} & -c_1\ell_{24} & c_2\ell_{13} & c_2\ell_{14} & 0 \\ c_1\ell_{23} & 0 & -c_1\ell_{34} & -c_3\ell_{12} & 0 & c_3\ell_{14} \\ c_1\ell_{24} & c_1\ell_{34} & 0 & 0 & -c_4\ell_{12} & -c_4\ell_{13} \\ -c_2\ell_{13} & c_3\ell_{12} & 0 & 0 & -c_2\ell_{34} & c_3\ell_{24} \\ -c_2\ell_{14} & 0 & c_4\ell_{12} & c_2\ell_{34} & 0 & -c_4\ell_{23} \\ 0 & -c_3\ell_{14} & c_4\ell_{13} & -c_3\ell_{24} & c_4\ell_{23} & 0 \end{pmatrix}.$$

In [BO09] it is shown that the Lie bundle $\lambda[\cdot, \cdot] - [\cdot, \cdot]_C = [\cdot, \cdot]_{\lambda I - C}$ where $\lambda \in \mathbb{R} \cup \infty$ is still a Lie bracket on $\mathfrak{so}(4)$. Similarly, $\lambda\{\cdot, \cdot\} - \{\cdot, \cdot\}_C = \{\cdot, \cdot\}_{\lambda I - C}$ is also a Poisson bracket on $\mathfrak{so}^*(4)$ giving us a set of compatible Poisson structures. Following Example B in [BO09], we can now study our system from the perspective of the compatible Poisson structures $\{\cdot, \cdot\}_{\lambda I - C}$ on $\mathfrak{so}^*(4)$. Expanding the Casimirs in terms of the parameter λ gives commuting integrals [BO09].

Proposition 23 ([BO09]). *The integrals (I_0, I_1, I_2) for the Poisson structure $(\mathfrak{so}^*(4), \{\cdot, \cdot\}_{\lambda I - C})$ with $C = diag(c_1, c_2, c_3, c_4)$ where c_i are real distinct constants can be obtained from the coefficients* *of the numerator of the rational function given by*

$$\psi(\lambda) = Tr((X(\lambda I - C)^{-1})^2) = 2\frac{I_0\lambda^2 + I_1\lambda + I_2}{(\lambda - c_1)(\lambda - c_2)(\lambda - c_3)(\lambda - c_4)} \tag{3.24}$$

where $X \in \mathfrak{so}(4)$. They are $I_0 = -\sum_{i,j}\ell_{ij}^2 = -2h,\ I_1 = \sum_{i<j}(c_n+c_m)\ell_{ij}^2,\ I_2 = -\sum_{i<j}c_nc_m\ell_{ij}^2$ where the indices m, n, i, j are all distinct.

Define $E = \operatorname{diag}(e_1, e_2, e_3, e_4)$ and using $C = E$ gives us the integrals $(I_0, I_1, I_2) = (-2h, \eta_1, -\eta_2)$ obtained from separation of variables in (3.13). This allows us to study the ellipsoidal integrable system on the reduced space $\mathfrak{so}^*(4)$ as a system of compatible Poisson structures and (3.24) becomes

$$\psi(\lambda) = 2\frac{-2h\lambda^2 + \eta_1\lambda - \eta_2}{(\lambda - e_1)(\lambda - e_2)(\lambda - e_3)(\lambda - e_4)}. \tag{3.25}$$

This is precisely the equation for the separated momenta in (3.14) with $\psi(s_i) = 4p_i^2$.

3.5.2. Critical Points

To find critical points, consider the lift of the standard endomorphism from $\mathfrak{so}(4, \mathbb{C})$ to $\mathfrak{so}(3) \oplus \mathfrak{so}(3)$ defined by $T : \boldsymbol{L} \mapsto (\boldsymbol{X}, \boldsymbol{Y})$ given in (3.20), where here $\boldsymbol{X}$ and $\boldsymbol{Y}$ are complex vectors. We will be using the map $\gamma_{\lambda I - E}$ in (3.23) to construct the map $T_2 = \gamma_{\lambda I - E}T^{-1}$ from $[\mathfrak{so}(3) \oplus \mathfrak{so}(3)]^*$ to $\mathfrak{so}^*(4, \{\cdot,\cdot\}_C)$. It is known from [BO09] that the set of singular points in $\mathfrak{so}(4, \mathbb{C}) \equiv \mathfrak{so}(3) \oplus \mathfrak{so}(3)$ under the standard bracket is given by $\{(\boldsymbol{X}, 0)\} \cup \{(0, \boldsymbol{Y})\}$. When the matrix $\lambda I - E$ is invertible (that is $\lambda \neq e_i$), the map $\gamma_{\lambda I - E}$ is an Poisson isomorphism between $\mathfrak{so}^*(4, \mathbb{C})$ and $\mathfrak{so}^*(4, \{\cdot,\cdot\}_{\lambda I - E})$ and so T_2 is also a Poisson isomorphism. The set of singular points of $\mathfrak{so}^*(4, \{\cdot,\cdot\}_{\lambda I - E})$ is the image of the singular points of $\mathfrak{so}(4, \mathbb{C})$ under T_2, that is $T_2(\{(\boldsymbol{X}, 0)\} \cup \{(0, \boldsymbol{Y})\})$. The set of critical points of the ellipsoidal integrable system is precisely the set of singular points of $\mathfrak{so}^*(4, \{\cdot,\cdot\}_{\lambda I - E})$ by Theorem 2 in [BO09]. We have an analogous result:

Proposition 24. *An element of $\boldsymbol{L} \in \mathfrak{so}^*(4)$ is critical if*

1. *$\lambda \neq e_i$ and $\boldsymbol{L} \in \Re e(T_2(0, \boldsymbol{X}) \cup T_2(\boldsymbol{Y}, 0))$.*

2. *$\lambda = e_i$ and $\boldsymbol{L}$ is such that the Poisson bracket $\{\cdot,\cdot\}_C$ drops rank.*

Using Proposition 24 we start by finding the general solutions for case 1 with $\lambda \neq e_i$. The critical points are given by $\boldsymbol{L} \in \Re e(T_2(0, \boldsymbol{Y}) \cup T_2(\boldsymbol{X}, 0))$. Let $\boldsymbol{z} = (z_1, z_2, z_3) \in \mathbb{C}^3$, define

$\mathrm{Sing}_+ = \{(\boldsymbol{z}, 0)\}$, $\mathrm{Sing}_- = \{(0, \boldsymbol{z})\}$ and $\mathrm{Sing} = \mathrm{Sing}_+ \cup \mathrm{Sing}_-$. We have

$$T_2(\lambda)(\mathrm{Sing}_\pm) = \Bigg(\frac{z_1\sqrt{\lambda-e_1}\sqrt{\lambda-e_2}}{\sqrt{2}}, \pm\frac{z_2\sqrt{\lambda-e_1}\sqrt{\lambda-e_3}}{\sqrt{2}}, \frac{z_3\sqrt{\lambda-e_1}\sqrt{\lambda-e_4}}{\sqrt{2}}, \pm\frac{z_3\sqrt{\lambda-e_2}\sqrt{\lambda-e_3}}{\sqrt{2}}, -\frac{z_2\sqrt{\lambda-e_2}\sqrt{\lambda-e_4}}{\sqrt{2}}, \pm\frac{z_1\sqrt{\lambda-e_3}\sqrt{\lambda-e_4}}{\sqrt{2}}\Bigg), \tag{3.26}$$

where $z_j = a_j + ib_j$ with $a_i, b_i \in \mathbb{R}$. Substituting these into the integrals gives $(I_1, I_2) = (4h\lambda, 2h\lambda^2)$ which is the curve $I_2 = \frac{I_1^2}{8h}$. This is precisely when λ is a double root of (3.25). It is easily seen that the values of λ that permit a double root while keeping $\psi > 0$ are in the interval $\lambda \in [e_2, e_3]$. After taking the real part this gives the critical points

$$\boldsymbol{L}_\pm = \Bigg(\frac{a_1\sqrt{\lambda-e_1}\sqrt{\lambda-e_2}}{\sqrt{2}}, \mp\frac{b_2\sqrt{\lambda-e_1}\sqrt{e_3-\lambda}}{\sqrt{2}}, -\frac{b_3\sqrt{\lambda-e_1}\sqrt{e_4-\lambda}}{\sqrt{2}}, \mp\frac{b_3\sqrt{\lambda-e_2}\sqrt{e_3-\lambda}}{\sqrt{2}}, \frac{b_2\sqrt{\lambda-e_2}\sqrt{e_4-\lambda}}{\sqrt{2}}, \mp\frac{a_1\sqrt{e_3-\lambda}\sqrt{e_4-\lambda}}{\sqrt{2}}\Bigg). \tag{3.27}$$

We can verify that these are critical points of the system (η_1, η_2) by noting that $B(\nabla\eta_0 - \lambda\nabla\eta_1 - \nabla\eta_2)|_{\boldsymbol{L}=\boldsymbol{L}_\pm} = 0$. Substituting (3.27) into the Plücker relation forces

$$a_1^2 = b_2^2 + b_3^2. \tag{3.28}$$

Using $\boldsymbol{L}\cdot\boldsymbol{L} = 2h$ gives the conic

$$(e_1e_2 - e_1e_3 - e_2e_4 + e_3e_4)b_2^2 + (e_1e_2 - e_2e_3 - e_1e_4 + e_3e_4)b_3^2 = 4h. \tag{3.29}$$

The conditions (3.28) and (3.29) when combined with (3.27) gives the explicit parametrisation for the 4 topological S^1 of critical points for case 1 with $\lambda \neq e_i$.

In case 2 where $\lambda = e_i$, the map $\gamma_{\lambda I-E}$ still exists but it is not invertible and so $T_2(e_i)(\mathrm{Sing})$ is still a subset of the critical points of the bracket $\{\cdot,\cdot\}_{C(e_i)}$. Let us consider $\lambda = e_1$, then we have

$$T_2(e_1)(\mathrm{Sing}_\pm) = \Bigg(0, 0, 0, \pm\frac{z_3\sqrt{e_1-e_2}\sqrt{e_1-e_3}}{\sqrt{2}}, -\frac{z_2\sqrt{e_1-e_2}\sqrt{e_1-e_4}}{\sqrt{2}}, \pm\frac{z_1\sqrt{e_1-e_3}\sqrt{e_1-e_4}}{\sqrt{2}}\Bigg).$$

These naturally satisfies the Plücker relations giving us solutions of the form $\boldsymbol{L} = (0, 0, 0, \ell_{23}, \ell_{24}, \ell_{34})$ after taking the real part with constraint $\ell_{23}^2 + \ell_{24}^2 + \ell_{34}^2 = 2h$. This means that the set of all critical points corresponding to case 2 with $\lambda = e_1$ is the sphere $\ell_{23}^2 + \ell_{24}^2 + \ell_{34}^2 = 2h$.

In order to show these are all the critical points for $\lambda = e_1$, recall that the singular points of $\{\cdot,\cdot\}_{C(e_i)}$ occurs when $B_{C(e_i)}$ drops rank. We perform the change of variables $(\boldsymbol{U}, \boldsymbol{V})$ where $\boldsymbol{U} = (u_{12}, u_{13,}, u_{14})$ and $\boldsymbol{V} = (v_{34}, v_{24}, v_{23})$ with $u_{ij} = \sqrt{(e_i - e_k)(e_i - e_m)}\ell_{ij}$, $v_{km} = \frac{1}{\sqrt{(e_i-e_k)(e_i-e_m)}}\ell_{km}$ and i, j, k, m are all distinct. This transforms $B_{e_1 I-E}$ into the standard

$\mathfrak{e}^*(3)$ algebra given by

$$B_3 = \begin{pmatrix} \mathbf{0} & \hat{\boldsymbol{U}} \\ \hat{\boldsymbol{U}} & \hat{\boldsymbol{V}} \end{pmatrix}.$$

Singular orbits of B_3 are given by $\boldsymbol{U} = \mathbf{0}$, giving $\ell_{12} = \ell_{13} = \ell_{14} = 0$ for all $j \neq i$. These are the critical points described above.

For $\lambda = e_2, e_3, e_4$ we have an isomorphism between $B_{\lambda I - E}$ and $\mathfrak{e}^*(1,2)$, $\mathfrak{e}^*(2,1)$, $\mathfrak{e}^*(0,3)$ respectively, all of which have singular orbits iff $\boldsymbol{U} = \mathbf{0}$ giving $\ell_{ik} = 0$ for all $k \neq i$ if $\lambda = e_i$.

3.5.3. Bifurcation diagram

Using the critical points described in the previous section we have the following result for the critical values.

Corolary 1. *The critical values of the integrals (η_1, η_2) occur when λ is a real root of $\psi(\lambda)$ so that $\psi(\lambda) \geq 0$ and*

1) $\lambda = e_i$ or

2) λ is a double root of the numerator $\psi(\lambda) := 2h\lambda^2 - \eta_1\lambda + \eta_2$

Proof. By the Cayley Hamilton theorem, it is known that

$$\mathrm{Tr}(M^2) - (\mathrm{Tr}(M))^2 + 2\det(M) = 0.$$

We observe that if $M = XC^{-1}$, $\mathrm{Tr}(M) = 0$ and $\det(M) = \frac{(X_{12}X_{23} - X_{13}X_{24} + X_{12}X_{34})^2}{(\lambda - c_1)(\lambda - c_2)(\lambda - c_3)(\lambda - c_4)} = \frac{\mathcal{C}_2^2}{(\lambda - c_1)(\lambda - c_2)(\lambda - c_3)(\lambda - c_4)} = 0$ due to constraint on the Casimir. This implies that λ has to be a root of $\psi(\lambda)$ for valid motion. For critical points, we either have $\lambda = e_i$ or λ such that $(I_1, I_2) = (4h\lambda, 2h\lambda^2)$, that is λ is a double root of $\psi(\lambda)$.

■

Proposition 25. *The set of critical values for the reduced ellipsoidal integrable system $(\eta_1, \eta_2) : S^2 \times S^2 \to \mathbb{R}^2$ is composed of 4 straight lines and a quadratic curve. The lines are $\mathcal{L}_i : \eta_2 - e_i(\eta_1 - e_i) = 0$ for $i \in \{1,2,3,4\}$ and part of the parabola $\eta_2 = \frac{\eta_1^2}{4}$ given by $\mathcal{C} : (\eta_1, \eta_2) = (2t, t^2)$ for $e_2 \leq t \leq e_3$. There are 6 transverse intersections of the lines $\mathcal{L}_i \cap \mathcal{L}_j$ which occur at $(\eta_1, \eta_2) = d_{ij} := (e_i + e_j, e_i e_j)$ where $i \neq j$ and $i, j \in \{1,2,3,4\}$. The points $d_i := (2e_i, e_i^2)$ where $i \in \{2,3\}$ correspond to the two tangential intersections of $\mathcal{L}_2$ and $\mathcal{L}_3$ with $\mathcal{C}$. The bifurcation diagram with $2h = 1$ is shown in Figure 3.3 b).*

Proof. Using Proposition 23 and Corollary 1, when $\lambda = e_i$ in (3.25) we must have $\eta_2 = e_i(\eta_1 - 2he_i)$ for the numerator of $\psi(\lambda)$ to be identically 0 . If λ is a double root, then taking the discriminant of the numerator gives the curve $\eta_2 = \frac{\eta_1^2}{8h}$. With $2h = 1$, we obtain the formulae for the lines $\mathcal{L}_i$ and the curve $\mathcal{C}$ which make up the boundary of the image of the momentum map. Since the bifurcation diagram is necessarily compact we must also determine the regions for which the momenta are real. To do this, recall that $\psi(s_i) = 4p_i^2$ can be factored as follows

$$\psi(s_i) = 4p_i^2 = -2\frac{(s_i - r_1)(s_i - r_2)}{(z - e_1)(z - e_2)(z - e_3)(z - e_4)}, \tag{3.30}$$

where $e_1 \leq r_1 \leq r_2 \leq e_4$, $\eta_1 = r_1 + r_2$ and $\eta_2 = r_1 r_2$. The denominator of (3.30) defines 4 poles at e_j and so divides the interval $[e_1, e_4]$ into three intervals $[e_i, e_{i+1}]$ where $i \in \{1, 2, 3\}$. To distribute the roots r_k, we require that p_i^2 takes on non negative values in each interval $[e_i, e_{i+1}]$ for valid motion. This gives 4 regions of motion which we represent in Figure 3.3 a). We call this the root diagram for the ellipsoidal system. The mapping from the root diagram to the bifurcation diagram is smooth on the interior and all edges of the root diagrams except on the diagonal cyan segment where $r_1 = r_2$. The image of the momentum map is the region enclosed by the lines $\mathcal{L}_i$ and the curve $\mathcal{C}$ presented in Figure 3.3 b).

From the root diagram, we find that each of the lines $\mathcal{L}_i$ is defined over $\eta_1 \in [e_1 + e_j, e_4 + e_k], \eta_2 \in [e_1 e_j, e_4 e_k]$ where $j = \max(2, i)$ and $k = \min(3, i)$. Hence the end points of $\mathcal{L}_i$ are d_{ij} and $d_{k4} = d_{4k}$. The critical points on each line $\lambda = e_i$ described in the previous section represents the geodeosic subflow on the great 2-sphere $x_i = 0$ under elliptical coordinates on S^2 with axes given by the remaining e_k with $k \neq i$. Consider the case with $\lambda = e_1$, for each critical value (η_1, η_2) on the line $\mathcal{L}_1$, its set of critical points is the intersection of the sphere $\ell_{23}^2 + \ell_{24}^2 + \ell_{34}^2 = 2h$ with the ellipsoids $\eta_2(\boldsymbol{L}) = e_1(e_4\ell_{23}^2 + e_3\ell_{24}^2 + e_2\ell_{34}^2) = \eta_2$. These are precisely the fibres of the geodesic flow on S^2 when separation of variables is performed in the elliptical coordinates on S^2 with semi-axes (e_2, e_3, e_4) (see Appendix A.2.1). Indeed, when $\ell_{12} = \ell_{13} = \ell_{14} = 0$, we have $x_1 = y_1 = 0$ and we have geodesic motion restricted on the great 2-sphere $x_1 = 0$.

In the case where there is a double root in the numerator, i.e. $t = r_1 = r_2$, we obtain the curve $\mathcal{C} : (\eta_1, \eta_2) = (2t, t^2)$ where $e_2 \leq t \leq e_3$.

It is clear that the intersections between $\mathcal{L}_i$ and $\mathcal{L}_j$ are transverse and are located at $(\eta_1, \eta_2) = (e_i + e_j, e_i e_j) = d_{ij}$ where $i \neq j$ and $i, j \in \{1, 2, 3, 4\}$. Similarly, it is easy to see by computing the tangents that only $\mathcal{L}_2$ and $\mathcal{L}_3$ intersect $\mathcal{C}$ tangentially at $d_2 = (2e_2, e_2^2)$ and $d_3 = (2e_3, e_3^2)$ respectively.

$\blacksquare$

Corolary 2. *The Uhlenbeck integral $F_i = 0$ if and only if $\eta_2 - e_i(\eta_1 - e_i) = 0$, i.e. F_i vanishes*

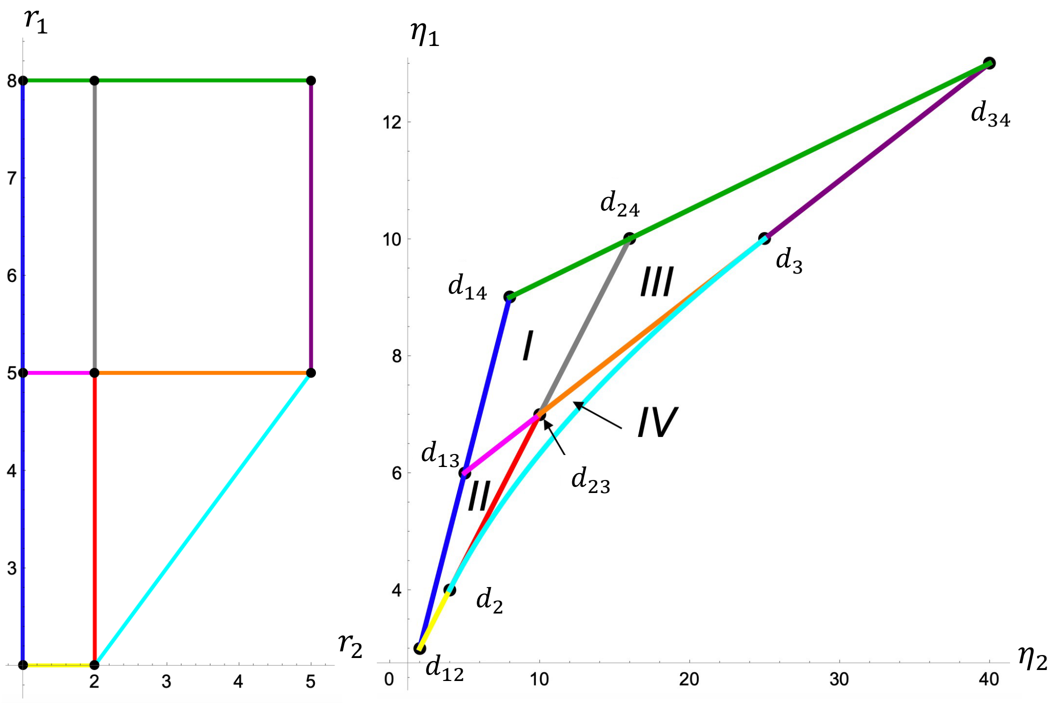

Figure 3.3: a) Root diagram of the reduced ellipsoidal system with $(e_1, e_2, e_3, e_4) = (1, 2, 5, 8)$. b) Corresponding bifurcation diagram. The four chambers of the image of the momentum map are labelled $I - IV$. The colours of the various lines will be kept in further figures.

along $\mathcal{L}_i$.

Proof. Taking the residue at e_i of both sides of (3.16) gives

$$F_i = -\frac{e_i^2 - e_i\eta_1 + \eta_2}{(e_i - e_k)(e_i - e_l)(e_i - e_m)}$$

where indicies i, k, l, m are all distinct. Since we have assumed all semi major axes are distinct, $F_i = 0$ if and only if (η_1, η_2) lie on $\mathcal{L}_i$.

■

To classify the nature of the critical points, we compute the eigenvalues of the linearisation $\nabla[B(\lambda\nabla\eta_1 + \nabla\eta_2)]$. The intersections d_{12}, d_{14} and d_{34} are all elliptic-elliptic critical values, d_{13} and d_{24} are of elliptic-hyperbolic type and d_{23} is hyperbolic-hyperbolic. The tangential intersections d_2 and d_3 are degenerate. The lines $\mathcal{L}_1, \mathcal{L}_4$, the curve $\mathcal{C}$, as well as the yellow and purple parts of $\mathcal{L}_2$ and $\mathcal{L}_3$ respectively have one pair of imaginary eigenvalues and so are codimension one elliptic. The magenta, orange and grey, red segments of $\mathcal{L}_3$ and $\mathcal{L}_2$ give one pair of real eigenvalues and so are codimension one hyperbolic.

3.5.4. Critical Fibres

Unlike the critical points, the parametrisation of the critical fibre cannot be computed algebraically. We will instead provide informal description and topological classification of the fibres on $S^2 \times S^2$ instead.

Firstly, by Louvile-Arnold theorem, the preimage of regular values in regions I, II, III, IV are $\mathbb{T}^2$ in $S^2 \times S^2$.

Since d_{12}, d_{14}, d_{34} are elliptic-elliptic, their preimage on $S^2 \times S^2$ are 2 points each, the critical points found earlier.

Next, consider the lines immediately connected to d_{12}, d_{14}, d_{34} These are the lines $\mathcal{L}_1, \mathcal{L}_4$, as well as the yellow and purple parts of $\mathcal{L}_2$ and $\mathcal{L}_3$ respectively. They are codimension one elliptic and so their fibres are circles S^1 and only contain critical points. The multiplicity of these circles is two as a result of extending the multiplicities of d_{12}, d_{14} and d_{34}.

Similarly, d_{13} and d_{24} are elliptic-hyperbolic critical values. There are 2 intersecting circles of critical points in their fibres. To obtain the full fibre, we observe that as we move along $\mathcal{L}_1$ (resp. $\mathcal{L}_4$) and pass by d_{13} (resp. d_{24}), two S^1 bifurcate into two S^1. Such a bifurcation is represented by the Fomenko atom C_2.

The magenta and grey segments of $\mathcal{L}_3$ and $\mathcal{L}_2$ are extensions of d_{13} and d_{24} respectively, the fibres of these segments are $S^1 \times C_2$.

Since the grey and magneta lines both have a C_2 type singularity, we know that the fibre of d_{23} is of type (C_2, C_2) l-type of complexity 2 with loop molecule number 17 in [BF04]. The critical fibre is simpler, there are only 4 types after symmetry reduction [DN07].

Since the 17 saddle saddle singularity contains 4 B atoms, it follows that the fibres of the red and orange lines are $2B \times S^1$.

The cyan curve is codimension one elliptic and so its fibre is a circle S^1. To find the multiplicity of these S^1, we note that the fibre of d_{23} contains $4S^1$. Extending d_{23} into chamber IV, we multiply by S^1. Hence, the fibre of a regular value in chamber IV is $4T^2$. Continuing onto $\mathcal{C}$, we see that the fibre along the curve must be $4S^1$.

The fibre type does not change at the degenerate points d_2 and d_3, hence are simply $2S^1$. Approaching d_2 and d_3 along the yellow and purple lines respectively, we see $2S^1$ bifurcate into $4S^1$ (along the curve $\mathcal{C}$) as well as a hyperbolic fibre ($2B \times S^1$). This means d_2 and d_3 are pitchfork bifurcations as described in [BF04].

Extending the codimension 1 lines $\mathcal{L}_1$ and $\mathcal{L}_4$ into chambers $I - III$ gives the following corollary.

Corolary 3. *The fibre of a regular point on the momentum map is a torus T^2. The multiplicity of the tori in chambers $I - III$ is 2, while tori in chamber IV have multiplicity 4.*

3.5.5. The Action Map

Recall that the Liouville tori of the ellipsoidal integrable system are certain coverings of the real parts of the Jacobi variety of the genus 3 hyperelliptic curve defined by $w^2(z) = -R(z)A(z)$. The actions of this system are the periods of the Abelian integral

$$I_j = \frac{1}{2\pi}\oint_{\gamma_j} p_j(s)ds = \frac{1}{2\pi}\oint_{\gamma_j}\sqrt{\frac{-R(s)}{4A(s)}}ds = \frac{1}{2\pi}\oint_{\gamma_j}\frac{-R(s)}{2w(s)}ds.$$

The actions I_j are discontinuous on phase space as we cross boundaries of chambers of the bifurcation diagram. To construct a set of continuous actions, we perform discrete symmetry reduction by the 2^4 discrete symmetries generated by the reflections

$$\sigma_i : (x_i, p_i) \to (-x_i, -p_i).$$

Following [Gur95], we can construct symmetry reduced actions that are continuous accross all chambers of the momentum map. A detailed explanation can be found in [DRVW01].

Lemma 26. *The continuous actions of the ellipsoidal integrable system (J_1, J_2, J_3) are*

$$J_1 = \frac{2}{\pi}\int_{e_1}^{\min(r_1,e_2)} p(s)ds, \quad J_2 = \frac{2}{\pi}\int_{\max(r_1,e_2)}^{\min(r_2,e_3)} p(s)ds, \quad J_3 = \frac{2}{\pi}\int_{\max(r_2,e_3)}^{e_4} p(s)ds. \tag{3.31}$$

This discrete symmetry reduction reduces the multiplicities of T^2 in all chambers to 1 and this is the reason why the discrete symmetry reduced system has a globally continuous action map. The actions J_i are independent on T^*S^3 but since H is a superintegrable Hamiltonian, they are related on an energy surface, and hence become dependent for the reduced system on $S^2 \times S^2$.

Lemma 27. *The continuous actions satisfy the relation*

$$J_1 + J_2 + J_3 = \sqrt{2h}. \tag{3.32}$$

Proof. Let β_i be cycles that enclose the bounds of J_i respectively. I.e. β_1 encloses the interval $[e_1, \min(r_1, e_2)]$ and similarly for β_2, β_3. By deforming the cycles on the hyperelliptic curve $w^2 = -R(z)A(z)$ we have

$$J_1 + J_2 + J_3 = -\frac{1}{2\pi}\oint_{\gamma} pdz \tag{3.33}$$

where γ is a cycle that encircles the point at infinity. It is easily shown that

$$\text{Res}(p, \infty) = -\sqrt{-2h}. \tag{3.34}$$

Combining (3.34) with (3.33) gives the desired result.

■

Theorem 28. *The image of the action map (3.31) is an equilateral triangle $\mathcal{T}$ (see Figure 3.4).*

Proof. From Lemma 5, we know that the image of the action map is constrained to the plane $J_1 + J_2 + J_3 = \sqrt{2h}$. This is bounded by $J_i \geq 0$ and hence the image is contained in the intersection of the plane $J_1 + J_2 + J_3 = \sqrt{2h}$ with the positive quadrant. Since the maps J_i are continuous on the reduced phase space, every point in the interior of $\mathcal{T}$ must be a point in the image of the action map. On the boundary of $\mathcal{T}$, the lines $J_1 = 0$ and $J_3 = 0$ are the image of the lines $\mathcal{L}_1$ and $\mathcal{L}_4$ respectively while $J_2 = 0$ is the image of the cyan curve $\mathcal{C}$ together with the yellow and purple segments of $\mathcal{L}_2$ and $\mathcal{L}_3$. Thus, the triangle $\mathcal{T}$ formed by intersecting the plane $J_1 + J_2 + J_3 = \sqrt{2h}$ with the positive quadrant is the image of the symmetry reduced phase space under the action map.

■

The action map calculated using (3.31) is shown in Figure 3.4 for $h = \frac{1}{2}$. Let lines $J_i = 0$ be $\mathfrak{J}_i$ and call the interior lines γ_1 (red and grey) and γ_2 (magenta and orange). We denote by A_{ij} the intersection of $\mathfrak{J}_i$ and γ_j. Similar polytopes are known to classify toric systems (two dimensional integrable systems where both integrals are global S^1 actions). For more details on this, see [Del88]. In our case, the γ_i in the interior of the action map reflect the non-toric nature of the ellipsoidal integrable system. Along these lines the hyperelliptic action integrals (26) become elliptic. Let

$$\mathcal{T}(u, v, \alpha) = \frac{(u - v)K(k) + (e_4 - e_1)\Pi(\alpha, k)}{\pi\sqrt{(e_1 - e_3)(e_2 - e_4)}}$$

where $k^2 = \frac{(e_4-e_3)(e_2-e_1)}{(e_4-e_2)(e_3-e_1)}$ and $K(k)$, $\Pi(\alpha, k)$ are the complete elliptic integrals of the first and third kind respectively. The tangential intersections of $\mathfrak{J}_2$ with γ_1, γ_2 occur at A_{21} and A_{22}. These are given by

$$A_{21} = (\mathcal{T}(e_2, e_4, \alpha_1), 0, \mathcal{T}(e_1, e_2, \alpha_2)), \quad A_{22} = (\mathcal{T}(e_3, e_4, \alpha_1), 0, \mathcal{T}(e_1, e_3, \alpha_2))$$

where $\alpha_1 = \frac{e_2-e_1}{e_2-e_4}$ and $\alpha_3 = \frac{e_4-e_3}{e_1-e_3}$. Transverse intersections of $\mathfrak{J}_i$ with γ_j occur at A_{31} and A_{12} given by

$$A_{31} = \frac{2}{\pi}(\sin^{-1}(u_1), \cos^{-1}(u_1), 0) \quad A_{12} = \frac{2}{\pi}(0, \sin^{-1}(u_2), \cos^{-1}(u_2))$$

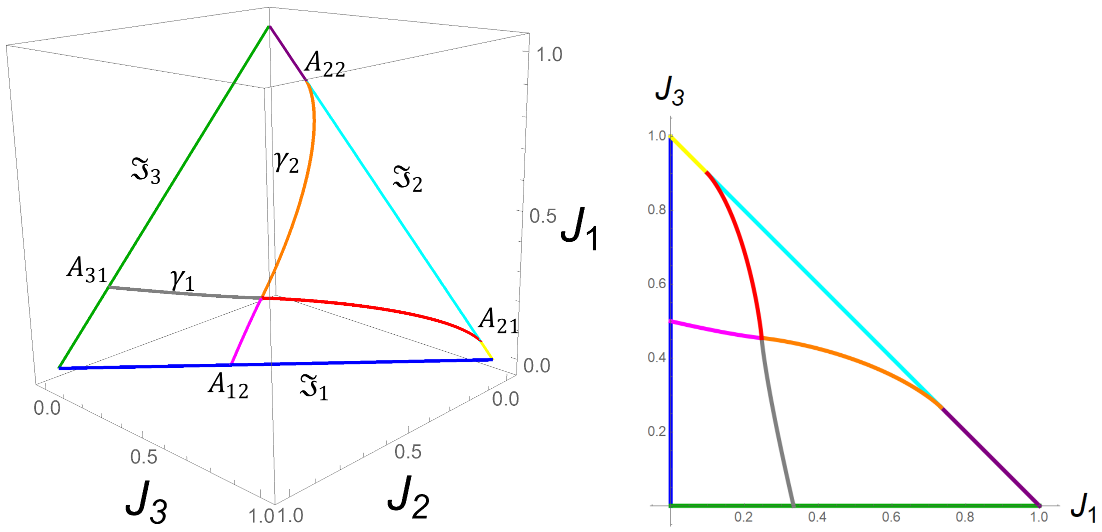

Figure 3.4: a) Action map of the ellipsoidal integrable system with $(e_1, e_2, e_3, e_4) = (1, 2, 5, 8)$. b) Corresponding reduced action map (J_1, J_3)

where $u_1 = \sqrt{\frac{e_1-e_2}{e_1-e_3}}$ and $u_2 = \sqrt{\frac{e_2-e_3}{e_2-e_4}}$. The intersection of γ_1 and γ_2 is located at

$$(J_1, J_2, J_3) = \frac{2}{\pi}(\sin^{-1}(v_1), \sin^{-1}(v_2) - \sin^{-1}(v_1), \cos^{-1}(v_2)) \tag{3.35}$$

where $v_1 = \sqrt{\frac{e_1-e_2}{e_1-e_4}}$ and $v_2 = \sqrt{\frac{e_1-e_3}{e_1-e_4}}$. Notice that these intersection points are invariant under affine transformations of (e_1, e_2, e_3, e_4) as expected.

The action map (J_1, J_2, J_3) is equivalent to the map $(J_1, J_1 + J_2 + J_3, J_3)$ by a uni-modular transformation. Since $J_1 + J_2 + J_3 = 1$ for the reduced system on $S^2 \times S^2$, we have 2 actions only, ie. (J_1, J_3). By using similar transformations, any pair (J_i, J_j) can be chosen as the actions for the reduced system. The resulting image of the corresponding action map is the projection of the action map in Figure 3.4 onto the J_iJ_j plane.

Corolary 4. *A possible set of actions for the reduced ellipsoidal integrable system is (J_1, J_3). The image of the reduced space $S^2 \times S^2$ under this map is a right-angled isosceles triangle obtained from projecting Figure 3.4 onto the $J_2 = 0$ plane.*

Proof. The reduction can be done in appropriate action variables directly. Since $J_1+J_2+J_3$ is a global action variable that is equal to the square root of twice the Hamiltonian, reduction means the following two things. Fix the action (i.e. fix the energy), and quotient by its flow. The flow of this action only changes it's conjugate angle, and so the quotient identifies this angle to a point. The remaining system with two degrees of freedom has action variables J_1, J_3, and the image of the action map of the reduced system is the projection of the "spatial" fixed energy triangle in Figure 3.4 a) onto the appropriate coordinate plane in Figure 3.4 b).

■

The choice of which action variable to present the reduced system in is somewhat arbitrary, and we prefer not to make any choice and hence keep showing the "spatial" picture of the triangle in $J_1J_2J_3$-space in the following section, even when discussing the reduced system on $S^2 \times S^2$. In general an integrable system can be represented by its energy surface in action space, which means the surface $H(J_1, J_2, J_3) = h$, which will depend on h, and may not even be continuous. However, in our setting we have simplest possible case of a maximally superintegrable system for which $H(J_1 + J_2 + J_3) = h$, and so the triangle in action space occurs for every superintegrable system for which globally continuous actions can be defined.

The position of the hyperbolic-hyperbolic point in the image of the action map (the intersections of the lines γ_1 and γ_2) is uniquely determined by the reduced parameters $1 < a < b$ of the system. In fact, the map $(1/b, a/b) \mapsto \frac{2}{\pi}(\sin^{-1}\sqrt{1/b}, \cos^{-1}\sqrt{a/b})$ maps the triangle in parameter space Figure 3.2 a) to the triangle in action space Figure 3.4 b). The involution in parameter space (3.22) becomes the reflection across the diagonal $(J_1, J_3) \mapsto (J_3, J_1)$.

Performing the affine transformation of e_i directly in the action integral and applying the same transformation to the integration variable s does change the integral. However, then also transforming (η_1, η_2) according to Lemma 21 recovers the original integral, as expected.

3.6. Degenerate Systems on $S^2 \times S^2$

In this section, we study all systems arising from separating the geodesic flow in degenerate coordinates on S^3. We begin by focusing on the following 3 systems: prolate $(1\ (2\ 3)\ 4)$, oblate $(1\ 2\ (3\ 4))$ and Lamé $(1\ (2\ 3\ 4))$. These correspond to the edges of the Stasheff polytope. Further degenerations of these coordinates, cylindrical $((1\,2)(3\,4))$ and two forms of spherical $(1\ (2\ (3\ 4)), (1\ ((2\ 3)\ 4))$ form the corners of the polytope.

It will be shown that the integrable systems (reduced and un-reduced) corresponding to these degenerate coordinate systems can also be obtained by smoothly deforming their ellipsoidal counterparts. Thus, we will establish the analogue of the result by Schöbel and Veselov [Sch14], namely that the correct moduli space for this family of integrable systems is the Stasheff polytope.

The main feature of the degenerate systems corresponding to the lower-dimensional faces of the Stasheff polytope is the appearance of global symmetries, in the case of S^3 either $SO(2)$ and $SO(3)$. The results of this section described in detail below can be summarised in the following theorem. Consider the designation of a separable coordinate system on S^3 by pairs of nested brackets inserted into 4 objects as shown in Figure 3.1.

Theorem 29. *For each pair of brackets that enclose two adjacent members, the corresponding (reduced) integrable system has an $SO(2)$ symmetry. For each pair of brackets that enclose three adjacent members the corresponding (reduced) integrable system has a global $SO(3)$ symmetry. The generic ellipsoidal integrable system with quadratic integrals degenerates to an integrable system with quadratic integrals. If there is an $SO(k)$ symmetry the corresponding quadratic integral is replaced by its square root. For $SO(2)$ this gives a global S^1 action, while for $SO(3)$ this gives an almost global S^1 action.*

In particular, the oblate, prolate, and spherical systems have one global S^1 action each, the cylindrical system has two global S^1 actions, and the spherical and the Lamé system have an almost-global S^1 action each. In addition, we find that the prolate system is generalised semi-toric and the cylindrical system is toric but the $S^1 \times S^1$ action is not effective. By almost global S^1 action we mean that the action fails in the preimage of an isolated point of the image of the momentum map. The corresponding spherical singularity in the spherical system [Ker22] also appears in the Lamé system.

3.6.1. Prolate Coordinates

We begin by considering prolate coordinates. It will be shown that the corresponding integrable system is generalised semi-toric and has non-trivial monodromy. In addition, the global action triangle is half of the semi-toric polygon invariant.

Separation of Variables

Prolate coordinates on S^3, denoted by $(1\,(2\,3)\,4)$, are a degeneration of ellipsoidal coordinates arising from setting the middle two semi major axes equal, i.e. $e_2 = e_3$. We normalise the e_j according to $(e_1, e_2 = e_3, e_4) = (0, 1 = a, b)$. From [KM86], an explicit representation of prolate coordinates is

$$x_1^2 = \frac{s_1 s_3}{b}, \qquad x_2^2 = -\frac{(s_1-1)\,s_2\,(s_3-1)}{b-1},$$
$$x_3^2 = \frac{(s_1-1)\,(s_2-1)\,(s_3-1)}{b-1}, \quad x_4^2 = \frac{(b-s_1)\,(b-s_3)}{(b-1)b},$$

where $0 \le s_1, s_2 \le 1 \le s_3 \le b$. Since s_2 is an ignorable coordinate, the Hamilton Jacobi equation can be separated easily to give integrals $(2H, G_{pro}, \ell_{23})$ where $G_{pro} = b\ell_{12}^2 + b\ell_{13}^2 + \ell_{14}^2$. The corresponding momenta are

$$p_i^2 = \frac{-2hs_i^2 + (g + 2h + (b-1)l^2)s_i - g}{4s_i(s_i-b)(s_i-1)^2}, \qquad p_2^2 = \frac{l^2}{4s_2(1-s_2)} \tag{3.36}$$

where $i \in \{1, 3\}$ and (l, g) are the values of ℓ_{23} and G_{pro}, respectively. We call the triple $(2H, \ell_{23}, G_{pro})$ on T^*S^3 the 1-parameter family of prolate integrable systems. Similarly, (ℓ_{23}, G_{pro}) gives a 1-parameter family of reduced prolate integrable systems on $S^2 \times S^2$.

Note that we have chosen ℓ_{23} as an integral since it is naturally a global S^1 action, unlike its square. The quadratic integrals can be obtained as a limit of the ellipsoidal integrable system.

Lemma 30. *The integrals* $\left(\ell_{23}^2, G_{pro}\right)$ *as well as the separated momenta* (3.36) *can be obtained by smoothly degenerating their ellipsoidal counterparts* (3.13) *and* (3.14)*.*

Proof. The transformation from ellipsoidal to prolate coordinates is given by

$$e_3 = e_2 + \varepsilon \qquad s_2 = e_2 + \varepsilon \tilde{s}_2 \qquad p_2 = \frac{\tilde{p}_2}{\varepsilon} \tag{3.37}$$

in the limit $\varepsilon \to 0$ where $\tilde{s}_2 \in [0,1]$. The transformation from (s_2, p_2) to $(\tilde{s}_2, \tilde{p}_2)$ is canonical. Let $(\tilde{\eta}_1, \tilde{\eta}_2) = (\eta_1, \eta_2)|_{e_3=e_2+\varepsilon}$. Substituting (3.37) into (3.13) and taking the limit gives

$$G_{pro} = \tilde{\eta}_2 \qquad \ell_{23}^2 = \frac{1}{b-1}(\tilde{\eta}_1 - \tilde{\eta}_2 - 2H)$$

where we have normalised the e_j by setting $(e_1, e_2 = e_3, e_4) = (0, 1, b)$.

For the separated equations, we insert (3.37) into (3.14) and expand about $\varepsilon = 0$ to obtain

$$p_i^2 = \frac{\tilde{\eta}_1 + s_i\left(s_i - \tilde{\eta}_2\right)}{4\left(e_1 - s_i\right)\left(s_i - e_2\right)^2\left(s_i - e_4\right)} + O(\varepsilon) \qquad \tilde{p}_2^2 = \frac{e_2(e_2 - \tilde{\eta}_2) + \tilde{\eta}_1}{4\tilde{s}_2(\tilde{s}_2 - 1)(e_1 - e_2)(e_2 - e_4)} + O(\varepsilon). \tag{3.38}$$

Taking the limit of (3.38) as $\varepsilon \to 0$ and dropping the tildes gives (3.36).

■

In the prolate limit, F_2 and F_3 become singular. However, multiplying both integrals by $(e_3 - e_2)$ gives

$$\lim_{\varepsilon \to 0}(e_3 - e_2)F_2 = -\lim_{\varepsilon \to 0}(e_3 - e_2)F_3 = \ell_{23}^2.$$

The other two integrals F_1 and F_4 degenerate smoothly to

$$F_{1,pro} = \frac{-G_{pro}}{b}, \quad F_{4,pro} = \frac{2Hb - G_{pro} - b\ell_{23}^2}{(b-1)b}.$$

Critical Points and Momentum Map

Since the integrals of the prolate system are significantly simpler than those of the ellipsoidal system, we can easily compute the critical points and values directly. However, it is interesting to note that we can also use the method of compatible Poisson structures with the matrix $C = \text{diag}(0, 1, 1+\varepsilon, b)$ for $0 < \varepsilon < b - 1$ for this computation.

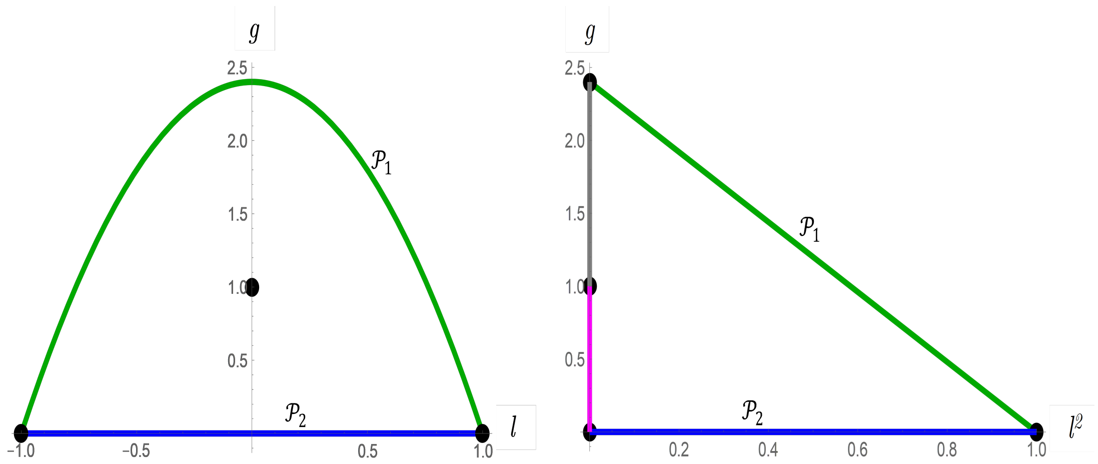

Figure 3.5: a) "Opened" momentum map with $b = 2.4$. b) "Unopened" momentum map using ℓ_{23}^2 as an integral.

Using Proposition 23 with this C, we get

$$\psi_{pro}(\lambda) = 2\frac{-2h\lambda^2 + I_1\lambda + I_2}{\lambda(\lambda-1)(\lambda-1-\varepsilon)(\lambda-b)}$$

with $(I_1, I_2) = (G_{pro} + 2h + (b-1)\ell_{23}^2 + \varepsilon(\ell_{12}^2 + \ell_{14}^2 + \ell_{24}^2), G_{pro} + \varepsilon(b\ell_{12}^2 + \ell_{14}^2))$. While the integrals I_1 and I_2 may appear complicated, the system (I_1, I_2) is equivalent to the system (G_{pro}, ℓ_{23}^2) in the limit as $\varepsilon \to 0$. We can find the critical points and values of the system (I_1, I_2) then taking the limit as $\varepsilon \to 0$ at the end of calculations to recover the correct results for the system (G_{pro}, ℓ_{23}^2).

Proposition 31. *The momentum map for the reduced prolate integrable system is the region bounded by the curve $\mathcal{P}_1 : G_{pro} = b(1 - \ell_{23}^2)$ and line $\mathcal{P}_2 : G_{pro} = 0$ shown in Figure 3.5 a). There is an isolated critical value at* $(0, 1)$.

Proof. Critical points of the system (ℓ_{23}^2, G_{pro}) can be computed directly or by applying Proposition 24:

1) The blue line $\mathcal{P}_2 : G_{pro} = 0$ has $\lambda = 0$ and the critical points are parametrised by $\boldsymbol{L} = (0, 0, 0, \ell_{23}, \ell_{24}, \ell_{34})$ with $\ell_{23}^2 + \ell_{24}^2 + \ell_{34}^3 = 1$ and $\ell_{23} = l$. These are co-dimension 1 elliptic points.

2) The green line $\mathcal{P}_1 : G_{pro} = b(1 - \ell_{23}^2)$ in Figure 3.5 b) has $\lambda = a$ and the critical points are parametrised by $\boldsymbol{L} = (\ell_{12}, \ell_{13}, 0, \ell_{23}, 0, 0)$ with $\ell_{12}^2 + \ell_{13}^2 + \ell_{23}^3 = 1$ and $\ell_{23} = l$. These are co-dimension 1 elliptic point.

3) The lines $\ell_{23}^2 = 0$ has both $\lambda = 1$, $\lambda = 1+\varepsilon$ as well as the curve $I_2 = \frac{I_1^2}{8h}$ corresponding to the double root $\lambda \in [1, 1+\varepsilon]$. These are degenerate critical values of system (ℓ_{23}^2, G_{pro}).

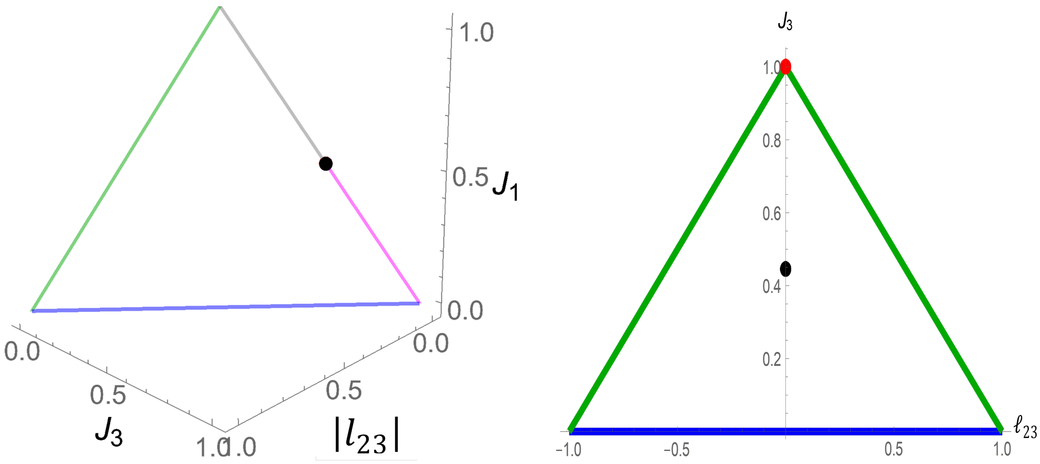

Figure 3.6: a) Action map for the prolate system with $b = 2.4$ where the black dot is the image of the focus-focus point. b) Semi-toric polygon invariant for the reduced prolate system.

For the reduced prolate integrable system (ℓ_{23}, G_{pro}), we see that the line $\mathcal{P}_2$ remains critical and has $l \in [-1, 1]$. The line P_1 for (ℓ_{23}^2, G_{pro}) becomes a parabola for (ℓ_{23}, G_{pro}). The line $\ell_{23} = 0$ becomes regular values after changing from ℓ_{23}^2 to ℓ_{23} with the exception of the isolated point $(\ell_{23}, G_{pro}) = (0, 1)$ which has critical points $\ell_{14} = \pm 1$. This is a focus-focus point and its fibre on $S^2 \times S^2$ a doubly pinched torus.

■

Action Map and Monodromy

From (3.36) and the same reasoning used to obtain (3.31), we have the following formulae for the actions

$$J_1 = \frac{2}{\pi} \int_0^{\min(r_1, 1)} p_1 ds \quad J_2 = \frac{2}{\pi} \int_0^1 p_2 ds \qquad J_3 = \frac{2}{\pi} \int_{\max(1, r_2)}^a p_3 ds \tag{3.39}$$

where the p_k are given in (3.36). Here (r_1, r_2) are the roots of $p_{1,3}^2$ from (3.36) where $0 \leq r_1 \leq 1 \leq r_2 \leq b$. Note that J_2 simplifies to $|\ell_{23}|$. Like for the ellipsoidal system, the prolate actions also satisfy (3.32). The action map for the prolate system is shown in Figure 3.6 a) where the black dot corresponding to the focus-focus point is located at $\frac{2}{\pi}(\sin^{-1}(\frac{1}{b}), 0, \frac{\pi}{2} - \sin^{-1}(\frac{1}{b}))$.

The reduced prolate system is a two degree of freedom integrable system where one of the integrals is a global S^1 action and all singularities are either elliptic or focus-focus type. Thus, we have the following.

Corolary 5. *The reduced prolate system (ℓ_{23}, G_{pro}) on $S^2 \times S^2$ is a generalised semi-toric system.*

Semi-toric systems have been globally classified using 5 symplectic invariants [PN09]. One of these is the polygon invariant, which is a family of rational convex polygons. This is a generalisation of the Delzant polytope (see, e.g., [Del88]) and allows us to compare the standard affine structure of $\mathbb{R}^2$ with that of the momentum map [AH19, SN17]. In Figure 3.6 b) we show one representative of the polygon invariant. This is simply the projection of the action map onto the (ℓ_{23}, J_1) axes with both signs of ℓ_{23} considered. The red vertex at $(0, 1)$ is a fake corner and is the result of "opening up" from $|\ell_{23}|$ to ℓ_{23}. For more information on the classification of semi-toric systems, see [SN17, AH19].

Another symplectic invariant of a semi-toric system is the height invariant, which is the position of the focus-focus point in the image of the action map. Note that this is the limit of the image of the hyperbolic-hyperbolic point in the action map for the degeneration $a = 1$. Specialising (3.35) to this case gives $\frac{2}{\pi}\cos^{-1}\sqrt{1/b}$ for the height invariant.

Another property of semi-toric systems is the non-trivial monodromy of the actions; the focus-focus equilibrium implies that one can only locally construct a smooth set of action variables. Monodromy has been well studied, both classically and quantum mechanically, see e.g. [DDN22, DW18, DDB07, CDEW19]. The prolate system has non-trivial monodromy.

Lemma 32. *The reduced prolate system has non-trivial monodromy with monodromy matrix*

$$\mathfrak{M} = \begin{pmatrix} 1 & 2 & 0 \\ 0 & 1 & 0 \\ 0 & -2 & 1 \end{pmatrix}. \tag{3.40}$$

Proof. Let C_1 and C_3 be cycles that enclose the intervals $[0, \min(1, r_1)]$ and $[\max(1, r_2), b]$ respectively. We rewrite (3.39) as

$$J_1 := \frac{1}{2\pi}\oint_{C_1} p_1 ds, \quad J_3 := \frac{1}{2\pi}\oint_{C_3} p_3 ds. \tag{3.41}$$

We observe that if $(l, g) = (0, g > 1)$ then $r_1 \to 1^-$. while if $g_{pro} < 1$, then $r_2 \to 1^+$. We now show that the actions (3.41), while continuous everywhere, are not globally smooth. Consider the slope of the action J_i considered as a function of l,

$$2\pi W_i := \frac{\partial J_i}{\partial l} = \oint_{C_i} \frac{(b-1)l}{2(b-s_i)(s_i-1)^2 p(s_i)} ds_i.$$

When $l = 0$, if C_i encloses $s_i = 1$ then $W_i = -\mathrm{sgn}(l)$, otherwise it vanishes. From our analysis of C_1 and C_2 around $s_i = 1$ we have

$$\lim_{l\to 0} \frac{\partial J_1}{\partial l} = -\,\kappa_1 \mathrm{sgn}(l) \quad \lim_{l\to 0} \frac{\partial J_3}{\partial l} = -\kappa_3 \mathrm{sgn}(l) \tag{3.42}$$

where $(\kappa_1, \kappa_3) = (1, 0)$ when $g_{pro} < 1$, otherwise $(\kappa_1, \kappa_3) = (0, 1)$. Thus, the actions J_1 and

J_3 are continuous but not differentiable at $l = 0$.

For $l > 0$, let $J_+ = (J_1, J_2, J_3)^t$ and similarly for J_-. Note that J_1 and J_3 are even functions of l while J_2 is odd. This means $J_-(-l) = SJ_+(l)$ where $S = \mathrm{diag}(1, -1, 1)$. We are now interested in finding unimodular matricies $M_1, M_2 \in SL(3, \mathbb{Z})$ such that J_+ and $M_i J_-$ are locally smooth across $l = 0$. To ensure continuity at $l = 0$ we require

$$
\begin{aligned}
J_+ &= M_1 J_- = M_1 S J_- = M_1 J_+, \quad g > 1 \\
J_+ &= M_2 J_- = M_2 S J_- = M_2 J_+, \quad g < 1.
\end{aligned}
$$

The above relations imply that $(J_1, 0, J_3)^t$ is an eigenvector of both M_1 and M_2 with eigenvalue $+1$. For arbitrary J_1, J_3 the corresponding eigenvector equation implies that M_i has the form

$$
M_i = \begin{pmatrix} 1 & \alpha_i & 0 \\ 0 & 1 & 0 \\ 0 & \beta_i & 1 \end{pmatrix}.
$$

For the actions to be smoothly joined when $g > 1$ we require

$$
M_1 \frac{\partial J_-}{\partial l} = \frac{\partial J_+}{\partial l}
$$

and similarly for $g < 1$ and M_2. The limits in (3.42) force $(\alpha_1, \beta_1) = (0, -2)$ and $(\alpha_2, \beta_2) = (-2, 0)$. The corresponding monodromy matrix is given by $M = (M_2 S)^{-1}(M_1 S)$ which we compute to be (3.40).

■

The monodromy of the reduce system with actions (J_1, ℓ_{23}) is obtained by the restriction to the top left block of $\mathfrak{M}$. It should be stressed that the integrable system with Hamiltonian H does not have monodromy, it is superintegrable, and does not even have dynamically defined tori. However, the fibration defined by the three commuting functions (H, ℓ_{23}, G_{pro}) on T^*S^3 has monodromy as computed. Similarly, the commuting function (ℓ_{23}, G_{pro}) on $S^2 \times S^2$ have monodromy given by the top left block of $\mathfrak{M}$.

3.6.2. Oblate Coordinates

Eventhough the definition of these coordinates is similar to the prolate case, the corresponding integrable system is significantly different. In particular, even though it does have a global S^1 action it is not semi-toric because of the appearance of hyperbolic and degenerate singularities.

Separation of Variables

Oblate coordinates, denoted by $(1\ 2\ (3\ 4))$ and $((1\ 2)\ 3\ 4)$, lie on opposite sides of the dotted line in Figure 3.1. They are equivalent by flipping the ordering of the e_i by applying $e_i \mapsto -e_i$ then reordering. Consequently, the corresponding integrable systems are equivalent. We focus on the $(1\ 2\ (3\ 4))$ coordinates and normalise according to $(e_1, e_2, e_3 = e_4) = (0, 1, a)$. This system is equivalent to the $((1\ 2)\ 3\ 4)$ with $(e_1 = e_2, e_3, e_4) = (0, 1, \frac{a}{a-1})$. An explicit definition of these coordinates is given by

$$\begin{aligned} x_1^2 &= \frac{s_1 s_2}{a}, & x_2^2 &= \frac{-(s_1-1)(s_2-1)}{a-1}, \\ x_3^2 &= \frac{(s_1-a)(s_2-a)\,s_3}{a(a-1)}, & x_4^2 &= \frac{(s_1-a)(s_2-a)(1-s_3)}{a(a-1)}, \end{aligned} \tag{3.43}$$

where $0 \le s_1, s_3 \le 1 \le s_2 \le a$. The integrals are $(2H, \ell_{34}, G_{obl})$ where $G_{obl} = a\ell_{12}^2 + \ell_{13}^2 + \ell_{14}^2$. Let (l, g) be functional values of ℓ_{34} and G_{obl} respectively, we obtain the separated momenta

$$p_i^2 = \frac{-2hs_i^2 + (2ah + g - (a-1)l^2)s_i - ag}{4s_i(s_i-1)(s_i-a)^2} \qquad p_3^2 = \frac{l^2}{4s_3(1-s_3)} \tag{3.44}$$

where $i \in \{1, 2\}$. We call the triple $(2H, \ell_{34}, G_{obl})$ on T^*S^3 the 1-parameter family of oblate integrable systems and (ℓ_{34}, G_{obl}) the corresponding reduced oblate integrable system.

We have a similar result to Lemma 30 for the oblate system.

Lemma 33. *The integrals (ℓ_{34}^2, G_{obl}) as well as the separated momenta (3.44) can be obtained by smoothly degenerating their ellipsoidal counterparts (3.13) and (3.14).*

Proof. Using the transformation

$$(e_4, s_3, p_3) = (e_3 + \varepsilon, e_3 + \varepsilon\tilde{s}_3, \frac{\tilde{p}_3}{\varepsilon})$$

where $\tilde{s}_3 \in [0, 1]$ and following the same procedure as Lemma 30 gives the result.

∎

In the oblate limit, the Uhlenbeck integrals F_i are

$$F_1 = -\frac{G_{obl}}{a}, \quad F_2 = \frac{G_{obl} + \ell_{34}^2 - 2h}{a-1}, \quad F_3 = \tilde{F}_4 = \ell_{34}^2.$$

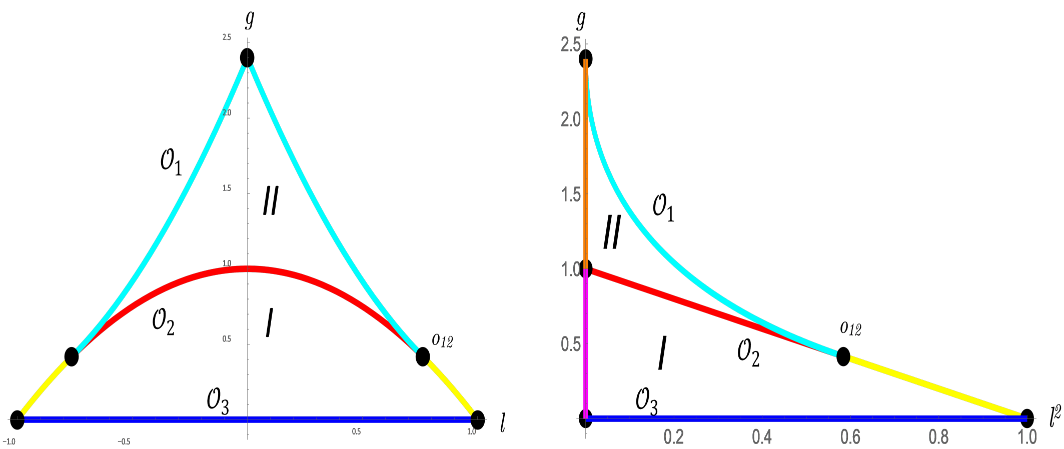

Figure 3.7: a) Momentum map for the oblate system (ℓ_{34}, G_{obl}) with $a = 2.4$. There are two chambers, labelled I and II. b) "Unopened" momentum map taking ℓ_{34}^2 as integral.

Critical Points and Momentum Map

We can also use the method of compatible Poisson structures to aid in studying this system. Using the matrix $C = \mathrm{diag}(0, 1, a, a+\varepsilon)$ in Proposition 23 gives the equation

$$\psi_{obl}(\lambda) = 2\frac{-2h\lambda^2 + I_1\lambda + I_2}{\lambda(\lambda-1)(\lambda-a)(\lambda-a-\varepsilon)}$$

where $(I_1, I_2) = (G_{obl} + 2ah - (a-1)\ell_{34}^2 + \varepsilon(\ell_{12}^2 + \ell_{13}^2 + \ell_{23}^2), -aG_{obl} - a\varepsilon\ell_{12}^2 - \varepsilon\ell_{13}^2)$. According to Corollary 1, the critical values occurs at the curve $I_2 = \frac{I_1^2}{8h}$ as well as the lines $I_2 = 0$, $I_2 = 2h - I_1$, $I_2 = 2ha^2 - aI_1$ and $I_2 = 2h(a+\varepsilon)^2 - (a+\varepsilon)I_1$ when $\lambda = 0, 1, a, a+\varepsilon$ respectively.

Proposition 34. *The critical values of the momentum map for the reduced oblate integrable system are the curves $\mathcal{O}_1 : G_{obl} = (\sqrt{a} - \sqrt{a-1}\,|\ell_{34}|)^2, \mathcal{O}_2 : G_{obl} = 1 - \ell_{34}^2$ and $\mathcal{O}_3 : G_{obl} = 0$. The momentum map is shown in Figure 3.7 a) with $2h = 1$.*

Proof. Applying Proposition 24 and following a similar calculation as the ellipsoidal case we get:

1) The blue line $\mathcal{O}_3 : G_{obl} = 0$ has $\lambda = 0$ and critical points parametrised by $\boldsymbol{L} = (0, 0, 0, \ell_{23}, \ell_{24}, \ell_{34})$ with $\ell_{23}^2 + \ell_{24}^2 + \ell_{34}^3 = 1$ and $\ell_{34} = l_{obl}$.

2) The red and yellow curve $\mathcal{O}_2 : G_{obl} = 1 - \ell_{34}^2$ has $\lambda = 1$ and the critical points are parametrised by $\boldsymbol{L} = (0, \ell_{13}, \ell_{14}, 0, 0, \ell_{34})$ with $\ell_{13}^2 + \ell_{14}^2 + \ell_{34}^3 = 1$ and $\ell_{34} = l_{obl}$.

3) The cyan curve $\mathcal{O}_1 : G_{obl} = (\sqrt{a} - \sqrt{a-1}\,|\ell_{34}|)^2$ has $\lambda \in [1, a]$ and critical points

$$\boldsymbol{L}_\pm = \left(\frac{a_1\sqrt{\lambda}\sqrt{\lambda-1}}{\sqrt{2}}, \mp\frac{b_2\sqrt{\lambda}\sqrt{a-\lambda}}{\sqrt{2}}, -\frac{b_3\sqrt{\lambda}\sqrt{a-\lambda}}{\sqrt{2}}, \right.$$
$$\left. \mp\frac{b_3\sqrt{\lambda-1}\sqrt{a-\lambda}}{\sqrt{2}}, \frac{b_2\sqrt{\lambda-1}\sqrt{a-\lambda}}{\sqrt{2}}, \mp\frac{a_1(a-\lambda)}{\sqrt{2}} \right)$$

with Plücker relation $a_1^2 = b_2^2 + b_3^2$ and $\boldsymbol{L}\cdot\boldsymbol{L} = \frac{1}{2}a(a-1)(b_2^2+b_3^2) = 1$. This forces $a_1 = \pm\frac{\sqrt{2}}{\sqrt{a(a-1)}}$ and gives a parametrisation $(\ell_{34}, G_{obl}) = \left(\mp\frac{(a-\lambda)}{\sqrt{a(a-1)}}, \frac{\lambda^2}{a}\right)$ in terms of λ. This curve exists only for $0 < |\ell_{34}| < \sqrt{\frac{a-1}{a}}$ which corresponds to a double root $1 < \lambda < a$.

The lines $I_2 = 2ha^2 - aI_1$ and $I_2 = 2h(a+\varepsilon)^2 - (a+\varepsilon)I_1$ both gives the line $\ell_{34} = 0$ (orange and magenta segments in Figure 3.7 b)) which are degenerate critical values for the system (ℓ_{34}^2, G_{obl}) since the vector field generated by ℓ_{34}^2 vanishes at $\ell_{34} = 0$. However, for the oblate integrable system (ℓ_{34}, G_{obl}) the line $\ell_{34} = 0$ becomes a set of regular values (except at three points). Direct computation using the vector fields of (ℓ_{34}, G_{obl}) confirms these results.

■

Let the intersection of $\mathcal{O}_i$ and $\mathcal{O}_j$ be denoted by $o_{ij\pm}$ where the sign is determined by whether the intersection occurs for a positive or negative value of ℓ_{34}. The intersections $o_{12\pm}$ at $(\ell_{34}, G_{obl}) = (\pm\sqrt{\frac{a-1}{a}}, \frac{1}{a})$ are tangential. The other 3 intersections at $o_{11} = (0, a)$ and $o_{23\pm} = (\pm 1, 0)$ are transverse.

The tangential intersections $o_{12\pm}$ are degenerate pitchfork singularities and their fibres are single circles S^1 on $S^2 \times S^2$. The points $o_{23\pm}$ are of elliptic-elliptic type. The point o_{11} is also elliptic-elliptic with 2 critical points $\boldsymbol{L} = (\pm 1, 0, 0, 0, 0, 0)$.

The curves $\mathcal{O}_1, \mathcal{O}_3$ as well as the yellow parts of $\mathcal{O}_2$ are all codimension one elliptic. The fibre of $\mathcal{O}_3$ and the yellow segments are single S^1, while the fibre of $\mathcal{O}_1$ is $2S^1$. The red part of $\mathcal{O}_2$ is codimension one hyperbolic and its fibre is $B \times S^1$.

The fibre of a regular value in chamber I is T^2 while the fibre of a regular value in chamber II is $2T^2$.

Actions

Like in the prolate case, one action for the oblate system $J_{3,obl} := |\ell_{34}|$ is trivial. The other two non trivial actions are

$$J_1 = \frac{2}{\pi}\int_0^{\min(r_1,1)} p_1 ds, \quad J_2 = \frac{2}{\pi}\int_{\max(r_1,1)}^{\min(r_2,a)} p_2 ds$$

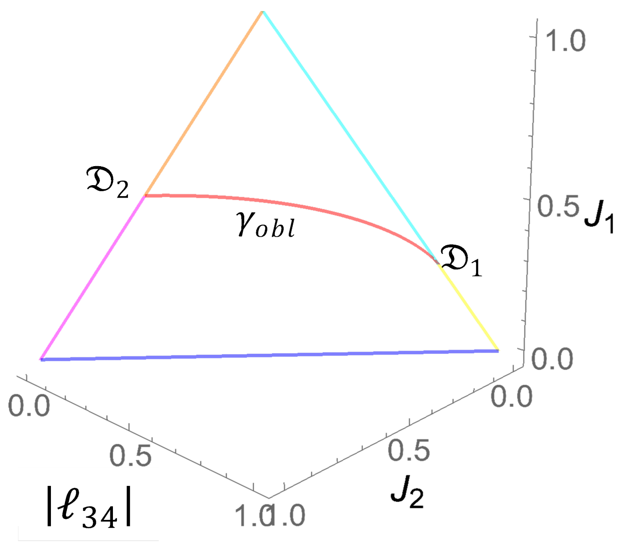

Figure 3.8: Action Map for the oblate system with $a = 2.4$.

where $r_2 \geq 1$ and $0 \leq r_1 \leq r_2 \leq a$. Theorem 28 also applies here. The action map is shown in Figure 3.8. For the interior (red) curve γ_{obl} we have $r_1 = 1$, $r_2 = a(1-l^2) \geq 1$ with $g = 1 - l^2$ for $|l| \leq \sqrt{\frac{a-1}{a}}$. The parametrisation of this curve in terms of the angular momentum l where $|l| \leq \sqrt{\frac{a-1}{a}}$ is given by

$$\gamma_{obl}(l) = \left(\frac{2}{\pi}\left(\sin^{-1}(t_1) + l\tan^{-1}(t_2)\right) - |l|, 1 - \frac{2}{\pi}\left(\sin^{-1}(t_1) + l\tan^{-1}(t_2)\right), |l|\right)$$

where $t_1 = \frac{1}{\sqrt{a(1-l^2)}}$ and $t_2 = \frac{\sqrt{a(1-l^2)-1}}{l}$. Call the intersections of γ_{obl} with the boundary of the action map $\mathfrak{D}_1$ (yellow/cyan) and $\mathfrak{D}_2$ (magenta/orange). The point $\mathfrak{D}_1$ has coordinates $\gamma_{obl}(\sqrt{\frac{a-1}{a}}) = (1-\sqrt{\frac{a-1}{a}}, 0, \sqrt{\frac{a-1}{a}})$, while $\mathfrak{D}_2$ is located at $\gamma_{obl}(0) = \frac{2}{\pi}(\sin^{-1}\left(\frac{1}{\sqrt{a}}\right), \cos^{-1}\left(\frac{1}{\sqrt{a}}\right), 0)$.

3.6.3. Lamé Coordinates

The Lamé system is unusual in a number of ways. In this case we actually need to make use of the fact that the parameters e_i live on the real projective line. This is the reason why this case is not visible in the original normalised ab-parameter space and a blow-up is required. Furthermore, it is a family that has larger symmetry group $SO(3)$. A larger symmetry group is in some sense related to super-integrability, however, since we don't have a Hamiltonian in the reduced system it is harder to define what this means. As we will see after another reduction, this system becomes the Euler top (see the Appendix).

Separation of Variables and Stäckel System

Lamé coordinates are an extension of ellipsoidal coordinates from S^2 onto S^3 and arise from limiting to three equal semi-major axes. As with oblate, there are two cases to consider:

(1 (2 3 4)) and ((1 2 3) 4) which are equivalent. Here we only discuss the (1 (2 3 4)) coordinates which are defined as follows

$$\begin{aligned} x_1^2 &= s_1, & x_3^2 &= \frac{(s_1-1)(f_2-s_2)(f_2-s_3)}{(f_1-f_2)(f_2-f_3)}, \\ x_2^2 &= -\frac{(s_1-1)(s_2-f_1)(s_3-f_1)}{(f_2-f_1)(f_3-f_1)} & x_4^2, &= \frac{(s_1-1)(f_3-s_2)(f_3-s_3)}{(f_2-f_3)(f_3-f_1)}, \end{aligned} \tag{3.45}$$

where $0 \le s_1 \le 1$ and $0 \le f_1 \le s_2 \le f_2 \le s_3 \le f_3$. A possible Stäckel matrix for these coordinates is

$$\Phi_L = \frac{1}{4}\begin{pmatrix} -\frac{1}{(s_1-1)s_1} & -\frac{1}{(s_1-1)^2 s_1} & 0 \\ 0 & \frac{1}{(f_3-s_2)(s_2-f_2)} & \frac{1}{(f_3-s_2)(s_2-f_1)(s_2-f_2)} \\ 0 & \frac{1}{(f_3-s_3)(s_3-f_2)} & \frac{1}{(f_3-s_3)(s_3-f_1)(s_3-f_2)}, \end{pmatrix}. \tag{3.46}$$

with integrals $(2H, 2H - F_L, G_L - f_1(2H - F_L))$ where $(F_L, G_L) = (\ell_{12}^2 + \ell_{13}^2 + \ell_{14}^2, f_1 l_{34}^2 + f_2 l_{24}^2 + f_3 l_{23}^2)$. From (3.46), the separated momenta are given by

$$p_1^2 = \frac{f_L - 2hs_1}{4(s_1-1)^2 s_1}, \qquad p_k^2 = -\frac{(f_L - 2h)s_k + g_L}{4(f_3-s_k)(s_k-f_1)(s_k-f_2)}, \tag{3.47}$$

where $k = 2, 3$ and (f_L, g_L) are functional values of (F_L, G_L). We call the triple $(2H, F_L, G_L)$ on T^*S^3 the Lamé integrable system and (F_L, G_L) the corresponding reduced Lamé integrable system on $S^2 \times S^2$.

The important feature of this case is the appearance of the integral F_L with a $SO(3)$ symmetry given by the rotations generated by ℓ_{1i} using B_L. Similar to the prolate and oblate families, the Lamé system can also be obtained as a limit of the ellipsoidal system.

Lemma 35. *The integrals (F_L, G_L) and separated momenta (3.47) for the Lamé integrable system can be obtained from their ellipsoidal counterparts* (3.13) *and* (3.14)*.*

Proof. A possible limiting process from ellipsoidal to Lamé coordinates is given in [KKM18]. However in this case, it is much simpler to use the transformation

$$\begin{aligned} (e_1, e_2, e_3, e_4) &= \left(-\frac{1}{\varepsilon}, f_1, f_2, f_3\right) \\ (s_1, p_1) &= \left(f_2 - \frac{\tilde{s}_1}{\varepsilon}, \varepsilon\tilde{p}_1\right) \end{aligned} \tag{3.48}$$

for $\varepsilon > 0$ and $\tilde{s}_1 \in [0, 1]$. Applying (3.48) and taking the limit as $\varepsilon \to 0$ immediately gives

$$(\tilde{\eta}_1, \tilde{\eta}_2) = \left(-\frac{2H - F_L}{\varepsilon}, \frac{-G_L}{\varepsilon}\right)$$

The separated momenta are obtained using the same method as in the prolate case.

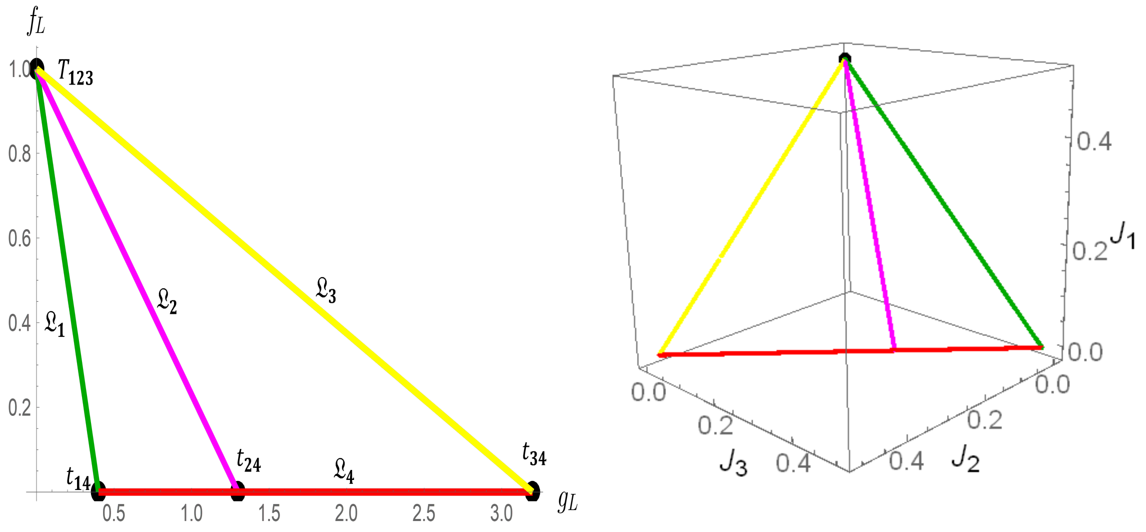

Figure 3.9: a) Momentum map for the Lamé system with $(f_1, f_2, f_3) = (0.4, 1.3, 3.2)$. b) Corresponding action map.

■

In the Lamé limit, the Uhlenbeck integrals F_i are as follows

$$F_1 = -F_L, \quad F_2 = \frac{\ell_{23}^2}{f_1 - f_2} + \frac{\ell_{24}^2}{f_1 - f_3}, \quad F_3 = \frac{\ell_{23}^2}{f_2 - f_1} + \frac{\ell_{34}^2}{f_2 - f_3}, \quad F_4 = \frac{\ell_{24}^2}{f_3 - f_1} + \frac{\ell_{34}^2}{f_3 - f_2}.$$

Note that up to projective transformations, the system only has one parameter $\frac{f_3 - f_1}{f_2 - f_1}$, but we use f_i to keep the higher symmetry.

The vector field of G_L given by $B_L \nabla G_L$ has a semi-direct product stucture: the equations for $\ell_{23}, \ell_{24}, \ell_{34}$ decouple from the others, and they are in fact Euler's equations for the rigid body on $SO(3)$ with moments of inertia given by f_i^{-1}. The equation for the remaining three variables are linear equations with time-varying coefficients given by the solution of Euler's equation.

Critical Points and Momentum Map

Using the matrix $C = \text{diag}(-\frac{1}{\varepsilon}, f_1, f_2, f_3)$ gives the integrals

$$(I_1, I_2) = -\frac{1}{\varepsilon} \left(2h - F_L + O(\varepsilon), G_L + O(\varepsilon)\right).$$

We need consider the $\frac{1}{\varepsilon}$ order term since the limit as $\varepsilon \to 0$ of (I_1, I_2) is infinite.

Proposition 36. *The set of critical values of the momentum map for the Lamé system is composed of four straight lines $\mathfrak{L}_j : F_L = 1 - \frac{1}{f_j} G_L$ for $j = 1, 2, 3$ and $\mathfrak{L}_4 : F_L = 0$. This is shown in Figure 3.9 a).*

Proof. The critical points for the Lamé integrable systems are similar to those for the lines in the ellipsoidal system:

1) The line $\mathfrak{L}_4 : F_L = 0$ is the limit as $\varepsilon \to 0$ of the line $I_2 = -\frac{1}{\varepsilon}(I_1 + \frac{1}{\varepsilon})$ with $\lambda = -\frac{1}{\varepsilon}$ and the critical points are parametrised by $\boldsymbol{L} = (0, 0, 0, \ell_{23}, \ell_{24}, \ell_{34})$ with $\ell_{23}^2 + \ell_{24}^2 + \ell_{34}^2 = 1$ and $f_1\ell_{34}^2 + f_2\ell_{24}^2 + f_3\ell_{23}^2 = g_L$.

2) The line $\mathfrak{L}_1 : F_L = 1 - \frac{1}{f_1}G_L$ is the limit as $\varepsilon \to 0$ of the line $I_2 = f_1(I_1 - f_1)$ with $\lambda = f_1$ and the critical points are parametrised by $\boldsymbol{L} = (0, \ell_{13}, \ell_{14}, 0, 0, \ell_{34})$ with $\ell_{13}^2 + \ell_{14}^2 + \ell_{34}^2 = 1$ and $f_1\ell_{34}^2 = g_L$.

3) The line $\mathfrak{L}_2 : F_L = 1 - \frac{1}{f_2}G_L$ is the limit as $\varepsilon \to 0$ of the line $I_2 = f_2(I_1 - f_2)$ with $\lambda = f_2$ and the critical points are parametrised by $\boldsymbol{L} = (\ell_{12}, 0, \ell_{14}, 0, \ell_{24}, 0)$ with $\ell_{12}^2 + \ell_{14}^2 + \ell_{24}^2 = 1$ and $f_2\ell_{24}^2 = g_L$.

4) The line $\mathfrak{L}_3 : F_L = 1 - \frac{1}{f_3}G_L$ is the limit as $\varepsilon \to 0$ of the line $I_2 = f_3(I_1 - f_3)$ with $\lambda = f_3$ and the critical points are parametrised by $\boldsymbol{L} = (\ell_{12}, \ell_{13}, 0, \ell_{23}, 0, 0)$ with $\ell_{12}^2 + \ell_{13}^2 + \ell_{23}^2 = 1$ and $f_3\ell_{23}^2 = g_L$.

The curve $I_2 = \frac{I_1^2}{8h}$ for $\lambda \in [f_1, f_2]$ shrinks to the degenerate point $(F_L, G_L) = (1, 0)$ in the limit $\varepsilon \to 0$.

■

Let the intersections of $\mathfrak{L}_i$ and $\mathfrak{L}_j$ be denoted by t_{ij} and the three way intersection of $\mathfrak{L}_1$, $\mathfrak{L}_2$, $\mathfrak{L}_3$ by T_{123}. The intersections t_{14} and t_{34} are elliptic-elliptic critical values with 2 points in their fibres $2S^1$ on $S^2 \times S^2$. The point t_{24} is elliptic hyperbolic and its fibre is C_2.

Lemma 37. *The three-way intersection T_{123} at $(F_L, G_L) = (1, 0)$ is a degenerate singularity of spherical type.*

Proof. The linearisation of the vector field generated by F_L and G_L is $\nabla_{\boldsymbol{L}} B_{\boldsymbol{L}}(\alpha \nabla_{\boldsymbol{L}} F_L + \beta \nabla_{\boldsymbol{L}} G_L)$. At the three-way intersection T_{123}, this matrix becomes

$$\begin{pmatrix} \mathbf{0} & \begin{matrix} 2(\alpha - f_3\beta)\ell_{13} & 2(\alpha - f_2\beta)\ell_{14} & 0 \\ -2(\alpha - f_3\beta)\ell_{12} & 0 & 2(\alpha - f_1\beta)\ell_{14} \\ 0 & -2(\alpha - f_2\beta)\ell_{12} & -2(\alpha - f_1\beta)\ell_{13} \end{matrix} \\ \mathbf{0} & \mathbf{0} \end{pmatrix} \tag{3.49}$$

where $\mathbf{0}$ is a 3×3 matrix of all zeros. The eigenvalue of (3.49) is $(0, 0, 0, 0, 0, 0)$ meaning that T_{123} is a degenerate critical value. The rank of the differential of the moment map drops by 1 at T_{123}. This is known as a spherical type singularity studied in the thesis [Ker22]. Systems with a spherical type singularity are characterised by the presence of a globally defined, continuous but not smooth action. The fibre of a spherical type singularity is diffeomorphic to a product of spheres. In this case the preimage of T_{123} is S^2 and every point in this fibre is critical.

■

It was shown in [Ker22] that the geodesic flow on S^n in polyspherical coordinates gives rise to systems containing a spherical type singularity. While the Lamé coordinate system is not polyspherical, the reduced Lamé integrable system is an example of a system that has a spherical singularity that was not studied in [Ker22]. Since the Lamé coordinate system is obtained by extending the ellipsoidal coordinates on S^2 to S^3, we can conjecture that systems originating from the geodesic flow on S^n in coordinates obtained from extending a coordinate system from S^k to S^n where $2 \leq k < n$ will contain a spherical type singularity.

Actions

The actions of the Lamé system are given by

$$J_1 = \frac{2}{\pi}\int_0^{f_L} p_1 \qquad J_2 = \frac{2}{\pi}\int_{f_1}^{\min(r_2,f_2)} p_2 ds \qquad J_3 = \frac{2}{\pi}\int_{\max(f_2,r_2)}^{f_3} p_3 ds$$

where $r_2 = \frac{g_L}{1-f_L}$. Theorem 28 applies for the Lamé system also. The first action evaluates to

$$J_1 = 1 - \sqrt{1-f_L}. \tag{3.50}$$

Notice that F_L has a vector field $B_{\boldsymbol{L}}\nabla F_L$ has a flow that is the rotation of $(\ell_{12}, \ell_{13}, \ell_{14})$ about the fixed axis given by $(\ell_{34}, -\ell_{24}, \ell_{23})$. The frequency of this rotation is given by the length of the axis, and is hence not constant.

Lemma 38. *$J_1 = 1 - \sqrt{1-F_L}$ is an almost global S^1-action.*

Proof. The vector field $B_{\boldsymbol{L}}\nabla J_1$ has periodic flow which is given by the rotation about the same axis as the flow of F_L, but here the axis is normalised because we need to divide by $\sqrt{1-F_L}$ and using the Casimir $2h = 1$ this means to divide by the length of the axis. It is only "almost" global because when $2h - F_L = \ell_{34}^2 + \ell_{24}^2 + \ell_{23}^2 = 0$ the normalisation factor vanishes and the vector field is not defined. Because of $2h = 1$ this occurs on the sphere S^2 given by $\ell_{12}^2 + \ell_{13}^2 + \ell_{14}^2 = 1$.

■

Note that (3.50) means that lines of constant f_L correspond to lines of constant J_1 in action space. In general, we have

Lemma 39. *Straight lines in the image of the momentum map (F_L, G_L) of the reduced Lamé system on $S^2 \times S^2$ given by $F_L = 1 - \frac{1}{r_2} G_L$ maps to straight lines in action space.*

Proof. Observe that

$$J_2 = \sqrt{1 - f_L} \int_{f_1}^{\gamma} \sqrt{\frac{r_2 - s}{(s - f_1)(s - f_2)(s - f_3)}} ds = (1 - J_1)\mathcal{F}(r_2)$$

where $\gamma = \min(r_2, f_2)$, $r_2 = \frac{g_L}{1 - f_L}$ and $\mathcal{F}$ is function of r_2 only. Since $J_3 = 1 - J_1 - J_2$, this implies that the image of a straight line $F_L = 1 - \frac{1}{r_2} G_L$ with constant slope $\frac{1}{r_2}$ under the action map is again a straight line.

■

Figure 3.9 b) shows an example of the action map. Let the magenta line in the interior of the action map be denoted by $\mathfrak{L}_M$. This has parameterisation

$$(J_1, J_2, J_3) = (J_1, \frac{2}{\pi}(1 - J_{1,L}) \sin^{-1} \Delta, \frac{2}{\pi}(1 - J_{1,L}) \cos^{-1} \Delta)$$

where $\Delta = \sqrt{\frac{f_1 - f_2}{f_1 - f_3}}$. The line intersects the boundary of the action map at $(1, 0, 0)$ and $\frac{2}{\pi}(0, \sin^{-1}(\Delta), \cos^{-1}(\Delta))$.

The fact that lines of constant f_L and lines through T_{123} are mapped to straight lines does not imply it is a linear map, because the map along these lines is determined by the non-linear map $\mathcal{F}$.

Since away from $f_l = 1$, the action variable J_1 is defined we can consider reduction with respect to the flow of J_1 on levels with $0 < f_L < 1$. Fixing the action and identifying the corresponding angle variable to a point gives the action J_2 for that constant value of f_L, and up to an overall constant factor this is the action of the Euler top.

3.6.4. Spherical Coordinates

Spherical coordinates (or rather poly-spherical coordinates) correspond to the case where simultaneously there is an $SO(2)$ and an $SO(3)$ symmetry. Accordingly we do have a global S^1 action. However, the induced integrable system on $S^2 \times S^2$ is not semi-toric because it has a degenerate point, which corresponds to the critical values at which the almost global action is not differentiable.

Separation of Variables

The two forms of spherical coordinates are found by setting $f_1 = f_2$ or $f_2 = f_3$ in Lamé coordinates. We call these the 12 and 23 spherical coordinates. The two systems are equivalent by a permutation of coordinates. These can also be obtained by setting $a = 1$ in prolate and oblate coordinates, respectively. The 23−spherical coordinate system $(1\ (2\ (3\ 4)))$ is defined by

$$\begin{aligned} x_1^2 &= s_1, & x_2^2 &= (1-s_1)\, s_2, \\ x_3^2 &= (1-s_1)(1-s_2)\, s_3, & x_4^2 &= (1-s_1)(1-s_2)(1-s_3)\,, \end{aligned} \tag{3.51}$$

where $0 \le s_k \le 1$ and $k = 1, 2, 3$. Due to the simplicity of these coordinates, we can manually separate the corresponding Hamilton-Jacobi equation. The geodesic Hamiltonian can be expressed as

$$H_{23} = \frac{2\left(p_2^2\,(s_2-1)\,s_2 - p_1^2\,(s_1-1)^{\,2}s_1 - \frac{p_3^2(s_3-1)s_3}{s_2-1}\right)}{s_1-1}. \tag{3.52}$$

The integrals are $(2H_{23}, \ell_{34}, G_{23})$ with separated momenta

$$p_1^2 = \frac{g_{23} - 2hs_1}{4s_1\,(s_1-1)^2} \qquad p_2^2 = \frac{(g_{23}-2h)(s_2-1) - l_{34}^2}{4s_2\,(s_2-1)^2} \qquad p_3^2 = \frac{l_{34}^2}{4s_3\,(1-s_3)} \tag{3.53}$$

where $G_{23} = \ell_{12}^2 + \ell_{13}^2 + \ell_{14}^2$ and (l_{34}, g_{23}) are functional values of (ℓ_{34}^2, G_{23}).

To obtain (ℓ_{34}, G_{23}) and (3.53) from the Lamé system, we set $(f_3, s_3, p_3) = (f_2 + \varepsilon, f_2 + \varepsilon\tilde{s}_3, \tilde{p}_3/\varepsilon)$ where $\tilde{s}_3 \in [0, 1]$ and normalise $(f_1, f_2) = (0, 1)$. To come from oblate, we let $(a, s_3, p_3) = (1 + \varepsilon, 1 + \varepsilon\tilde{s}_3, \tilde{p}_3/\varepsilon)$.

Critical Points and Momentum Map

The critical points and values are easily obtained by direct computation to give

Proposition 40. *The image of momentum map for the* 23−*spherical system* (ℓ_{34}, G_{23}) *with* $2h = 1$ *has critical values* $\mathfrak{C}_1 : G_{23} = 1 - \ell_{34}^2$ *and* $\mathfrak{C}_2 : G_{23} = 0$ *which are both codimension one elliptic (see Figure 3.10).*

Proof. The computation of critical points and values are straight forward for this system.

■

The fibre of a regular value on $S^2 \times S^2$ is a torus T^2 with multiplicity one. The fibres along $\mathfrak{C}_1$ and $\mathfrak{C}_2$ are single S^1. The intersections of $\mathfrak{C}_1$ and $\mathfrak{C}_2$ are codimension 2 elliptic points and have 1 critical point in their fibres. The linearisation $\nabla_{\boldsymbol{L}} B_{\boldsymbol{L}}(\alpha\nabla_{\boldsymbol{L}} G_{23} + \beta\nabla_{\boldsymbol{L}}\ell_{34})$ has eigenvalues $(0, 0, -i\beta, i\beta, -i\beta, i\beta)$ at $D_{23} = (0, 1)$ making the peak of the parabola D_{23} a degenerate singularity. Similar to the Lamé system the rank of the differential of the moment map drops by 1 at D_{23} and it's fibre is S^2. This is also an example of a spherical type singularity. Spherical coordinates is a type of polyspherical coordinates and these have been studied in detail in [Ker22].

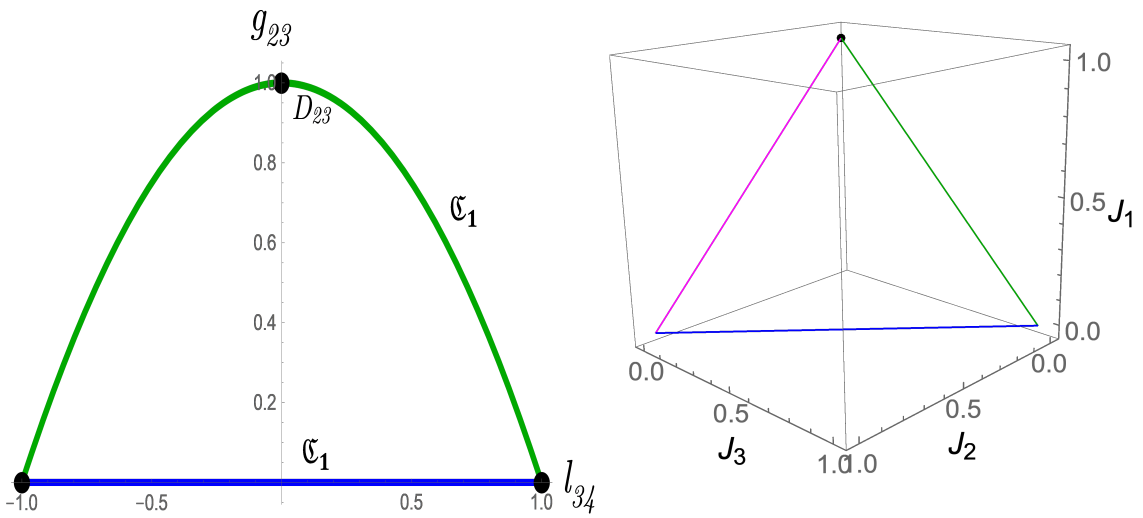

Figure 3.10: a) Momentum map and b) Action map for the 23-spherical system.

In the limit $a \to 1$, the bifurcation diagram for the oblate coordinates in Figure 3.7 a) degenerates to Figure 3.10 a). In particular, the elliptic-elliptic point o_{11} collides with the hyperbolic line $\mathcal{O}_2$ and becomes degenerate. Similarly, setting $f_2 = f_3$ in the Lamé system causes the elliptic-hyperbolic point t_{24} to collide with the elliptic-elliptic point at t_{34} while T_{123} remains degenerate.

Actions

The action variables for the 23−spherical system are given by

$$J_1 = \frac{2}{\pi}\int_0^{r_1} p_1(s)ds \qquad J_2 = \frac{2}{\pi}\int_0^{r_2} p_2(s)ds \qquad J_3 = |\ell_{34}|$$

where $0 \leq r_1 = g_{23} \leq 1$ and $0 \leq r_2 = 1 - \frac{l_{23}^2}{1-g_{23}} \leq 1$. We can simplify the non trivial actions to

$$J_1 = 1 - \sqrt{1 - g_{23}} \quad J_2 = \sqrt{1 - g_{23}} - |l_{34}|.$$

The action map is shown in Figure 3.10 b). Note that $(\ell_{34}, \sqrt{1 - G_{23}})$ defines continuous global action variables that are not differentiable at $G_{23} = 1$. This is a system obtained from toric degeneration, see [Ker22].

3.6.5. Cylindrical Coordinates

The coordinate system with the highest symmetry has two global S^1 action, and there is only a single point in the Stasheff polytope for which this happens. The corresponding reduced system on $S^2 \times S^2$ is toric.

Separation of Variables

The cylindrical coordinates (also called Hopf coordinates) $((1\,2)\,(3\,4))$ are a further degeneration of the oblate coordinates obtained by setting both $e_1 = e_2$ and $e_3 = e_4$. Specifically, the transformation $(e_2, e_4) \to (e_1 + \varepsilon, e_3 + \varepsilon)$ along with $(s_1, p_1, s_3, p_3) \to (e_1 + \varepsilon\tilde{s}_1, \tilde{p_1}/\varepsilon, e_3 + \varepsilon\tilde{s}_3, \tilde{p_3}/\varepsilon)$ gives the following relationship between Cartesian coordinates and cylindrical coordinates:

$$\begin{aligned} x_1^2 &= s_1 s_2, & x_2^2 &= s_2\left(1 - s_1\right), \\ x_3^2 &= s_3\left(1 - s_2\right), & x_4^2 &= \left(1 - s_2\right)\left(1 - s_3\right), \end{aligned}$$

where $0 \le s_k \le 1$ and $k = 1, 2, 3$. The geodesic Hamiltonian in these coordinates is

$$H_{Cyl} = -\frac{2p_1^2\left(s_1 - 1\right)s_1}{s_2} - 2p_2^2\left(s_2 - 1\right)s_2 + \frac{2p_3^2\left(s_3 - 1\right)s_3}{s_2 - 1}$$

which trivially separates to give integrals $(H_{Cyl}, \ell_{34}^2, \ell_{12}^2)$ The separated equations are

$$p_2^2 = \frac{l_{12}^2(s_2 - 1) - s_2\left(2h(s_2 - 1) + l_{34}^2\right)}{4(s_2 - 1)^2 s_2^2} \qquad p_k^2 = \frac{l_\nu^2}{4s_k(1 - s_k)} \tag{3.54}$$

where $\nu = 12$ if $k = 1$, $\nu = 34$ if $k = 3$ and l_ν denoted the functional value of ℓ_ν.

Critical Points and Momentum map

Proposition 41. *The bifurcation diagram for the cylindrical system (ℓ_{12}, ℓ_{34}) on $S^2 \times S^2$ with $2h = 1$ is composed of 4 straight lines $\ell_{34} = \pm(1 \pm \ell_{12})$ which intersect transversally at $(\pm 1, 0)$ and $(0, \pm 1)$ (see Figure 3.11).*

The fibre of a regular point on $S^2 \times S^2$ is T^2 with multiplicity one. The lines are all codimension one elliptic and their fibres are single S^1. The intersections of the lines are elliptic-elliptic critical values with a single critical point in their fibres.

Actions

The trivial actions for the cylindrical system are $(J_1, J_3) = (|\ell_{12}|, |\ell_{34}|)$ while the "non trivial" action is easily determined by $J_1 + J_2 + J_3 = 1$. The action map is shown in Figure 3.11 b). The relation between the symmetry reduced actions $|\ell_{12}|$ and $|\ell_{34}|$ and the global S^1 actions is to forget the absolute value sign. In this way 4 copies of the right triangle in J_1, J_3 are glued together to a diamond in ℓ_{12}, ℓ_{34}.

Proposition 42. *The system (X_1, Y_1) is a toric system on $S^2 \times S^2$ where X_1 and Y_1 are defined in* (3.20).

Proof. Both ℓ_{12} and ℓ_{34} define smooth global S^1 action on $S^2 \times S^2$. However, the torus action (ℓ_{12}, ℓ_{34}) is not effective. Note that ℓ_{ij} is the generator of rotation in the $x_i x_j$-plane

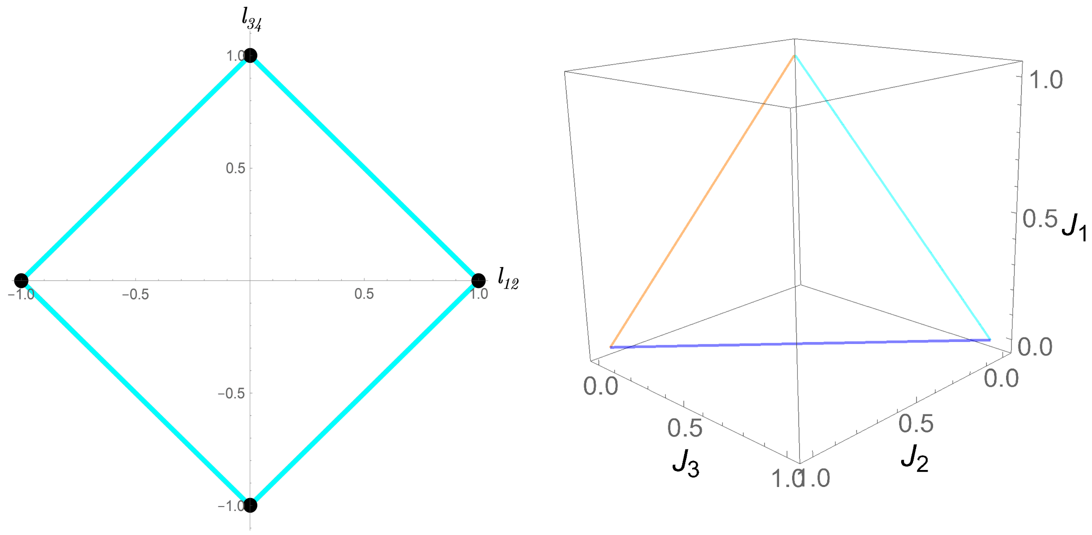

Figure 3.11: (a) Momentum map and (b) action map of the cylindrical system.

represented by $\exp(it_{ij}\hat{\boldsymbol{x}}_i \wedge \hat{\boldsymbol{x}}_j)$ where $\hat{\boldsymbol{x}}_i$ is the unit vector in the x_i axis. The action on the momenta $\boldsymbol{y}$ is the same. A rotation by $t_{ij} = \pi$ in the $x_i x_j$-plane has the effect

$$x_i \mapsto -x_i, \qquad y_i \mapsto -y_i,$$
$$x_j \mapsto -x_j, \qquad y_j \mapsto -y_j,$$

on T^*S^3. This induces the map

$$\ell_{ij} \mapsto \ell_{ij}, \qquad \ell_{mn} \mapsto \ell_{mn},$$

for i, j, m, n all distinct, and

$$\ell_{ik} \mapsto -\ell_{ik}, \qquad \ell_{kj} \mapsto -\ell_{kj},$$

for all $k \neq i, j$. In particular, the action with $t_{12} = \pi$ and $t_{34} = \pi$ both generate the same map

$$(\boldsymbol{X}, \boldsymbol{Y}) \mapsto (X_1, -X_2, -X_3, Y_1, -Y_2, -Y_3) \tag{3.55}$$

on $S^2 \times S^2$. Since the flows of ℓ_{12} and ℓ_{34} commute and (3.55) is an involution, we see that $(t_{12}, t_{34}) = (\pi, \pi)$ is the identity on $S^2 \times S^2$, so the action is not effective. By taking half of the sum and difference, we see that $(X_1, Y_1) = \frac{1}{2}(\ell_{12} + \ell_{34}, \ell_{12} - \ell_{34})$ is faithful with 2π period giving us a toric system on $S^2 \times S^2$. The image of the momentum map of (X_1, Y_1) is the unit square - the standard Delzant polytope for $S^2 \times S^2$.

Note that the torus action of (ℓ_{12}, ℓ_{34}) is effective on T^*S^3 as $(t_{12}, t_{34}) = (\pi, \pi)$ gives $\boldsymbol{x} \mapsto -\boldsymbol{x}$ and $\boldsymbol{y} \mapsto -\boldsymbol{y}$. However, the points $(\boldsymbol{x}, \boldsymbol{y})$ and $(-\boldsymbol{x}, -\boldsymbol{y})$ are anti-podal points on the same great circle and thus become the same point on $S^2 \times S^2$ after reduction.

■

3.7. Conclusion

The main novelty in this paper is the construction of a natural family of integrable system on $S^2 \times S^2$ in section 3.4, and the analysis of its Liouville foliation in section 3.6. It turns out that many properties of the reduced system are visible already in one way or another in the original Stäckel system on T^*S^3. However, it should be pointed out that the upstairs system does not even have a natural Liouville foliation because it is superintegrable, and hence dynamically does not possess invariant tori, but just periodic orbits. After reduction by the flow of the Hamiltonian, which after extracting the square root is a global S^1 action, an integrable system on $S^2 \times S^2$ is obtained. The reduced system is Lie-Poisson with Lie-algebra $\mathfrak{so}(4)$.

Since the reduction is done by the flow of the Hamiltonian the reduced system does not have a Hamiltonian any more, it just has commuting integrals. The definition of Liouville integrable system does not require a Hamiltonian, and the foliation into tori as defined by the integrals is defined independently of a Hamiltonian. What is missing is the possibility to define the Hamiltonian vector field which induces a flow on these tori. But this is not necessary in order to study the equivalence of Liouville foliations of integrable systems.

At first it may be surprising that in the Liouville-Arnold theorem the existence of action-angle variables near a regular torus does not need a Hamiltonian either. In fact, the action-angle variables are such that all of the integrals can be expressed as functions of the action variables. Moreover, considering diffeomorphism of the integrals changes the integrals, but does not change the action variables. We saw this explicitly for a restricted class of transformations of the integrals in our case. Since after reduction by the Hamiltonian there is no distinguished function anymore, the focus is fully on the action variables. For the foliation it makes sense to consider leaf-preserving homeomorphisms or diffeomorphisms, but from the point of view of the action variables the natural class is symplectomorphisms. Since the reduced symplectic manifold is compact the image of the momentum map is compact as well, and we have shown that the image of the action map (appropriately modified so that it is continuous!) is a right triangle. This triangle is rigid, which means that it is the same for the whole family. What does change are the position and organisation of action values in the triangle that correspond to critical values of the momentum map. These play the role of the height invariant, and in fact for the prolate system which is semi-toric these turn into the height invariant.

The Liouville-Arnold theorem holds near regular tori, and can be extended to open subsets of phase space bounded by separatrices. Only in rare cases are there no separatrices, essentially this means that the system is toric. But most integrable systems do have singular fibres that are not just tori, and the classification of integrable system needs to take these into account. It is crucial to note that the actions of the action-angle variables can in general not be extended globally in phase space. If this is possible we call them global S^1 actions. Instead of S^1 action we may also speak of a global $SO(2)$ symmetry. A slightly less optimal situation occurs for a global $SO(3)$ symmetry, which leads to almost global S^1 actions, as described for the Lamé system, with an almost global S^1 action and a spherical type singularity. Examples of global S^1 actions do appear in our family through degenerations, and when they do appear they unfold the action map into the polygon invariant in the semi-toric case (prolate system) and into the Delzant polygon in the toric case (cylindrical system).

Thus, for our family we have some analogues of important symplectic invariants, namely a convex polygon and generalisations of the height invariant. Certainly the semi-global symplectic invariants would need to be added, and at least in principle this is understood for the hyperbolic-hyperbolic point in the ellipsoidal family [DN07], and generalisations to elliptic-hyperbolic points, degenerate points and the rank 1 hyperbolic lines would need to be worked out. The interesting question is what kind of global invariants (like the twisting index invariant for semi-toric systems) would need to be added to the list so that it becomes the complete list of global symplectic invariants.

Chapter 4

The Harmonic Lagrange Top and the Confluent Heun Equation

Abstract

The harmonic Lagrange top is the Lagrange top plus a quadratic (harmonic) potential term. We describe the top in the space fixed frame using a global description with a Poisson structure on T^*S^3. This global description naturally leads to a rational parametrisation of the set of critical values of the energy-momentum map. We show that there are 4 different topological types for generic parameter values. The quantum mechanics of the harmonic Lagrange top is described by the most general confluent Heun equation (also known as the generalised spheroidal wave equation). We derive formulas for an infinite pentadiagonal symmetric matrix representing the Hamiltonian from which the spectrum is computed.

4.1. Introduction

The Lagrange top is a prime example of classical mechanics. Over centuries, it has been studied starting with Euler and Lagrange, and interest in its various features is blossoming again and again. Almost every modern development in mechanics has lead to new insights about the Lagrange top. Before we attempt to describe the place of the Lagrange top in mechanics in the remainder of this introduction, let us formulate our main observation: the quantum mechanics of the harmonic Lagrange top is described by the most general confluent Heun equation (also known as the generalised spheroidal wave equation). By harmonic Lagrange top we mean the Lagrange top with an added harmonic (i.e. quadratic) potential. It provides an example of the subcritical and the supercritical Hamiltonian Hopf bifurcation and hence the quantisation of these bifurcations. The bulk of the paper is devoted to the description of the classical integrable system.

Rigid body dynamics is treated in most mechanics textbooks, e.g. [Whi37, LL84, Arn78, Gol80, MR94]. Of the books devoted specifically to rigid body dynamics we highlight the monumental volumes of Klein & Sommerfeld [KS10] and the recent addition by Borisov & Mamayev [BM18]. Many special cases of rigid body dynamics including the Lagrange top are completely integrable Hamiltonian systems, and as such have been studied in detail in Bolsinov & Fomenko [BF04] and Cushman & Bates [CB15]. For all the references we inevitably missed in this introduction we refer to the extensive bibliography in [BM18].

In modern mechanics the (energy)-momentum map plays a central role. Singularity theory's swallowtail was found as the set of critical values of the energy-momentum map of the Lagrange top in [CK85], also see [CB15]. The meaning of the swallowtail from the point of view of bifurcation theory, specifically the supercritical Hamiltonian Hopf bifurcation in the Lagrange top was described in [CvdM90]. The fact that the swallowtail may make the set of regular values in the image of the energy-momentum map non-simply connected is the essential observation that explains why the Lagrange top does not possess global action variables [Dui80, CD88]. Hamiltonian monodromy of the Lagrange top is described in [Viv03]. Integrable discretisations of the integrable Lagrange top were found in [BS99]. The complex algebraic geometry of the Lagrange top was described in [GZ98], and its bi-Hamiltonian structure in [Tsi08]. In KAM theory perturbations of the Lagrange top give a beautiful example worked out in detail in [HBHN06].

The quantisation of the symmetric top was first done in the early days of quantum mechanics [Rei26] and leads to a hypergeometric equation, also see [LL77]. The study of polar molecules in an electric field leads to a Hamiltonian that is equivalent to the Lagrange top. In the physics literature this is referred to as the Stark effect, and was first studied in [Sch55]. Matrix elements for the numerical computation of the spectrum were given in [Shi63], and nearly 30 years later again in [HO91].

The discovery of quantum monodromy [Dui80] was in the smaller brother of the Lagrange top, the spherical pendulum, in [CD88]. The quantum monodromy in the Lagrange top itself has been studied in [KR03].

While so-called semi-toric systems with two degrees of freedom (somewhat like the spherical pendulum) are now in a precise sense completely understood classically [PN09] and quantum mechanically [FS21], the Lagrange top is still out of reach from this point of view. We should mention that many generalisations of the spherical pendulum have been studied, in particular the magnetic spherical pendulum [CB95, CB15], also see [Sak02], and the quadratic spherical pendulum [Zou92, Efs05]. The combination of both is the harmonic Lagrange top, which is the object of this paper. To our knowledge, it has not been considered in the literature in full generality. The so-called Kirchhoff top which has only quadratic terms in the potential has been studied in [Bog92, BZ93]. A general potential with linear and quadratic terms was considered in [Han97] from the point of view of perturbation theory of the Euler top. The harmonic Lagrange top can also be considered as an example of the general idea described in [DP16], where a semi-toric system is deformed preserving integrability. In particular, we find that the harmonic Lagrange top exhibits the subcritical and the supercritical Hamiltonian Hopf bifurcations.

As mentioned in the beginning, we want to draw attention to the fact that the quantisation of the Lagrange top leads to the confluent Heun equation. The Heun equation is a Fuchsian equation with 4 regular singular points, thus generalising the hypergeometric equation by one singularity, see, e.g., [Ars64, RA95, SL00, DLMF]. An important physical application of the confluent Heun equation appears in the perturbation theory of a rotating black hole in general relativity [Teu73, PT73, Lea86]. In this context, expansions in terms of Jacobi polynomials have been given in [FC77], and series expansion for small potential are given in [Sei89]. As we show below, the harmonic Lagrange top leads to the most general confluent Heun equation, unlike the above application in general relativity, which does not have enough parameters.

After this work was completed we learned that a physical interpretation for the additional quadratic ("harmonic") term in the potential is provided by considering the Lagrange top on a vibrating suspension [Mar09, Mar12]. In this context the focus-focus points in the model have been analysed in [BRS20], also see [BI22]. Some of our results about the threads of focus-focus points in the bifurcation diagram overlap with [BRS20], also see [RS21].

The structure of this paper is as follows. We give an introduction to the Lagrange top in the next section, where we emphasise the description in the spatial frame using quaternions and the corresponding Poisson structure. The various periodic flows and their differences when considering $T^*SO(3)$ or T^*S^3 (the quaternions) is discussed in section 3, and the reductions to two degrees of freedom in section 4. The traditional description in Euler angles is recalled in section 5, which is needed for the quantisation. The main classical results are the description of the critical points in phase space and the corresponding critical values in the image of the energy-momentum map. There are 4 different cases, with one thread (the original Lagrange top), with two threads, with a triangular tube instead of the thread, and a triangular tube shrinking to a thread. In the final section we show that the quantum harmonic Lagrange top leads to the most general confluent Heun equation and compute the spectrum, which is displayed overlayed with (slices) of the classical energy-momentum map. A new method for the computation of the spectrum is presented.

4.2. Heavy Symmetric Top

Consider a general rigid body with a fixed point. Assume that the symmetric inertia tensor I with respect to that point has three distinct eigenvalues I_1, I_2, I_3, the moments of inertia, and assume that a body frame has been chosen in which the tensor of inertia is diagonal. For the symmetric top with $I_1 = I_2$ the location of the corresponding basis vectors is only defined up to a rotation about the symmetry axis (or figure axis) of the body. In the spatial coordinate frame, the z-axis is parallel to the direction of gravity. Let $\boldsymbol{V}$ be the coordinate vector of a point in the body frame. The orthogonal matrix $R \in SO(3)$ describes how this point is moving in time when viewed in the spatial frame, $\boldsymbol{v} = R\boldsymbol{V}$.

For the free rigid body (Euler top), the fixed point of the body is the centre of gravity of the body. For the Lagrange top, the centre of gravity is on the figure axis but does not coincide with the fixed point of the body, which also lies on said axis. Denote the unit vector along the figure axis of the top by $\boldsymbol{a}$ (in the spatial frame), then the potential energy in the field of gravity is $V = c_1 a_z$. In this paper, we are going to study the more general case

$$V(a_z) = c_1 a_z + c_2 a_z^2 \,.$$

The angular velocity $\boldsymbol{\Omega}$ in the body frame is defined through R by $R^t \dot{R}\boldsymbol{V} = \Omega \times \boldsymbol{V}$ for any vector $\boldsymbol{V}$, or, equivalently, by $\hat{\boldsymbol{\Omega}} = R^t \dot{R}$. The kinetic energy of the rigid body is

$$T = \frac{1}{2}\boldsymbol{\Omega} \cdot I\boldsymbol{\Omega}$$

where I is the diagonal tensor of inertia and $\cdot$ denotes the Euclidean scalar product.

The angular momentum vector is defined by $\boldsymbol{L} = I\boldsymbol{\Omega}$. For the free rigid body $\boldsymbol{l} = R\boldsymbol{L}$ is a constant vector. For the Lagrange top instead there are only two conserved quantities given by

$$l_z = \boldsymbol{l} \cdot \boldsymbol{e}_z, \quad L_3 = \boldsymbol{L} \cdot \boldsymbol{e}_3 = R^t \boldsymbol{l} \cdot \boldsymbol{e}_3 = \boldsymbol{l} \cdot R\boldsymbol{e}_3 = \boldsymbol{l} \cdot \boldsymbol{a} \,.$$

In the spatial frame we have $\boldsymbol{e}_z = (0,0,1)^t$ and in the body frame we have $\boldsymbol{e}_3 = (0,0,1)^t$.

A beautiful global description of the dynamics of rigid bodies uses quaternions $\boldsymbol{x} = (x_0, x_1, x_2, x_3)$ which are coordinates on the double cover of $SO(3)$ which is $S^3 \in \mathbb{R}^4$ given by $x_0^2 + x_1^2 + x_2^2 + x_3^2 = 1$. Define

$$\boldsymbol{x}_\pm = \begin{pmatrix} x_1 & -x_0 & \mp x_3 & \pm x_2 \\ x_2 & \pm x_3 & -x_0 & \mp x_1 \\ x_3 & \mp x_2 & \pm x_1 & -x_0 \end{pmatrix}$$

which satisfy $\boldsymbol{x}_+ \boldsymbol{x}_+^t = id$, $\boldsymbol{x}_- \boldsymbol{x}_-^t = id$, $\boldsymbol{x}_+^t \boldsymbol{x}_+ \boldsymbol{x}_-^t = \boldsymbol{x}_-^t$, and $\boldsymbol{x}_-^t \boldsymbol{x}_- \boldsymbol{x}_+^t = \boldsymbol{x}_+^t$ on the unit sphere. Then an orthogonal 3×3 matrix is given by $R = \boldsymbol{x}_+ \boldsymbol{x}_-^t$ and the last two identities in the previous sentence become $\boldsymbol{x}_+^t R = \boldsymbol{x}_-^t$ and $\boldsymbol{x}_-^t R^t = \boldsymbol{x}_+^t$. The matrices $\boldsymbol{x}_\pm$ relate the angular velocities to the tangent vector of the sphere $\dot{\boldsymbol{x}}$ by $\boldsymbol{\Omega} = 2\boldsymbol{x}_- \dot{\boldsymbol{x}}$ and $\boldsymbol{\omega} = 2\boldsymbol{x}_+ \dot{\boldsymbol{x}}$, see, e.g., [Whi37, Section 16]. To see this, differentiate R with respect to time, observe that $\dot{\boldsymbol{x}}_+ \boldsymbol{x}_-^t = \boldsymbol{x}_+ \dot{\boldsymbol{x}}_-^t$, and use $R^t \boldsymbol{x}_+ = \boldsymbol{x}_-$. Substituting $\boldsymbol{\Omega} = 2\boldsymbol{x}_- \dot{\boldsymbol{x}}$ into the expression for T gives

$$T = 2\dot{\boldsymbol{x}}^t (\boldsymbol{x}_-^t I \boldsymbol{x}_-) \dot{\boldsymbol{x}} \,.$$

Differentiating with respect to $\dot{\boldsymbol{x}}$ gives the conjugate momenta $\boldsymbol{p} = 4(\boldsymbol{x}_-^t I \boldsymbol{x}_-)\dot{\boldsymbol{x}}$ on T^*S^3. Using $\boldsymbol{L} = I\boldsymbol{\Omega} = 2I\boldsymbol{x}_-\dot{\boldsymbol{x}}$ we see that

$$\boldsymbol{L} = 2I\boldsymbol{x}_-\dot{\boldsymbol{x}} = 2(\boldsymbol{x}_-\boldsymbol{x}_-^t)I\boldsymbol{x}_-\dot{\boldsymbol{x}} = \frac{1}{2}\boldsymbol{x}_-\boldsymbol{p}\,.$$

Similarly, we have $\boldsymbol{l} = \frac{1}{2}\boldsymbol{x}_+\boldsymbol{p}$. It is valid to use the canonical bracket between $\boldsymbol{x}$ and $\boldsymbol{p}$ because the resulting Hamiltonian automatically preserves $|\boldsymbol{x}| = 1$ and $\boldsymbol{x}\cdot\boldsymbol{p} = 0$.

Now changing from canonical variables $(\boldsymbol{x}, \boldsymbol{p})$ to non-canonical variables $(\boldsymbol{x}, \boldsymbol{L})$ gives the Lie-Poisson structure in the body frame as [BM97, BM18]

$$B_- = \begin{pmatrix} 0 & \frac{1}{2}\boldsymbol{x}_-^t \\ -\frac{1}{2}\boldsymbol{x}_- & \hat{\boldsymbol{L}} \end{pmatrix}, \quad \dot{\boldsymbol{x}} = \tfrac{1}{2}x_-^t \nabla_L H, \quad \dot{\boldsymbol{L}} = -\tfrac{1}{2}x_-\nabla_x H + \boldsymbol{L}\times\nabla_L H\,.$$

Similarly, the Lie-Poisson structure in the space fixed frame is

$$B_+ = \begin{pmatrix} 0 & \frac{1}{2}\boldsymbol{x}_+^t \\ -\frac{1}{2}\boldsymbol{x}_+ & -\hat{\boldsymbol{l}} \end{pmatrix}, \quad \dot{\boldsymbol{x}} = \tfrac{1}{2}x_+^t \nabla_l H, \quad \dot{\boldsymbol{l}} = -\tfrac{1}{2}x_+\nabla_x H - \boldsymbol{l}\times\nabla_l H\,.$$

Both Poisson structures have the Casimir $x_0^2 + x_1^2 + x_2^2 + x_3^2$. The Poisson structure B_+ is found by sandwiching the symplectic structure of the $(\boldsymbol{x}, \boldsymbol{p})$ variables by the Jacobian of the transformation of $(\boldsymbol{x}, \boldsymbol{l})$ and its transpose.

For the Euler top the usual Hamiltonian in the body frame is $H = \frac{1}{2}\boldsymbol{L}\cdot I^{-1}\boldsymbol{L}$, and the complicated integrals are $R\boldsymbol{L}$ (which imply the simple integral $|\boldsymbol{L}|^2$). In the space fixed frame instead we have the complicated Hamiltonian $H = \frac{1}{2}\boldsymbol{l}\cdot RI^{-1}R^t\boldsymbol{l}$ with the simple integrals $\boldsymbol{l}$. We mention the Euler top here to make the point that for general moments of inertia, the description in the body frame is simpler. However, for a round rigid body with $I_1 = I_2 = I_3$ both Hamiltonians are equally simple. Also for a symmetric rigid body with say $I_1 = I_2$, the spatial frame is useful because

$$2T = \boldsymbol{l}\cdot RI^{-1}R^t\boldsymbol{l} = \boldsymbol{l}\cdot\frac{1}{I_1}R(id + \delta\boldsymbol{e}_3\boldsymbol{e}_3^t)R^t\boldsymbol{l} = \frac{1}{I_1}\left(\boldsymbol{l}^2 + \delta L_3^2\right)$$

where $\delta = I_1/I_3 - 1$. The important point is that $L_3 = \boldsymbol{e}_3\cdot\boldsymbol{L} = \boldsymbol{e}_3\cdot R^t\boldsymbol{l} = R\boldsymbol{e}_3\cdot\boldsymbol{l} = \boldsymbol{l}\cdot\boldsymbol{a}$ is the angular momentum about the body's symmetry axis $\boldsymbol{e}_3$ and hence a constant of motion for the symmetric top.

Theorem 3. *The Lagrange top (symmetric heavy rigid body with a fixed point on the symmetry axis) in coordinates $\boldsymbol{x}\in S^3\subset\mathbb{R}^4$ and angular momenta $\boldsymbol{l}$ in the space fixed frame has Hamiltonian*

$$H = \frac{1}{2I_1}(l_x^2 + l_y^2 + l_z^2 + \delta L_3^2) + V(x_0^2 + x_3^2 - x_1^2 - x_2^2)$$

and Poisson structure B_+, with integrals l_z and

$$L_3 = 2l_x(-x_0x_2 + x_1x_3) + 2l_y(x_0x_1 + x_2x_3) + l_z(x_0^2 + x_3^2 - x_1^2 - x_2^2).$$

The vector fields of l_z and L_3 generate a T^2 action with isotropies. The vector field of the Hamiltonian is

$$X_H = \frac{1}{2I_1}X_{l^2} + \frac{\delta L_3}{I_1}X_{L_3} - \frac{1}{2}(0,0,0,0,\boldsymbol{x}_+\nabla_x V)^t \,. \tag{4.1}$$

The functions H, l_z, L_3 have pairwise vanishing Poisson bracket. The vector fields X_H, X_{L_3} and X_{l_z} are independent almost everywhere.

This theorem is well known for the case of a linear potential, and when using Euler angles it is part of most mechanics textbooks. Instead we offer a global description in the spatial frame with a Poisson structure. In addition, in order to make the connection with the general confluent Heun equation, we consider not just a linear potential (gravity), but in addition a quadratic term. After some preparations in the next sections discussing the torus action, the reduction, and briefly recalling Euler angles, the main technical part is the description of the set of critical values of the energy-momentum map in Theorem 2.

4.3. TORUS ACTION

The vector field generated by L_3 in the space fixed coordinate system is

$$X_{L_3} = B_+\nabla L_3 = \tfrac{1}{2}(\boldsymbol{x}_+^t R\boldsymbol{e}_3, 0,0,0)^t = (\tfrac{1}{2}\boldsymbol{x}_-^t\boldsymbol{e}_3, 0,0,0)^t \tag{4.2}$$

where we used the identity $\boldsymbol{x}_+^t R = \boldsymbol{x}_-^t$. This vector field can be easily integrated (two harmonic oscillators) to give the flow $\Phi_{L_3}^{\psi}$. This flow rotates (x_0, x_3) and (x_1, x_2) by $\psi/2$ clockwise. However, when the flow acts on R it acts by multiplication by a counterclockwise rotation about the z-axis through ψ (not $\psi/2$!) from the right. Thus L_3 has 2π-periodic flow on $T^*SO(3)$ and hence is an action variable.

The vector field generated by the integral l_z is

$$X_{l_z} = B_+\nabla l_z = (\tfrac{1}{2}\boldsymbol{x}_+^t\boldsymbol{e}_z, -\boldsymbol{l}\times\boldsymbol{e}_z)^t. \tag{4.3}$$

Again, this vector field is easily integrated (three harmonic oscillators) giving the flow $\Phi_{l_z}^{\phi}$. The action on R is by multiplication with a counterclockwise rotation about the z-axis through ϕ from the left. In addition, the momentum vector $\boldsymbol{l}$ is rotated by the same rotation matrix. Thus l_z has 2π-periodic flow on $T^*SO(3)$ and hence is an action variable.

The vector fields X_{L_3} and X_{l_z} are parallel when $l_x = l_y = 0$ and either $x_0 = x_3 = 0$ or $x_1 = x_2 = 0$. These critical points have $\boldsymbol{l}||\boldsymbol{a}||\boldsymbol{e}_z$ and are called sleeping tops. In the first case $a_z = -1$ (hanging sleeping top), while in the second case $a_z = +1$ (upright sleeping top).

The torus action is not free at these points because the rotations coincide. Since $L_3 = \boldsymbol{l} \cdot \boldsymbol{a}$ we see that $L_3 = -l_z$ for the hanging sleeping top and $L_3 = l_z$ for the upright sleeping top. The corresponding critical points of H are two parabolas above $l_z \pm L_3 = 0$.

The vector fields X_{l_z} and X_{L_3} both have 2π periodic flows on $T^*SO(3)$, i.e. they map $\boldsymbol{x}$ to $-\boldsymbol{x}$ after time 2π. When considered as flows on S^3 both flows have period 4π. Now consider the vector fields generated by $l_z \pm L_3$. These are both 2π periodic vector fields on T^*S^3. Points with $l_x = l_y = 0$ and either $x_0 = x_3 = 0$ or $x_1 = x_2 = 0$, respectively, are fixed points of these flows. Nevertheless, they are action variables on T^*S^3. Notice that as flows on $T^*SO(3)$ the orbits of $l_z \pm L_3$ do not all have the same minimal period, since points with $l_x = l_y = 0$ and either $x_0 = x_3$ or $x_1 = x_2$ have minimal period π, while all other non-fixed points have minimal period 2π. The T^2 action on T^*S^3 is of course still not free, the difference is that now the exceptional sets of points are found as those where one of the vector fields vanishes.

The vector field of the spherical Euler top is that of $\boldsymbol{l}^2 = l_x^2 + l_y^2 + l_z^2$. The vector fields of l_x and l_y are permutations to that of l_z given in (4.3). Combining these gives

$$X_{l^2} = (\boldsymbol{x}_+^t \boldsymbol{l}, 0, 0, 0)^t \,.$$

Here the components of $\boldsymbol{l}$ are all constant, and the flow of this vector field is a rotation about the axis $\boldsymbol{l}$. This is also a periodic flow, but the period is not constant. To obtain constant period, we consider the flow generated by $l = \sqrt{\boldsymbol{l}^2}$, which we denote by X_l. This flow commutes with the flows of l_z and L_3, but not with that of H. The flow of $\boldsymbol{l}^2$ leaves $\boldsymbol{l}$ constant and so

$$\begin{aligned}\Phi_l^\alpha &= \exp\left(\frac{\alpha}{2l}\begin{pmatrix} 0 & l_x & l_y & l_z \\ -l_x & 0 & -l_z & l_y \\ -l_y & l_z & 0 & -l_x \\ -l_z & -l_y & l_x & 0 \end{pmatrix}\right) \\ &= \begin{pmatrix} \cos\frac{\alpha}{2} & l_x/l\sin\frac{\alpha}{2} & l_y/l\sin\frac{\alpha}{2} & l_z/l\sin\frac{\alpha}{2} \\ -l_x/l\sin\frac{\alpha}{2} & \cos\frac{\alpha}{2} & -l_z/l\sin\frac{\alpha}{2} & l_y/l\sin\frac{\alpha}{2} \\ -l_y/l\sin\frac{\alpha}{2} & l_z/l\sin\frac{\alpha}{2} & \cos\frac{\alpha}{2} & -l_x/l\sin\frac{\alpha}{2} \\ -l_z/l\sin\frac{\alpha}{2} & -l_y/l\sin\frac{\alpha}{2} & l_x/l\sin\frac{\alpha}{2} & \cos\frac{\alpha}{2} \end{pmatrix}.\end{aligned}$$

When acting with this flow on the rotation matrix R with initial condition $\boldsymbol{x} = (1, 0, 0, 0)$ gives Rodrigues' parametrisation of $SO(3)$ with rotation axis $\boldsymbol{l}/l$ and rotation angle α. Thus Rodrigues' formula gives the geodesics of the spherical top. When acting with this flow on S^3 it is periodic with period 4π.

The reason we are including this flow is that there is an interesting difference between $SO(3)$ and S^3. On $T^*SO(3)$ the singular T^3 torus action generated by the commuting flows of l_z,

L_3, and l is faithful. This means that outside the singularity where $l_z \pm L_3 = 0$ the action on each T^3 obtained by fixing the values of the generators is faithful. By contrast, when considering the T^3 torus action generated by $l_z + L_3$, $l_z - L_3$, and $l + l$ on T^*S^3 the action is not faithful on regular tori. The reason is that when flowing each flow only for angle π, then the first two flows together achieve $\boldsymbol{x} \to -\boldsymbol{x}$, and this is cancelled by the flow $\Phi^{\pi}_{2l} = \Phi^{2\pi}_{l}$.

4.4. Reductions

The flows of l_z and L_3 are global S^1 actions, and hence allow for regular reduction. It is straightforward to obtain the reduced system from the global system with Poisson structure $B_\pm$. The l_z-reduced system gives the well known Euler-Poisson equations, while the L_3-reduced equations are somewhat less well known in classical mechanics (see, e.g., [BS99, CB15, Dul04]). The full reduction is singular because the T^2 action of l_z and L_3 is not free. The standard description of reduction uses zxz-Euler angles, the singular reduction using invariants is in [CB15]. A peculiar property of Euler angles is that the ψ-rotation leaves the figure axis invariant (it acts on the right) while the ϕ-rotation leaves the direction of gravity invariant (it acts on the left), and hence Euler angles are neither space-fixed nor body-fixed. The quantisation of the top (see below) starts out with Euler angles [LL77], but in the end, writing the Hamiltonian using $\boldsymbol{l}^2$ and L_3^2 shows that for the quantum mechanical description the spatial frame is also useful.

The reduction by the symmetry $\Phi^{\psi}_{L_3}$ introduces the coordinates of the axis of the top $\boldsymbol{a} = R\boldsymbol{e}_3$ as new coordinates. This is, in fact, reduction by invariants, since the third column of R is given by $(2(x_0x_2 + x_1x_3), -2x_0x_1 + 2x_2x_3, x_0^2 + x_3^2 - x_1^2 - x_2^2)$ and these are all invariant under the two-oscillator flow $\Phi^{\psi}_{L_3}$. We already noted that $\Phi^{\psi}_{L_3}$ acts on R by multiplication by $R_z(\psi)$ from the right, where $R_z(\psi)$ denotes a counterclockwise rotation about the z-axis by ψ. Hence $RR_z(\psi)\boldsymbol{e}_3 = R\boldsymbol{e}_3 = \boldsymbol{a}$ is invariant. The resulting reduced system has Poisson structure

$$B_+^r = \begin{pmatrix} 0 & -\hat{\boldsymbol{a}} \\ -\hat{\boldsymbol{a}} & -\hat{\boldsymbol{l}} \end{pmatrix}, \quad \dot{\boldsymbol{a}} = -\boldsymbol{a} \times \nabla_l H, \quad \dot{\boldsymbol{l}} = -\boldsymbol{a} \times \nabla_a H - \boldsymbol{l} \times \nabla_l H \,.$$

Denote the Jacobian of the transformation from $(\boldsymbol{x}, \boldsymbol{l})$ to $(\boldsymbol{a}, \boldsymbol{l})$ by A. Then $B_+^r = A^t B_+ A$ when expressed in the new variables. The main identity in the reduction from B_+ to B_+^r is $\frac{1}{2}\frac{\partial \boldsymbol{a}}{\partial \boldsymbol{x}} \boldsymbol{x}_+^t = \hat{\boldsymbol{a}}$. The Poisson structure B_+^r has Casimirs $\boldsymbol{a}^2 = 1$ and $\boldsymbol{a} \cdot \boldsymbol{l}$ and the reduced Hamiltonian is

$$H = \frac{1}{2I_1}(\boldsymbol{l}^2 + \delta(\boldsymbol{a} \cdot \boldsymbol{l})^2) + V(a_z).$$

Since $\boldsymbol{a} \cdot \boldsymbol{l}$ is a Casimir (equal in value to the generator of the symmetry L_3) it does not contribute to the dynamics but merely changes the value of the Hamiltonian.

Note that reduction by the symmetry generated by the integral l_z is more complicated in the spatial frame since the flow is a rotation in $\boldsymbol{x}$ and in l_x, l_y. However, when switching to the body frame then the flow of l_z (written in terms of $\boldsymbol{L}$) is simpler. Reduction is achieved by introducing the invariant of the left action generated by l_z, which is $\boldsymbol{e}_3^t R_z(\phi) R = \boldsymbol{e}_3^t R = \boldsymbol{\Gamma}^t$ with Poisson structure

$$B_-^r = \begin{pmatrix} 0 & \hat{\boldsymbol{\Gamma}} \\ \hat{\boldsymbol{\Gamma}} & \hat{\boldsymbol{L}} \end{pmatrix}, \quad \dot{\boldsymbol{\Gamma}} = \boldsymbol{\Gamma} \times \nabla_L H, \quad \dot{\boldsymbol{L}} = \boldsymbol{\Gamma} \times \nabla_\Gamma H + \boldsymbol{L} \times \nabla_L H \,.$$

The reduction leads to the more familiar Hamiltonian of the Lagrange top given by

$$H = \frac{1}{2I_1}(L_1^2 + L_2^2) + \frac{1}{2I_3} L_3^2 + V(\Gamma_3)$$

where $\boldsymbol{\Gamma}$ is $\boldsymbol{e}_z$ viewed from the body frame. The Poisson structure is B_-^r with the opposite sign than B_+^r. These are the equations usually called Euler-Poisson equations. Their advantage is that this reduction remains valid for an arbitrary rigid body with a fixed point, and this family for appropriate moments of inertia and position of the centre of mass contains the Kovalevskaya top, the Euler top, and all other (non-integrable) tops.

The Hamiltonian Hopf bifurcation in the sleeping top with $\boldsymbol{a}||\boldsymbol{l}||\boldsymbol{e}_z$ respectively $\boldsymbol{\Gamma}||\boldsymbol{L}||\boldsymbol{e}_3$ is best described in the reduced system(s), because the corresponding periodic orbit becomes a relative equilibrium after reduction. It is easy to check that indeed these are equilibria, and linearising the Hamiltonian vector field about these equilibria yields a 6×6 matrix with 2 eigenvalues zero corresponding to the two Casimirs. The characteristic polynomial for the remaining non-trivial eigenvalues is

$$P_+(\lambda) = \lambda^4 + \lambda^2(\kappa^2 - 2f) + f^2 = 0, \quad \kappa = l_z/I_1 = \omega I_3/I_1, \quad f = a_z V'(a_z)/I_1, \quad a_z = \pm 1 \,.$$

in the spatial frame and

$$P_-(\lambda) = P_+(\lambda) + \omega(\omega - \kappa)(2\lambda^2 + 2f + \omega(\omega - \kappa)), \quad \omega = l_z/I_3$$

in the body frame. The eigenvalues given by the roots of P_+ in the spatial frame are not the same as the eigenvalues given by the roots of P_- in the body frame because in the latter case the system is described in a frame rotating with angular velocity ω. However, they differ only by $\pm i\omega$. More precisely, let $\lambda_1, \bar{\lambda}_1, \lambda_2, \bar{\lambda}_2$ be the roots of P_+, then the roots of P_- are $\lambda_1 + i\omega, \bar{\lambda}_1 - i\omega, \lambda_2 + i\omega, \bar{\lambda}_2 - i\omega$ such that the Floquet multipliers $\mu = \exp(\lambda T)$ of the periodic orbit with period $T = 2\pi/\omega$ are the same. The description in the spatial frame gives simpler formulas.

At the Hamiltonian Hopf bifurcation the eigenvalues change from all purely imaginary via a collision on the imaginary axis to a quadruple of complex eigenvalues. This occurs when the discriminant of $P_+(\lambda)$ considered as a quadratic equation in λ^2 changes from positive to negative. The discriminant is given by $\kappa^2(\kappa^2 - 4f)$. When f is negative the eigenvalues are purely imaginary for any κ. When f is positive eigenvalues are purely imaginary when $\kappa^2 > 4f$, while the top is unstable with non-zero real parts of the eigenvalues when $\kappa^2 < 4f$. This is the classical stability condition for the Lagrange top, here obtained for arbitrary potential. At the critical case $\kappa^2 = 4f$ the eigenvalues collide and $\lambda^2 = -\kappa^2/4$.

4.5. EULER ANGLES

The Poisson structures $B_\pm$ allow for a global description of rigid body dynamics free of coordinate singularities. However, often explicit canonical coordinates are more convenient, and even essential for the quantisation of the problem. Such a coordinate system adapted to the symmetries is given by zxz-Euler angles such that

$$R = R_z(\phi)R_x(\theta)R_z(\psi)\,.$$

The canonically conjugate momenta are denoted by p_ϕ, p_θ, p_ψ, respectively. Then we have that $l_z = p_\phi$ and $L_3 = p_\psi$. The Hamiltonian in these coordinates is

$$H = \frac{1}{2I_1}(2T_{round} + \delta p_\psi^2) + V(\cos\theta)$$

where T_{round} is the kinetic energy of the spherical top with moment of inertia 1:

$$T_{round} = \frac{1}{2}\left(p_\theta^2 + \frac{1}{\sin^2\theta}\left(p_\phi^2 + p_\psi^2 - 2p_\phi p_\psi \cos\theta\right)\right) = \frac{1}{2}\boldsymbol{l}^2\,.$$

Notice that this round metric on $SO(3)$ is a metric of constant curvature and hence up to a covering equivalent to the metric of the round sphere S^3.

Away from the coordinate singularity where the torus action is not free, Euler angles are a smooth local coordinate system. Equilibrium points in θ are determined by $\partial H/\partial\theta = 0$. For later use, we denote this function by H_θ, and similarly the 2nd derivative by $H_{\theta\theta}$.

4.6. BIFURCATION DIAGRAM

The energy-momentum map from $T^*SO(3)$ to $\mathbb{R}^3$ is given by (l_z, L_3, H) where L_3 is given in terms of $\boldsymbol{x}$ and $\boldsymbol{l}$ as in Theorem 1. The bifurcation diagram of this integrable system is the set of critical values of the energy-momentum map. Hence we are interested in the rank of (X_{l_z}, X_{L_3}, X_H). To determine where the rank drops we consider

$$\alpha X_{L_3} + \beta X_{l_z} + \gamma X_H = 0\,. \tag{4.4}$$

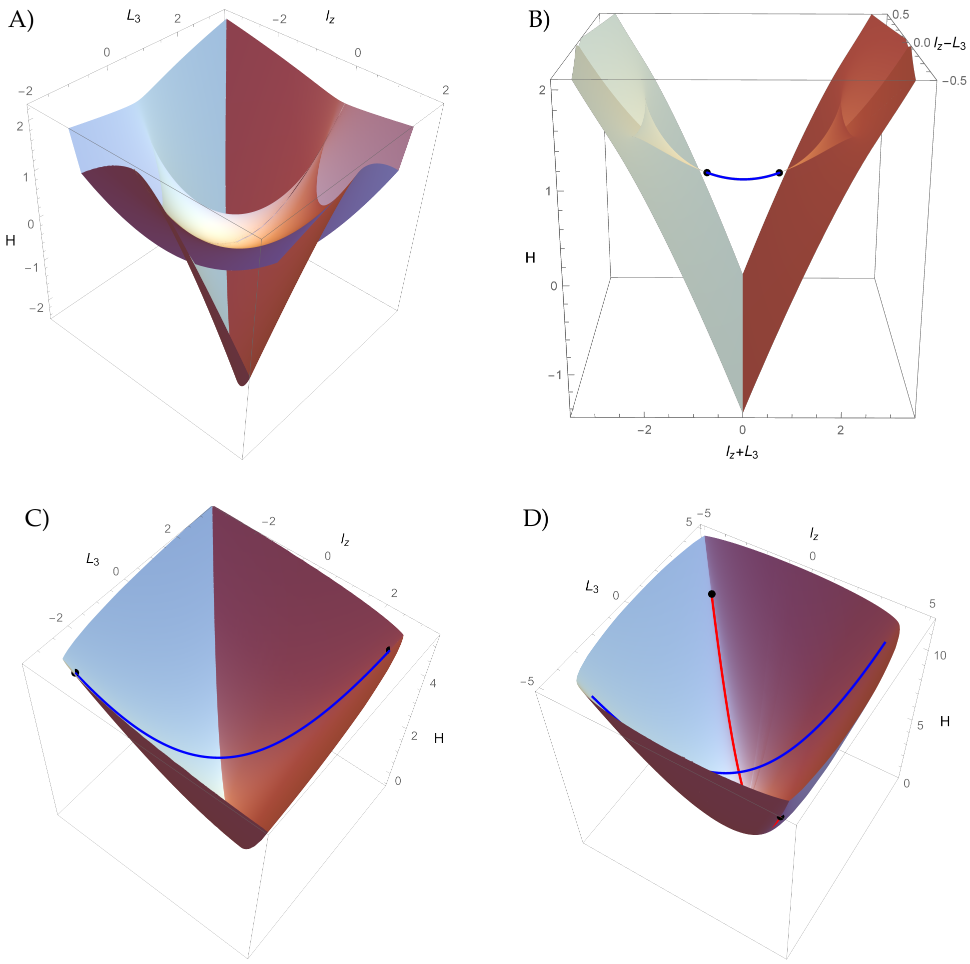

Figure 4.1: Examples of the four topologically different kinds of bifurcation diagrams. A) triangular tube, B) shrinking triangular tube and thread (zoomed in), C) one thread and D) two threads. All figures use $I_1 = 1, \delta = 0, c_1 = 1$. The values of c_2 are $-1.5, -0.48, 0.4, 2.5$ for A,B,C,D, respectively. In A) the ranges for l_z and L_3 are chosen as to cut away parts of the surface facing the viewer. In B) the ranges are even more restricted. The black dots mark the Hamiltonian Hopf bifurcations.

Theorem 4. *The rank 1 points of the energy-momentum map are given by two parabolas of sleeping tops*

$$(l_z, L_3, H) = \left(m, \pm m, \frac{m^2}{2I_1}(1+\delta) + V(\pm 1)\right). \tag{4.5}$$

The rank 2 points have a rational parametrisation determined by $\boldsymbol{l}(\beta, a_z) = \frac{1}{\beta} I_1 V'(a_z)\boldsymbol{a} + \beta \boldsymbol{e}_z$ *such that for* $a_z \in [-1, 1]$ *and* $\beta \in \mathbb{R}$ *the critical values of the energy-momentum map are*

$$\begin{aligned}
l_z(\beta, a_z) &= \frac{1}{\beta} I_1 V'(a_z) a_z + \beta, \\
L_3(\beta, a_z) &= \frac{1}{\beta} I_1 V'(a_z) + \beta a_z, \\
H(\beta, a_z) &= \frac{1}{2I_1}(\boldsymbol{l}(\beta, a_z)^2 + \delta L_3(\beta, a_z)^2) + V(a_z).
\end{aligned}$$

Proof. Notice that the last 3 components of X_V can be written as

$$-\tfrac{1}{2}\boldsymbol{x}_+ \nabla_x V(a_z(x)) = -\boldsymbol{a} \times \nabla_a V(a_z) = -\boldsymbol{a} \times \boldsymbol{e}_z V'(a_z).$$

Using $\boldsymbol{x}_-^t \boldsymbol{e}_3 = \boldsymbol{x}_+^t R \boldsymbol{e}_3 = \boldsymbol{x}_+^t \boldsymbol{a}$ in the flow of L_3, (4.4) becomes

$$\begin{pmatrix} \frac{1}{2}\boldsymbol{x}_+^t((\alpha + \gamma\delta L_3)\boldsymbol{a} + \beta \boldsymbol{e}_z + \gamma \boldsymbol{l}) \\ -(\gamma I_1 V' \boldsymbol{a} + \mu \boldsymbol{e}_z + \beta \boldsymbol{l}) \times \boldsymbol{e}_z \end{pmatrix} = \begin{pmatrix} 0 \\ 0 \end{pmatrix}.$$

This means critical points of the momentum map occur when

$$\begin{aligned}
(\alpha + \gamma\delta L_3)\boldsymbol{a} + \beta \boldsymbol{e}_z + \gamma \boldsymbol{l} &= 0 \\
\gamma I_1 V' \boldsymbol{a} + \mu \boldsymbol{e}_z + \beta \boldsymbol{l} &= 0.
\end{aligned} \tag{4.6}$$

for α, β, γ not all zero. Hence the three vectors $\boldsymbol{a}$, $\boldsymbol{l}$, $\boldsymbol{e}_z$ are co-planar. Since $\boldsymbol{a}$ and $\boldsymbol{e}_z$ never vanish, there is no rank 0 point. We have the following four cases.

1) $\boldsymbol{a} \parallel \boldsymbol{e}_z$. This means $a_x = a_y = 0$ and $a_z = \pm 1$. If $\boldsymbol{l} \neq 0$ and $\boldsymbol{l}$ not parallel to $\boldsymbol{e}_z$, then linear independence (4.6) implies $\alpha = \beta = \gamma = 0$. Hence $\boldsymbol{l} \parallel \boldsymbol{e}_z \parallel \boldsymbol{a}$ (including $\boldsymbol{l} = 0$), and we can use $l_z = m$ as parameter and thus showed the parametrisation of the sleeping tops (4.5). Recall that these are the points where the torus action is not free. All points along these parabolas have rank 1. Parts of these parabolas may be isolated threads of focus-focus type, while others form the edges of the surface of elliptic-elliptic type. The vertices of the parabolas where $m = 0$ and hence $\boldsymbol{l} = 0$ are equilibrium points of X_H with $a_z = \pm 1$.

2) $\boldsymbol{l} \parallel \boldsymbol{e}_z$. Set $\boldsymbol{l} = \lambda \boldsymbol{e}_z$. If $\boldsymbol{a} \parallel \boldsymbol{e}_z$ then this gives the sleeping top solution again. If $\boldsymbol{a}$ is not parallel to $\boldsymbol{e}_z$ then by linear independence, (4.6) implies $\alpha + \gamma\delta L_3 = \beta + \gamma\lambda = 0$ and $I_1 V' = \mu + \beta\lambda = 0$. If $\gamma = 0$ then this forces the trivial solution $\alpha = \beta = 0$ so $\gamma \neq 0$ and $V' = 0$. Since $V' = c_1 + 2c_2 a_z$ this means $a_z = \frac{-c_1}{2c_2} =: a_{z0}$. Normalising $\gamma = -1$ gives

$\lambda = \beta$ and hence $\boldsymbol{l} = \beta \boldsymbol{e}_z$, $\boldsymbol{a} = (a_x, a_y, a_{z0})$, $L_3 = \boldsymbol{l} \cdot \boldsymbol{a} = \beta a_{z0}$ and hence using $\beta = m$ as parameter gives

$$(l_z, L_3, H) = \left(m, m a_{z0}, \frac{m^2}{2I_1}(1 + \delta a_{z0}^2) + V(a_{z0}) \right). \tag{4.7}$$

Since $|a_z| \leq 1$ this parabola only exists when $2|c_2| > |c_1|$, while for $2|c_2| = \pm|c_1|$ it merges with the sleeping tops. The vertex of this parabola where $m = 0$ and hence $\boldsymbol{l} = 0$ is an equilibrium point of X_H with $|a_z| \leq 1$. This vertex lies above or below the vertices of the parabolas of sleeping tops (4.5) described in case 1, depending on whether $c_2 < -c_1/2$ or $c_2 > c_1/2$.

3) $\boldsymbol{l} \parallel \boldsymbol{a}$. This forces $\boldsymbol{l} = \lambda \boldsymbol{a} = L_3 \boldsymbol{a}$. If $\boldsymbol{a} \parallel \boldsymbol{e}_z$ then this gives the sleeping top solution again. If $\boldsymbol{a}$ is not parallel to $\boldsymbol{e}_z$ then linear independence and (4.6) implies $\alpha + \gamma(\delta + 1)L_3 = \beta = 0$ and $\gamma I_1 V' + \beta L_3 = \mu = 0$. Again $\gamma = 0$ gives the trivial solution, so we can normalise $\gamma = -1$ and find $\alpha = (1 + \delta)L_3$ and $V' = 0$, as in case 2. Using $L_3 = k$ as parameter gives

$$(l_z, L_3, H) = \left(k a_{z0}, k, \frac{k^2}{2I_1}(\delta + 1) + V(a_{z0}) \right). \tag{4.8}$$

Existence and limiting behaviour is as in case 2. The vertex of this parabola coincides with that of case 2.

4) General case where no pair of vectors is parallel. If $\gamma = 0$ then this gives $\alpha = \beta = 0$ while if $\beta = 0$ then this gives case 2. We now assume $\beta \neq 0$ and $\gamma \neq 0$. Eliminating $\boldsymbol{l}$ from (4.6) and using linear independence gives $\mu = \frac{\beta^2}{\gamma}$ and $\alpha + \gamma \delta L_3 = \frac{\gamma^2}{\beta} I_1 V'$. Using this to eliminate L_3 in (4.6) gives $-\boldsymbol{l} = \frac{\gamma}{\beta} I_1 V' \boldsymbol{a} + \frac{\beta}{\gamma} \boldsymbol{e}_z$. Normalising $\gamma = -1$ computing $l_z = \boldsymbol{l} \cdot \boldsymbol{e}_3$, $L_3 = \boldsymbol{l} \cdot \boldsymbol{a}$, and $\boldsymbol{l}^2 = \boldsymbol{l} \cdot \boldsymbol{l}$ gives the result. Notice that β is the angular velocity of the angle ϕ conjugate of p_ϕ.

■

Note that in cases 2 and 3 the parabolas (4.7) and (4.8) are embedded in the surface of critical values described in case 4. Unlike the parabolas (4.5) the rank of these points is 2. Since V' is linear in a_z we can eliminate a_z in favour of $\tilde{\alpha} = I_1 V'(a_z)/\beta$. Notice that α is the angular velocity of the angle ψ, and $\tilde{\alpha}$ is that angular velocity with $\delta = 0$. As a result we obtain a *polynomial* parametrisation of the critical values of the energy-momentum map which after non-dimensionalisation is given by

$$\left(\beta + a_{z0}\tilde{\alpha}(1 - \tilde{\alpha}\beta), \gamma + a_{z0}\beta(1 - \tilde{\alpha}\beta), \tfrac{1}{2}(\tilde{\alpha}^2 + \beta^2 + a_{z0}(1 - \tilde{\alpha}\beta)(3\tilde{\alpha}\beta + 1) + \delta(\tilde{\alpha} + a_{z0}\beta(1 - \tilde{\alpha}\beta))^2)\right)$$

with the constraint $-1 \leq a_{z0}(1 - \tilde{\alpha}\beta) \leq 1$ on the parameters $\tilde{\alpha}$ and β. When $\delta = 0$ any line

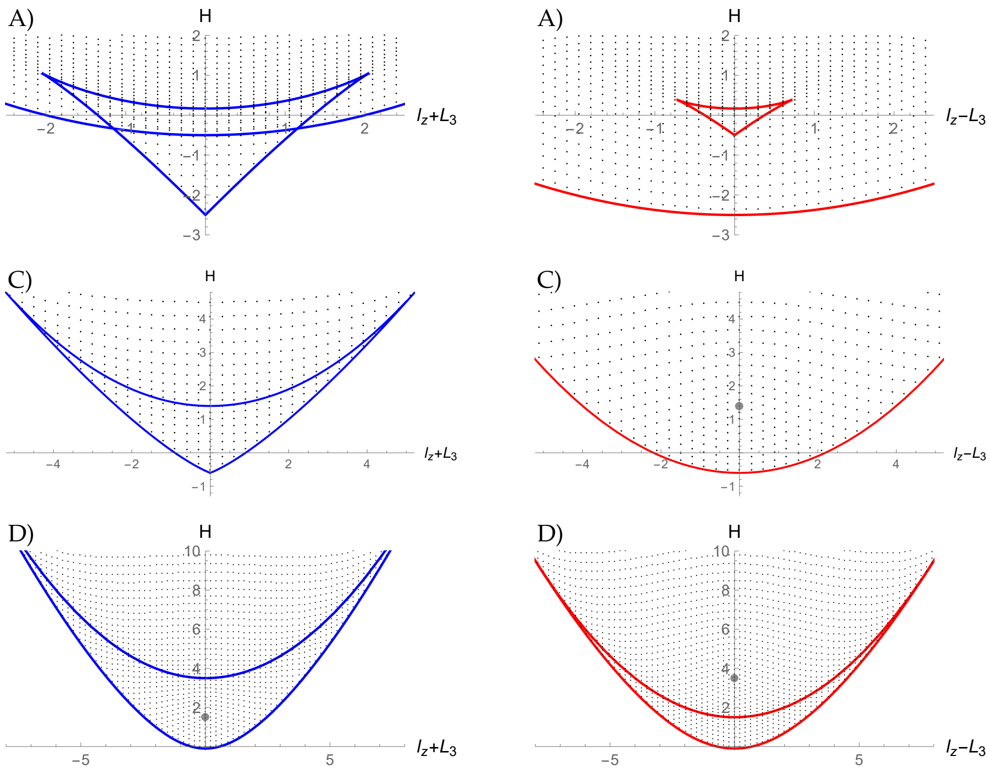

Figure 4.2: Slices through the bifurcation diagram along $l_z - L_3 = 0$ (blue) and $l_z + L_3 = 0$ (red) for Fig. 4.1 A,C,D using $\hbar = (0.075, 0.15, 0.11)$ for the quantum spectrum, respectively.

determined by fixing α and changing β or vice versa is a planar parabola. This means the surface is doubly foliated by (arcs of) planar parabolas. The two special parabolas (4.7) and (4.8) correspond to vanishing angular momentum $\tilde{\alpha} = 0$ and $\beta = 0$, respectively. Hence for points on (4.7) the top does not rotate about its figure axis while for points on (4.8) the figure axis does not rotate in space. Both are extreme cases of resonant 2-tori where one frequency vanishes. Note that such solutions are impossible in the ordinary Lagrange top with $c_2 = 0$. The parabolas of rank 1 points (4.5) are *not* part of this foliation, instead they mark the endpoints of the parabolic arcs where $a_{z0}(1 - \tilde{\alpha}\beta) = \pm 1$.

The rational parametrisation from Theorem 2 is also useful when using the Euler angles. Inserting the parametrisation into the condition for an equilibrium point $H_\theta = 0$ shows that it is identically satisfied. To determine the stability of the equilibrium we evaluate the second derivative $H_{\theta\theta}$ on the rational parametrisation and find

$$H_{\theta\theta}(\beta, a_z) = \beta^2 I_1 - 2a_z V'(a_z) + (1 - a_z^2)V''(a_z) + \frac{1}{\beta^2 I_1} V'(a_z)^2 \,. \tag{4.9}$$

The transverse stability of a 2-torus is determined by the sign of $H_{\theta\theta}$ since it gives the curvature of the effective potential. Computing $H_{\theta\theta}$ on the parabolas of sleeping top (4.5) gives $m^2/(4I_1) \mp V'(\pm 1)$, reproducing the classical condition for the Hamiltonian Hopf bifurcation in Lagrange's sleeping top found at the end of section 4. Evaluating $H_{\theta\theta}$ as given in (4.9) on the parabola (4.7) gives $m^2/I_1 + 2c_2(1 - a_{z0}^2)$, and on the parabola (4.8) similarly gives $k^2/I_1 + 2c_2(1 - a_{z0}^2)$. When $c_2 < -c_1/2$ these are both negative for small m or k, respectively, and hence unstable. These correspond to points on top of the triangular tube, which are hyperbolic. For sufficiently large angular momentum the sign flips, and they are points in the outer envelope surface of critical values. When $c_2 > c_1/2$ the 2nd derivative is always positive, hence in this case rank 2 points correspond to elliptic 2-tori.

Equating $H_{\theta\theta}$ to zero gives a relation between β and a_z which determines degenerate values in the bifurcation diagram. These are the cusp-shaped edges of the triangular tubes in Fig. 1A,B. The most degenerate situation occurs when simultaneously the 2nd and the 3rd θ-derivative of H vanish. This occurs for the special parameter values $a_z = -c_1/(2c_2)$, $\beta^2 = -c_1^2/(8c_2 I_1)$ and $a_z = -c_1/(4c_2)$, $\beta^2 = c_1^2/(2c_2 I_1) - 2c_2/I_1$. When these degenerate values for a_z collide with ± 1 then the degenerate points disappear and the topological structure of the bifurcation diagram changes. This occurs for $c_1 = \pm 2c_2$ and $c_1 = -4c_2$. The plus sign yields imaginary β. The sign of c_1 can be made positive by the original choice of body coordinate system. This can flip the sign of $c_1 a_z$ in the potential but leaves $c_2 a_z^2$ unchanged. Hence there are 4 topologically distinct cases illustrated in Fig. 1:

A) $c_2/c_1 < -1/2$: triangular tube Fig. 1A;

B) $-1/2 < c_2/c_1 < -1/4$: triangular tube shrinking to a thread Fig. 1B;

C) $-1/4 < c_2/c_1 < 1/2$: one thread Fig. 1C;

D) $c_2/c_1 > 1/2$: two threads Fig. 1D.

To understand the figures corresponding to these 4 cases it helps to consider how they bifurcate into each other. We stress again that we always consider $\delta = 0$, because adding the additional quadratic term in L_3 to the Hamiltonian deforms the bifurcation diagram, but does not essentially change it. Bifurcations similar to those found here have recently been described in [SZ07a, EHM19], in particular also the related quantum monodromy in [SZ07a].

Let us start with the ordinary Lagrange top, $c_2 = 0$, $c_1 = 1$ by choice of coordinate system and normalisation [CK85]. The bifurcation diagram for the harmonic Lagrange top is topologically the same for $-1/4 < c_2/c_1 < 1/2$. It is natural that a small enough quadratic term does not change the nature of the bifurcation diagram since the potential $V(a_z)$ is only changed a little since $|a_z| \leq 1$. The outer surface is a bowl that has at least two corners when cut at constant energy. For high energy there are four corners, while for low energy only two. The transitions are two supercritical Hamiltonian Hopf bifurcations where the sleeping top becomes stable. A thread of critical values detaches at these points of the surface. This thread is shown in blue in Fig. 1C. In Fig. 2 slices through the 3-dimensional bifurcation diagram are shown. Each blue curve is a slice with $l_z - L_3 = 0$ which contains the thread, while in the other slice $l_z + L_3 = 0$ the thread appears as a single isolated point. In these figures we also show the quantum spectrum, see the next section. This situation persists for non-zero c_2 not too large.

For $c_2/c_1 > 1/2$, a second thread emerges from the minimum of H, as shown in Fig. 1D and Fig. 2D. For low energies, the outer surface has no corners at all. For intermediate energy as visible at the top of Fig. 1D, there are 2 corners above where the red thread is attached, but the blue thread is not yet attached and the outer surface nearby is still smooth. For high energies, there are 4 corners.

A more dramatic change occurs when decreasing c_2/c_1 through $-1/4$. All attachment points of the threads in the two cases discussed so far are supercritical Hamiltonian Hopf bifurcations. When passing $-1/4$, the supercritical Hamiltonian Hopf bifurcation turns into a subcritical Hamiltonian Hopf bifurcation. The attachment point is replaced by a tube with triangular cross section that eventually contracts to a point and becomes a thread, as shown in Fig. 1B (zoomed in).

When decreasing c_2/c_1 further, the two subcritical Hamiltonian Hopf bifurcation values collide when $c_2/c_1 = -1/2$, and merge into a triangular tube shown in Fig. 1A and there is no bifurcation any more in the rank 1 points given by (4.5) with $L_3 = +m$. Instead this parabola marks the corner at the bottom of the triangular tube and for higher energies the corner in the outer surface. In this figure, the bounding box is chosen such that it cuts away parts of the surface facing the viewer so that the triangular tube becomes visible. The 0-slices are shown in Fig. 2A. The two bottom surfaces of the tube correspond to elliptic 2-tori, while the top surface of the tube corresponds to hyperbolic 2-tori. The top surface joins the bottom surfaces along a line of cusps where $H_{\theta\theta} = 0$. The merging of the triangular tube with the outer surface is illustrated in additional slices in Fig. 4.3. Consider the red triangle in Fig. 2A. It is obtained by slicing the tube orthogonal to its long direction in the middle. When moving this slice away from the middle the triangle moves up, but the bottom curve below it moves up faster, and eventually the corner of the triangle will pierce through that curve. When viewing the critical values from below the triangular tube pierces through the surface. The first bifurcation in the slice occurs when the top of the triangle (hyperbolic 2-tori) becomes tangent to the curve. This creates a pair of saddle-centre bifurcation of 2-tori and the corresponding critical values in the energy-momentum map are degenerate. In the rightmost slice the two cusps collide and annihilate and the slice becomes smooth. The reason that the two different slices in Fig. 3 appear somewhat similar is that when $c_1 \to 0$ they actually become identical, see Fig. 4 below. In the left pane a perspective view looking down along the H-axis from above is shown, while in the right pane we are looking up along the H-axis from below the surface. This concludes the description of the four generic cases of the bifurcation diagram.

There are 3 degenerate cases separating A,B,C,D from each other. In addition there are two non-generic cases that occur in the limit that $c_1 \to 0$. There are two different limiting cases depending on the sign of c_2. For positive c_2 we recover the case studied in [BZ93], for which the two threads (4.5) intersect at their vertex. The case of negative c_2 is fundamentally different and was not considered in [BZ93]. Again the two parabolas (4.5) intersect at their vertices, but they are now embedded in the surface of critical values and mark its edges, see Fig. 4. In addition the triangular tube becomes symmetric in this limit forming a kind of trampoline. The edge of the trampoline where $H_{\theta\theta} = 0$ is shown in orange. The cuspidal points of the trampoline touch the outer surface where the self-intersection of the surface stops, this is where the parabolas (4.7) and (4.8) (green and purple in Fig. 4) intersect the orange cusps. Viewed from below this point is where the self-intersection of the surface stops and the parabolas become visible as embedded in the smooth outer surface (Fig. 4 right). Slices of the set of critical values for constant energy in this case have D_4 symmetry.

4.7. Quantum Mechanics of the Harmonic Lagrange Top

The quantisation of the rigid body is textbook material, see, e.g., [LL77, §103]. The global action variables l_z and L_3 become operators $\hat{l}_z = -i\partial/\partial\phi$ and $\hat{L}_3 = -i\partial/\partial\psi$, measured in units of $\hbar$. We denote the corresponding integer eigenvalues by m and k such that $\hat{l}_z\Psi = m\Psi$ and $\hat{L}_3\Psi = k\Psi$ for a wave function Ψ.

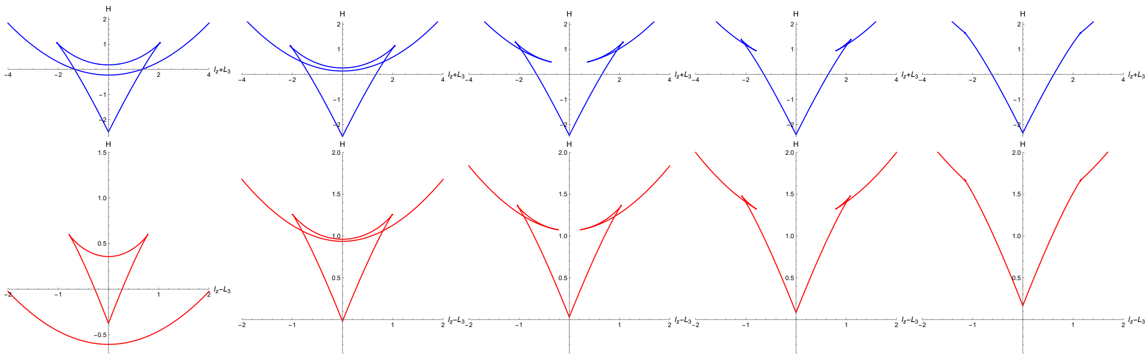

Figure 4.3: Slices of constant $l_z - L_3$ and $l_z + L_3$ near the most degenerate values. Top: slices with constant $l_z - L_3 = (0.200, 0.488, 0.755, 0.888, 1.15)$. Bottom: slices with constant $l_z + L_3 = (1.00, 1.96, 2.06, 2.16, 2.31)$. Parameters are the same as those in Fig. 1A.

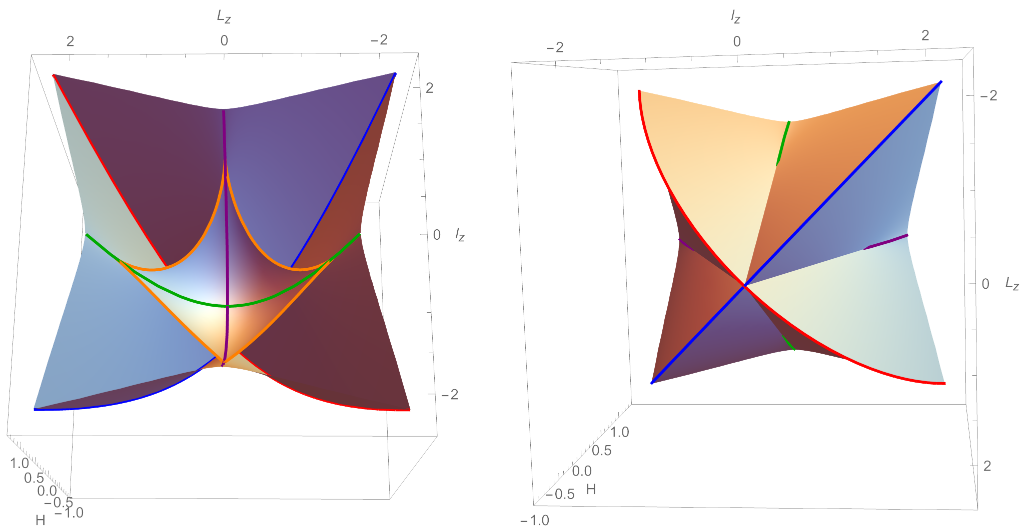

Figure 4.4: Top and bottom view (shown in the left and right pane, respectively) of the limiting case with $c_1 = 0$ and negative $c_2 = -1$. Four parabolas corresponding to (4.5) (red and blue), (4.7) (green), (4.8) (purple) are shown, in addition to the cuspidal edge of the "trampoline" (orange).

The quantum mechanical harmonic Lagrange top has the Hamiltonian operator

$$\hat{H} = \frac{1}{2I_1}\left(\hat{\boldsymbol{l}}^2 + \delta\hat{L}_3^2\right) + c_1\cos\theta + c_2\cos^2\theta \tag{4.10}$$

where $\hat{\boldsymbol{l}}$ is the total angular momentum operator. Explicitly the first part of the Hamiltonian operator is found as the Laplace-Beltrami operator of the metric T_{round} of the spherical top, hence

$$\hat{\boldsymbol{l}}^2 = -\frac{1}{\sin\theta}\partial_\theta(\sin\theta\,\partial_\theta) + \frac{1}{\sin^2\theta}(m^2+k^2-2mk\cos\theta)\,,$$

where we have already replaced the operators $\hat{l}_z$ and $\hat{L}_3$ by their respective eigenvalues. The equation $\hat{\boldsymbol{l}}^2 f = j(j+1)f$ is a self-adjoint form of the hypergeometric equation. Setting the eigenvalue of $\hat{\boldsymbol{l}}^2$ to $j(j+1)$ for positive integer j, solutions are given by $\sin^{|m+k|}\frac{\theta}{2}\cos^{|m-k|}\frac{\theta}{2}P^{|m+k|,|m-k|}_{j-\max(|k|,|m|)}(\cos\theta)$ where $P_n^{m_1,m_2}$ are the Jacobi polynomials. Up to normalisation and phase factors these are the Wigner-D functions [BLC81]. The equation has regular singular points at $\theta = 0,\pi$ with indices $\pm(m-k)$ and $\pm(m+k)$, respectively. Note that the global quantum numbers m and k appear as indices of regular singular points.

Adding the potential terms, and transforming to $z = \cos\theta$ brings us to the following observation.

Theorem 5. *The quantisation of the harmonic Lagrange top leads to the most general confluent Heun equation (aka generalised spheroidal wave equation) which has the self-adjoint form*

$$(-\partial_z((1-z^2)\partial_z + \frac{k^2+m^2-2kmz}{1-z^2} + \tilde{c}_1 z + \tilde{c}_2 z^2 - \lambda)\psi(z) = 0 \tag{4.11}$$

where $z = \cos\theta$ and λ is the spectral parameter related to the energy eigenvalue E of the Hamiltonian by $\lambda = 2I_1E/\hbar^2 - \delta k^2$, $\tilde{c}_1 = c_1 2I_1/\hbar^2$, $\tilde{c}_2 = c_2 2I_1/\hbar^2$,

In the form (4.11) the indices at $z = \pm 1$ are $\pm(m-k)/2$ and $\pm(m+k)/2$. This equation has an irregular singular point at infinity, which is obtained by the confluence of two regular singular points of the Heun equation. The Heun equation is the most general Fuchsian equation with 4 regular singular points. The Heun equation (after normalisation by Möbius transformations) has 6 parameters, 1 position of a pole, 4 indices, and the so called accessory parameter. The pole position is used for the confluence, after which only two regular singular points remain. Hence 2 indices remain as parameters (given by $\pm(m \pm k)/2$). Two additional parameters describe the behaviour near the irregular singular point, and the accessory parameter remains, so that there is a total of 5 parameters.

To transform into the standard form of the confluent Heun equation, see, e.g., [DLMF], first shift to the standard poles by $z \to (z+1)/2$, and then scale the dependent variable with $\exp(2\sqrt{\tilde{c}_2})z^{|m+k|}(z-1)^{|m-k|}$.

When considering the confluent Heun equation, the usual reference to its application in physics is to Teukolsky's master equation [Teu73], which appears in the perturbation theory around a rotating black hole, i.e. the Kerr metric. However, that equation only has 4 parameters, and one index-parameter is more restricted because it represents the spin of a particle. In this context, eigenvalues λ of the equation have been computed using expansion in Jacobi polynomials in [FC77]. Their results are not applicable to our case because their equation only has 4 parameters. To compute the spectrum in our case we generalise the papers [Shi63], [HO91] which treat the case of a symmetric molecule (i.e. top) in an electric field, hence the Lagrange top (without the harmonic field). To extend their method, which is also an expansion in Jacobi polynomials (or rather the related Wigner D-functions), we need to compute the matrix elements of $\cos^2\theta$. This leads to our final result.

Theorem 6. *The spectrum of the harmonic Lagrange top* (4.10) *which is equivalent to the most general confluent Heun equation* (4.11) *can be computed from a penta-diagonal symmetric matrix*

$$\hat{H} = \hat{H}_0 + c_1\hat{H}_1 + c_2\hat{H}_1^2\,. \tag{4.12}$$

For given fixed m, k the operator $\hat{H}_0$ is the diagonal representation of the Hamiltonian without potential and H_1 is the tri-diagonal representation of $\cos\theta$ *in terms of Wigner-D basis functions.*

Proof. The formulas for $\hat{H}_0$ and $\hat{H}_1$ are given in [Shi63]. We repeat them here for convenience. The diagonal entries of $\hat{H}_0$ are $\frac{\hbar^2}{2I_1}(j(j+1)+\delta k^2)$. The diagonal entries of $\hat{H}_1$ are $a_j = -km/(j(j+1))$ and the off-diagonal entries are $b_j = -\sqrt{(j^2-k^2)(j^2-m^2)/(j^2(4j^2-1))}$. The first entries in the matrix representing the operators have $j = \max(m,k)$. Note that for $m = k = 0$ the diverging terms in b_j cancel and b_0 is defined. It is easy to compute the matrix elements of $\cos^2\theta$. This can be done by noticing that $D_{2,0,0} = \frac{3}{2}\cos^2\theta - \frac{1}{2}$. The matrix representation of $D_{2,0,0}$ can be expressed in terms of Clebsch-Gordan coefficients. However, it is more efficient to use the fact that since $\hat{H}_1$ represents $\cos\theta$ the matrix $\hat{H}_1^2$ represents $\cos^2\theta$. So instead of computing matrix elements of $\cos^2\theta$ from scratch in terms of Clebsch-Gordan coefficients we can simply compute the square of the matrix representation of $\hat{H}_1$. In particular the entries in the 2nd off-diagonal are given by products $b_{j-1}b_j$.

■

The numerical convergence of these expressions is good, and the spectra displayed in Figure 2 were computed from these matrices truncated at twice the maximal needed quantum number j. Even though the term δL_3^2 in the Hamiltonian is important for the classical dynamics, its effect on the quantum spectrum is rather trivial, it simply adds δk^2. It does change the spectrum, but the change is simple, and for this reason in the figures we restricted attention to $\delta = 0$, the spherical top. Moreover, from the point of view of the computation of the spectrum of the general confluent Heun equation the term δk^2 is irrelevant.

Why is there a correspondence between the harmonic Lagrange top and the confluent Heun equation? This question may not have a definite answer, but it is suggestive that the harmonic potential is the most general potential for which the classical dynamics can be linearised using the Jacobian of an elliptic curve. This fact appears to be related to the fact that the corresponding quantum system is described by the confluent Heun equation. After adding higher order terms to the potential, the system remains integrable and separable in the same way, but the classical dynamics will involve hyperelliptic curves, and the quantum system will be described by higher order confluent Fuchsian equations. It would be interesting to make this observation more precise.

Chapter 5

Concluding Remarks and Future Work

In this thesis, we have used separation of variables and symmetry reduction to construct natural families of integrable systems that exhibit fascinating behaviours. In general, this technique can be used for all superintegrable systems to produce families of integrable systems which have significant applications for both classication of integrable systems and the theory of special functions.

The free particle in $\mathbb{R}^3$ is perhaps the simplest system in classical mechanics. We showed in Chapter 2 that separation of variables and symmetry reduction of this elementary system gave the prolate spheroidal integrable system on T^*S^2 which is generalised semi-toric and displays non-trivial monodromy. The semi-classical quantisation of this system exhibits quantum monodromy with a defect in the joint spectrum. The differential operator in the quantum spheroidal harmonics integrable system is the spheroidal wave equation which is a special case of the confluent Heun equation. The quantum monodromy in this system ultimately reveals quantum monodromy of the spheroidal wave functions which are a class of special functions and are solutions to the spheroidal wave equation.

A natural continuation to the free particle on $\mathbb{R}^3$ is the free motion on S^3. The geodesic flow on S^3 gave a 2-parameter family of integrable systems on $S^2 \times S^2$ whose moduli space is the Stashsheff polytope K^4. Of these, the cylindrical and prolate systems are toric and generalised semi-toric respectively, while the rest fall outside the realm of the current theory of classification. Since $S^2 \times S^2$ is a compact symplectic manifold, these systems are excellent candidates for new theories of classification. A detailed study of the corresponding quantum systems and their quantum spectra are planned for in a future article.

The Lagrange top is an extensively studied system in classical mechanics. In Chapter 4, we showed that by adding a quadratic potential we obtained the harmonic Lagrange top which remained integrable. Using symmetry reduction we studied the bifurcation diagram of this system for various values of parameters. The quantisation of the harmonic Lagrange top gives the general confluent Heun equation in its most general form.

Chapter A

Appendix

A.1. Identification of $\widetilde{Gr}(2,4)$ with $S^2 \times S^2$

There is a natural identification of $\widetilde{Gr}(2,4)$ with $S^2 \times S^2$ via the Plücker embedding

$$\begin{aligned} i : \widetilde{Gr}(2,4) &\to \Lambda^2(\mathbb{R}^4) \\ \text{span}(\boldsymbol{v}_i, \boldsymbol{v}_j) &\to \frac{1}{|\boldsymbol{v}_i|\,|\boldsymbol{v}_j|}\boldsymbol{v}_i \wedge \boldsymbol{v}_j. \end{aligned}$$

If $(\boldsymbol{v}_1, \boldsymbol{v}_2, \boldsymbol{v}_3, \boldsymbol{v}_4)$ is an ordered-orthonormal basis of $\mathbb{R}^4$ then

$$(\boldsymbol{v}_1 \wedge \boldsymbol{v}_2, \boldsymbol{v}_1 \wedge \boldsymbol{v}_3, \boldsymbol{v}_1 \wedge \boldsymbol{v}_4, \boldsymbol{v}_2 \wedge \boldsymbol{v}_3, \boldsymbol{v}_2 \wedge \boldsymbol{v}_4, \boldsymbol{v}_3 \wedge \boldsymbol{v}_4) \tag{A.1}$$

is a basis of $\Lambda^2(\mathbb{R}^4)$ and a $\boldsymbol{L} \in \Lambda^2(\mathbb{R}^4)$ is of the form

$$\boldsymbol{L} = \ell_{12}\boldsymbol{v}_1 \wedge \boldsymbol{v}_2 + \ell_{13}\boldsymbol{v}_1 \wedge \boldsymbol{v}_3 + \ell_{14}\boldsymbol{v}_1 \wedge \boldsymbol{v}_4 + \ell_{23}\boldsymbol{v}_2 \wedge \boldsymbol{v}_3 + \ell_{24}\boldsymbol{v}_2 \wedge \boldsymbol{v}_4 + \ell_{34}\boldsymbol{v}_3 \wedge \boldsymbol{v}_4.$$

The image of $\widetilde{Gr}(2,4)$ under i is totally decomposable, i.e. any $\boldsymbol{L} \in \widetilde{Gr}(2,4)$ can be expressed as $L = \boldsymbol{x} \wedge \boldsymbol{y}$ where $\boldsymbol{x}, \boldsymbol{y} \in \mathbb{R}^4$. Thus, $\boldsymbol{L} \in \text{im}(i)$ if and only if $\boldsymbol{L} \wedge \boldsymbol{L} = 0$. This yields the Plücker relation

$$\ell_{12}\ell_{34} - \ell_{13}\ell_{24} + \ell_{14}\ell_{23} = 0. \tag{A.2}$$

This relation defines the image of $\widetilde{Gr}(2,4)$ under i. On $\Lambda^2(\mathbb{R}^4)$ the Hodge star operator gives a decomposition

$$\star : \Lambda^2(\mathbb{R}^4) \to \Lambda^2_+(\mathbb{R}^4) \oplus \Lambda^2_-(\mathbb{R}^4)$$

where $\Lambda^2_\pm(\mathbb{R}^4)$ are the ± 1 eigenspaces. For convenience we let $\boldsymbol{V}_{ij} := \boldsymbol{v}_i \wedge \boldsymbol{v}_j$. Then the effect of $\star$ on the basis vectors (A.1) is as follows

$$\begin{aligned} \star(\boldsymbol{V}_{12}) &= \boldsymbol{V}_{34} & \star(\boldsymbol{V}_{34}) &= \boldsymbol{V}_{12} \\ \star(\boldsymbol{V}_{13}) &= -\boldsymbol{V}_{24} & \star(\boldsymbol{V}_{24}) &= -\boldsymbol{V}_{13} \\ \star(\boldsymbol{V}_{14}) &= \boldsymbol{V}_{23} & \star(\boldsymbol{V}_{23}) &= \boldsymbol{V}_{14}. \end{aligned}$$

This gives the following bases of $\Lambda^2_+(\mathbb{R}^4)$ and $\Lambda^2_-(\mathbb{R}^4)$:

$$\begin{aligned}\Lambda^2_+ :& \frac{1}{2}\langle \boldsymbol{V}_{12} + \boldsymbol{V}_{34}, \boldsymbol{V}_{13} - \boldsymbol{V}_{24}, \boldsymbol{V}_{14} + \boldsymbol{V}_{23}\rangle \\ \Lambda^2_- :& \frac{1}{2}\langle \boldsymbol{V}_{12} - \boldsymbol{V}_{34}, \boldsymbol{V}_{13} + \boldsymbol{V}_{24}, \boldsymbol{V}_{14} - \boldsymbol{V}_{23}\rangle .\end{aligned} \tag{A.3}$$

The Hodge star operator then induces a decomposition

$$\begin{aligned}\star \circ i :& \widetilde{Gr}(2,4) \to S^2_+ \times S^2_- \\ \text{span}(\boldsymbol{x}, \boldsymbol{y}) \to & \frac{1}{2\,|\boldsymbol{x}|\,|\boldsymbol{y}|}\left[(\boldsymbol{x} \wedge \boldsymbol{y} + \star(\boldsymbol{x} \wedge \boldsymbol{y})) + (\boldsymbol{x} \wedge \boldsymbol{y} - \star(\boldsymbol{x} \wedge \boldsymbol{y})\right]\end{aligned}$$

where $S^2_+ \subseteq \Lambda^2_+, S^2_- \subseteq \Lambda^2_-$. Note that

$$\boldsymbol{X} = \frac{1}{2\,|\boldsymbol{x}|\,|\boldsymbol{y}|}(\boldsymbol{x} \wedge \boldsymbol{y} + \star(\boldsymbol{x} \wedge \boldsymbol{y})) \qquad \boldsymbol{Y} = \frac{1}{2\,|\boldsymbol{x}|\,|\boldsymbol{y}|}(\boldsymbol{x} \wedge \boldsymbol{y} - \star(\boldsymbol{x} \wedge \boldsymbol{y}))$$

are are both unit vectors in $\mathbb{R}^3$ with the bases (A.3) of $\Lambda^2_\pm$. Thus, a plane spanned by $(\boldsymbol{x}, \boldsymbol{y})$ is identified with two unit vectors $(\boldsymbol{X}, \boldsymbol{Y})$ in $\mathbb{R}^3$, i.e $S^2 \times S^2$. Geometrically S^2_+ and S^2_- represent the left and right isoclinic rotations in $\mathbb{R}^4$. Note that $\exp(\boldsymbol{x} \wedge \boldsymbol{y})$ is a rotation in the plane spanned by $\boldsymbol{x}$ and $\boldsymbol{y}$.

For a given point $(\boldsymbol{X}, \boldsymbol{Y}) \in S^2 \times S^2$, we have $T^{-1}(\boldsymbol{X}, \boldsymbol{Y}) = (\ell_{12}, \ell_{13}, \ell_{14}, \ell_{23}, \ell_{24}, \ell_{34})$ defines an element $\boldsymbol{L} \in \Lambda^2(\mathbb{R}^4)$ where the map T is defined in (3.20). For a given $\boldsymbol{L}$ we can find the corresponding circle on S^3 by considering the linear map

$$\begin{aligned}M_{\boldsymbol{L}} : \Lambda^1(\mathbb{R}^4) &\to \Lambda^3(\mathbb{R}^4) \\ \boldsymbol{v} &\to \boldsymbol{v} \wedge \boldsymbol{L}.\end{aligned}$$

Since $\boldsymbol{L}$ is decomposable with $\boldsymbol{L} = \boldsymbol{x} \wedge \boldsymbol{y}$ then $\ker(()M_{\boldsymbol{L}}) = \text{span}(\boldsymbol{x}, \boldsymbol{y})$. Let (b_1, b_2, b_3, b_4) be a basis of $\mathbb{R}^4$ and $(b_{123}, b_{124}, b_{134}, b_{234})$ be bases of $\Lambda^3(\mathbb{R}^4)$. Then we can represent $M_{\boldsymbol{L}}$ as

$$M_{\boldsymbol{W}} = \begin{pmatrix} \ell_{23} & -\ell_{13} & \ell_{12} & 0 \\ \ell_{24} & -\ell_{14} & 0 & \ell_{12} \\ \ell_{34} & 0 & -\ell_{14} & \ell_{13} \\ 0 & \ell_{34} & -\ell_{24} & \ell_{23} \end{pmatrix}.$$

If $\boldsymbol{L}$ is in the image of the Plücker embedding then $\text{rank}(M_{\boldsymbol{L}})$ is exactly 2 as all 16 of the 3×3 minors vanishes under the Plücker relation. Thus, finding the nullspace of $M_{\boldsymbol{L}}$ gives us an unoriented plane in $\mathbb{R}^4$ whose intersection with S^3 is the fibre over $S^2 \times S^2$.

A.2. GEODESIC FLOW ON S^2

Following a similar construction to Section 3.3, we can define the geodesic flow on S^2 as a constrained system on $T^*\mathbb{R}^3$ with Cartesian coordinates $(\boldsymbol{x}, \boldsymbol{y})$ where $\boldsymbol{x} \cdot \boldsymbol{x} = 1$ and $\boldsymbol{x} \cdot \boldsymbol{y} = 0$. The Dirac bracket yields a Poisson structure that can still be accurately represented by the matrix $B_{(\boldsymbol{x},\boldsymbol{y})}$ in (3.7), where here $\boldsymbol{x}$ and $\boldsymbol{y}$ are vectors in $\mathbb{R}^3$. The invariants of the Hamiltonian $H = \frac{1}{2}\boldsymbol{y} \cdot \boldsymbol{y}$ are the three angular momenta $\boldsymbol{L} = (\ell_{12}, \ell_{13}, \ell_{23})$. Symplectic reduction by the S^1 action of $\sqrt{2H}$ gives a reduced space that is diffeomorphic to the sphere S^2 given by the Casimir $\ell_{12}^2 + \ell_{13}^2 + \ell_{23}^2 = 2h = 1$. The Poisson algebra of the invariants ℓ_{ij} is isomorphic to $\mathfrak{so}(3)$.

There are 2 non-equivalent orthogonal separable coordinates on the sphere S^2 leading to 2 distinct Stäckel systems. They are the spherical coordinates and the elliptic coordinates with semi-axes (e_1, e_2, e_3).

A.2.1. ELLIPTIC COORDINATES ON S^2

The elliptic coordinates with semi-axes (e_1, e_2, e_3) are defined by

$$
\begin{aligned}
x_1^2 &= \frac{(s_1 - e_1)(s_2 - e_1)}{(e_2 - e_1)(e_3 - e_1)} \\
x_2^2 &= \frac{(s_1 - e_2)(s_2 - e_2)}{(e_1 - e_2)(e_3 - e_2)} \\
x_3^2 &= \frac{(s_1 - e_3)(s_2 - e_3)}{(e_1 - e_3)(e_2 - e_3)}.
\end{aligned}
$$

Performing Stäckel separation or analysis using compatible Poisson structures both gives the separation constants $1 = \ell_{12}^2 + \ell_{13}^2 + \ell_{23}^2$ and $\eta_1 = e_3\ell_{12}^2 + e_2\ell_{13}^2 + e_1\ell_{23}^2$. Using the matrix $C = \mathrm{diag}(\lambda - c_1, \lambda - c_2, \lambda - c_3)$, the Poisson matrix for $(so_3^*, \{\cdot,\cdot\}_C)$ is given by

$$
B_C = \begin{pmatrix} 0 & \ell_{23}(\lambda - e_1) & \ell_{13}(e_2 - \lambda) \\ \ell_{23}(e_1 - \lambda) & 0 & \ell_{12}(\lambda - e_3) \\ \ell_{13}(\lambda - e_2) & \ell_{12}(e_3 - \lambda) & 0 \end{pmatrix}.
$$

The bracket $\{\cdot,\cdot\}_C$ drops rank only when exactly 2 of the $\ell_{ij}'s$ vanishes, giving the 6 poles $\pm(1,0,0)$, $\pm(0,1,0)$ and $\pm(0,0,1)$ as critical points on the sphere S^2 defined by fixing the Casimir. The image of the momentum map is the line segment $[e_1, e_3]$ with 3 critical values at e_1, e_2 and e_3. The critical points at e_1 and e_3 are elliptic and ones at e_2 are hyperbolic. The fibres of e_1 and e_3 are the poles $\pm(0,0,1)$ and $\pm(1,0,0)$ respectively. The preimage of e_2 is the intersection of the sphere $1 = \ell_{12}^2 + \ell_{13}^2 + \ell_{23}^2$ with the ellipsoid $e_2 = e_3\ell_{12}^2 + e_2\ell_{13}^2 + e_1\ell_{23}^2$. The sphere and this ellipsoid intersect tangentially at the poles $\pm(0,1,0)$.

The reduced system is of course the Euler top with phase space S^2 and Hamiltonian η_1, where (e_1, e_2, e_3) are the inverse moments of inertia of the top.

A.2.2. Spherical Coordinates on S^2

We define the spherical coordinates on S^2 with

$$\begin{aligned} x_1^2 &= s_1 \\ x_2^2 &= (1 - s_1)s_2 \\ x_3^2 &= (1 - s_1)(1 - s_2) \end{aligned} \quad .$$

This system easily separates with separation constants $1 = \ell_{12}^2 + \ell_{13}^2 + \ell_{23}^2$ and $\eta_1 = \ell_{23}^2$. The image of the momentum map is the line segment $[0, 1]$ with 2 critical values at 0 and 1. The critical points at 1 are the poles $\pm(0, 0, 1)$ and are elliptic. The point $\ell_{23}^2 = 0$ is degenerate and it's fibre is the equator of the sphere.

The reduced system is the symmetric Euler top with phase space S^2 and two equal moments of inertia.

Bibliography

[ADH19] J. Alonso, H. R. Dullin, and S. Hohloch. Symplectic classification of coupled angular momenta. *Nonlinearity*, 33(1):417–468, 2019. 10, 53

[AH19] J. Alonso and S. Hohloch. Survey on recent developments in semitoric systems. *arXiv preprint, arXiv:1901.10433v2*, 2019. 10, 53, 79

[AMV04] M. Adler, P. Moerbeke, and P. Vanhaecke. *Algebraic Integrability, Painlevé Geometry and Lie Algebras*. Springer Berlin Heidelberg, 2004. 15

[Arn78] V. I. Arnold. *Mathematical Methods of Classical Mechanics*. Springer, Berlin, 1978. 11, 15, 97

[Ars64] F. M. Arscott. *Periodic differential equations: an introduction to Mathieu, Lamé, and allied functions*. Pergamon Press, 1964. 20, 22, 28, 31, 98

[AS92] M. Abramowitz and I. A. Stegun, editors. *Handbook of mathematical functions with formulas, graphs, and mathematical tables*. Dover Publications Inc., New York, 1992. Reprint of the 1972 edition. 22, 29, 31

[Ati82] M. F. Atiyah. Convexity and commuting Hamiltonians. *Bulletin of the London Mathematical Society*, 14(1):1–15, 1982. 52

[BB02] A. V. Bolsinov and A. V. Borisov. Compatible Poisson brackets on Lie algebras. *Mathematical Notes*, 72(1/2):10–30, 2002. 53, 63

[Ben89] S. Benenti. Stäckel systems and Killing tensors. *Note di Matematica*, Volume 9, suppl., 1989. 53, 54

[BF04] A. V. Bolsinov and A. T. Fomenko. *Integrable Hamiltonian Systems. Geometry, Topology, Classification*. Chapman & Hall/CRC, London, 2004. 11, 15, 17, 52, 70, 97

[BI22] A. V. Borisov and A. P. Ivanov. A top on a vibrating base: New integrable problem of nonholonomic mechanics. *Regular and Chaotic Dynamics*, 27:2–10, 2022. 98

[BKM76] C. Boyer, E. Kalnins, and W. Miller. Symmetry and separation of variables for the helmholtz and laplace equations. *Nagoya Mathematical Journal*, 60:35–80, 1976. 20, 21

[BLC81] L. C. Biedenharn, J. D. Louck, and P. A. Carruthers. *Angular momentum in quantum physics: theory and application*, volume 8. Addison-Wesley Reading, MA, 1981. 114

[BM97] A. V. Borisov and I. S. Mamaev. Non-linear Poisson brackets and isomorphisms in dynamics (russian). *Regular and Chaotic Dynamics*, 2(3):72–89, 1997. 100

[BM18] A. V. Borisov and I. S. Mamaev. *Rigid body dynamics*. de Gruyter, 2018. 97, 100

[BMF90] A. V. Bolsinov, S. V. Matveev, and A. T. Fomenko. Topological classification of integrable Hamiltonian systems with two degrees of freedom. List of systems of small complexity. *Russian Mathematical Surveys*, 45(2):59–94, apr 1990. 17

[BO09] A. V. Bolsinov and A. A. Oshemkov. Bi-Hamiltonian structures and singularities of integrable systems. *Regular and Chaotic Dynamics*, 14:431–454, 2009. 53, 63, 64, 65

[Bog92] O. I. Bogoyavlenskii. Euler equations on finite-dimensional Lie coalgebras, arising in problems of mathematical physics. *Russ. Math. Surv.*, 47:117, 1992. 97

[Boy04] J. P. Boyd. Prolate spheroidal wavefunctions as an alternative to chebyshev and legendre polynomials for spectral element and pseudospectral algorithms. *Journal of Computational Physics*, 199(2):688–716, 2004. 28

[BRS20] A. V. Borisov, P. E. Ryabov, and S. V. Sokolov. On the existence of focus singularities in one model of a lagrange top with a vibrating suspension point. In *Doklady Mathematics*, volume 102, pages 468–471. Springer, 2020. 98

[BS99] A. I. Bobenko and Y. B. Suris. Discrete time Lagrangian mechanics on Lie groups, with an application to the Lagrange top. *Communications in mathematical physics*, 204(1):147–188, 1999. 97, 103

[BT92] O. Babelon and M. Talon. Separation of variables for the classical and quantum neumann model. *Nuclear Physics B*, 379(1-2):321–339, 1992. 36

[BZ93] L. Bates and M. Zou. Degeneration of hamiltonian monodromy cycles. *Nonlinearity*, 6(2):313, 1993. 22, 41, 97, 112

[CB95] R. Cushman and L. Bates. The magnetic spherical pendulum. *Meccanica*, 30(3):271–289, 1995. 11, 97

[CB15] R. H. Cushman and L. M. Bates. *Global aspects of classical integrable systems*. Birkhäuser Verlag, Basel, 2nd edition, 2015. 11, 14, 16, 17, 97, 103

[CD88] R. H. Cushman and J. J. Duistermaat. The quantum mechanical spherical pendulum. *Bull. Amer. Math. Soc.*, 19:475–479, 1988. 21, 97

[CDEW19] I. Chiscop, H. R. Dullin, K. Efstathiou, and H. Waalkens. A Lagrangian fibration of the Isotropic 3-Dimensional Harmonic Oscillator with monodromy. *Journal of Mathematical Physics*, 60(3):032103, 2019. 21, 79

[CIAD14] C. Chen, M. Ivory, S. Aubin, and J. Delos. Dynamical monodromy. *Physical Review E*, 89(1):012919, 2014. 22, 50

[CK85] R. Cushman and H. Knörrer. The energy momentum mapping of the Lagrange top. In *Differential Geometric Methods in Mathematical Physics*, pages 12–24. Springer, 1985. 97, 111

[CvdM90] R. Cushman and J.-C. van der Meer. The Hamiltonian Hopf bifurcation in the Lagrange top. In *Géométrie Symplectique et Mécanique*, pages 26–38. Springer, 1990. 97

[DD06] C. M. Davison and H. R. Dullin. *Geodesic flow on three-dimensional ellipsoids with equal semi-axes*. PhD thesis, Loughborough University, 2006. 18, 19

[DD07] C. M. Davison and H. R. Dullin. Geodesic flow on three dimensional ellipsoids with equal semi-axes. *Regular and Chaotic Dynamics*, 12:172–197, 2007. 53

[DDB07] C. M. Davison, H. R. Dullin, and A. V. Bolsinov. Geodesics on the ellipsoid and monodromy. *Journal of Geometry and Physics*, 57(12):2437 – 2454, 2007. 53, 58, 79

[DDN21] S. R. Dawson, H. R. Dullin, and D. M. H. Nguyen. Monodromy in Prolate Spheroidal harmonics. *Studies in Applied Mathematics*, 146(4):953–982, 2021. 1, 11

[DDN22] S. R. Dawson, H. R. Dullin, and D. M. H. Nguyen. The harmonic Lagrange top and the confluent Heun equation. *Regular and Chaotic Dynamics*, 27(4):443–459, 2022. 1, 11, 53, 79

[Del88] T. Delzant. Hamiltoniens périodiques et images convexes de l'application moment. *Bulletin de la Société Mathématique de France*, 116(3):315–339, 1988. 9, 52, 72, 79

[DH12] H. R. Dullin and H. Hanßmann. The degenerate C. Neumann system I: symmetry reduction and convexity. *Central European Journal of Mathematics*, 10(5):1627–1654, 2012. 22, 36, 37, 53, 54

[DLMF] *NIST Digital Library of Mathematical Functions*. http://dlmf.nist.gov/, Release 1.0.24 of 2019-09-15. F. W. J. Olver, A. B. Olde Daalhuis, D. W. Lozier, B. I. Schneider, R. F. Boisvert, C. W. Clark, B. R. Miller, B. V. Saunders, H. S. Cohl, and M. A. McClain, eds. 26, 28, 31, 98, 114

[DN07] H. R. Dullin and S. V. Ngọc. Symplectic invariants near hyperbolic-hyperbolic points. *Regular and Chaotic Dynamics*, 12(6):689–716, 2007. 70, 95

[DP16] H. R. Dullin and Á. Pelayo. Generating hyperbolic singularities in semitoric systems via Hopf bifurcations. *Journal of Nonlinear Science*, 26(3):787–811, 2016. 98

[DRVW01] H. R. Dullin, P. H. Richter, A. P. Veselov, and H. Waalkens. Actions of the Neumann systems via Picard–Fuchs equations. *Physica D: Nonlinear Phenomena*, 155:159–183, 2001. 36, 71

[DS07] H. R. Dullin and V. S. Symplectic invariants near hyperbolic-hyperbolic points. *Regul. Chaotic Dyn.*, 12:689–716, 2007. 36

[dS08] A. C. da Silva. *Lectures on Symplectic Geometry*. Springer Berlin Heidelberg, 2008. 11

[Dui80] J. J. Duistermaat. On global action-angle coordinates. *Comm. Pure Appl. Math.*, 33:687–706, 1980. 21, 50, 97

[Dul04] H. R. Dullin. Poisson integrator for symmetric rigid bodies. *Regul. Chaotic Dyn.*, 9:255–264, 2004. 103

[DW18] H. R. Dullin and H. Waalkens. Defect in the joint spectrum of hydrogen due to monodromy. *Phys. Rev. Lett.*, 120:020507, 2018. 21, 53, 79

[Efs05] K. Efstathiou. *Metamorphoses of Hamiltonian systems with symmetries*, volume 1864 of *Lecture Notes in Math.* Springer, 2005. 11, 17, 22, 41, 97

[EHM19] K. Efstathiou, H. Hanßmann, and A. Marchesiello. Bifurcations and monodromy of the axially symmetric 1: 1:- 2 resonance. *Journal of Geometry and Physics*, 146:103493, 2019. 111

[Eis34] L. P. Eisenhart. Separable systems of Stäckel. *Annals of Mathematics*, 35(2):284–305, 1934. 55

[Fas05] F. Fassò. Superintegrable Hamiltonian systems: Geometry and perturbations. *Acta Applicandae Mathematica*, 87(1-3):93–121, 2005. 53

[FAW03] P. E. Falloon, P. Abbott, and J. Wang. Theory and computation of spheroidal wavefunctions. *Journal of Physics A: Mathematical and General*, 36(20):5477, 2003. 28

[FC77] E. D. Fackerell and R. G. Crossman. Spin-weighted angular spheroidal functions. *Journal of Mathematical Physics*, 18(9):1849–1854, 1977. 98, 115

[Fla57] C. Flammer. *Spheroidal wave functions*. Stanford Research Institute, 1957. 20, 28

[FP18] Y. L. Floch and J. Palmer. Semitoric families. *arXiv preprint, arXiv:1810.06915*, 2018. 10, 53

[FS21] Y. L. Floch and V. N. San. The inverse spectral problem for quantum semitoric systems. *arXiv preprint arXiv:2104.06704*, 2021. 97

[Gol80] H. Goldstein. *Classical Mechanics*. Addison-Wesley, Reading, MA, 2nd edition, 1980. 97

[GS82] V. Guillemin and S. Sternberg. Convexity properties of the moment mapping. *Inventiones Mathematicae*, 67:491–513, 1982. 52

[Gur95] D. Gurarie. Quantized Neumann problem, separable potentials on S^n and the Lamé equation. *Journal of Mathematical Physics*, 36:5355–5391, 1995. 36, 71

[GZ98] L. Gavrilov and A. Zhivkov. The complex geometry of the Lagrange top. *Enseign. Math. (2)*, 44(1-2):133–170, 1998. 97

[Han97] H. Hanßmann. Quasi-periodic motions of a rigid body. I. Quadratic Hamiltonians on the sphere with a distinguished parameter. *Regular and Chaotic Dynamics*, 2(2):41–57, 1997. 97

[HBHN06] J. Hoo, H. Broer, H. Hanßmann, and V. Naudot. Nearly-integrable perturbations of the Lagrange top: applications of KAM-theory. In *Dynamics & Stochastics*, volume 48, pages 286–303. Institute of Mathematical Statistics, 2006. 97

[HO91] J. Hajnal and G. I. Opat. Stark effect for a rigid symmetric top molecule: exact solution. *Journal of Physics B: Atomic, Molecular and Optical Physics*, 24(12):2799, 1991. 97, 115

[HP17] S. Hohloch and J. Palmer. A family of compact semitoric systems with two focus-focus singularities. *Journal of Geometric Mechanics*, 10(3):331–357, 2017. 10, 53

[Ker22] R. Kerr. *On spherical type singularities in integrable systems*. Loughborough University, 2022. 10, 75, 87, 88, 90, 91

[KK91] I. V. Komarov and V. B. Kuznetsov. Quantum Euler-Manakov top on the three-sphere S^3. *Journal of Physics A: Mathematical and General*, 24(13):L737–L742, 1991. 53

[KKM05a] E. G. Kalnins, J. M. Kress, and W. Miller. Second-order superintegrable systems in conformally flat spaces. I. Two-dimensional classical structure theory. *Journal of Mathematical Physics*, 46(5):053509, May 2005. 10, 53

[KKM05b] E. G. Kalnins, J. M. Kress, and W. Miller. Second-order superintegrable systems in conformally flat spaces. II. the classical two-dimensional Stäckel transform. *Journal of Mathematical Physics*, 46(5):053510, May 2005. 10, 53

[KKM05c] E. G. Kalnins, J. M. Kress, and W. Miller. Second-order superintegrable systems in conformally flat spaces. III. Three-dimensional classical structure theory. *Journal of Mathematical Physics*, 46(10):103507, October 2005. 10, 53

[KKM06a] E. G. Kalnins, J. M. Kress, and W. Miller. Second-order superintegrable systems in conformally flat spaces. IV. The classical 3D Stäckel transform and 3D classification theory. *Journal of mathematical physics*, 47(4):043514, 2006. 10, 53

[KKM06b] E. G. Kalnins, J. M. Kress, and W. Miller. Second-order superintegrable systems in conformally flat spaces. V. Two- and three-dimensional quantum systems. *Journal of Mathematical Physics*, 47(9):093501, September 2006. 10, 53

[KKM18] E. G. Kalnins, J. M. Kress, and W. Miller. *Separation of Variables and Superintegrability*. Bristol: IOP Publishing, 2018. 10, 15, 20, 22, 53, 54, 56, 58, 85

[KM86] E. G. Kalnins and W. Miller. Separation of variables on n-dimensional Riemannian manifolds. i. the n-sphere S^n and Euclidean n-space $\mathbb{R}^n$. *Journal of Mathematical Physics*, 27(7):1721–1736, 1986. 10, 53, 55, 75

[Kn2] H. Knörrer. Geodesics on quadrics and a mechanical problem of c. neumann. *Journal für die reine und angewandte Mathematik (Crelles Journal)*, 1982(334):69–78, 1982. 18

[KR03] I. Kozin and R. Roberts. Monodromy in the spectrum of a rigid symmetric top molecule in an electric field. *The Journal of chemical physics*, 118(23):10523–10533, 2003. 97

[KS10] F. Klein and A. Sommerfeld. *Über die Theorie des Kreisels*. Teubner, Leipzig, 1910. 97

[KWMW76] E. G. Kalnins, J. W. Miller, and P. Winternitz. The group $O(4)$, separation of variables and the Hydrogen atom. *SIAM Journal on Applied Mathematics*, 30(4):630–664, 1976. 10, 53

[Lea86] E. W. Leaver. Solutions to a generalized spheroidal wave equation: Teukolsky's equations in general relativity, and the two-center problem in molecular quantum mechanics. *Journal of mathematical physics*, 27(5):1238–1265, 1986. 98

[LGMV10] C. Laurent-Gengoux, E. Miranda, and P. Vanhaecke. Action-angle coordinates for integrable systems on poisson manifolds. *International Mathematics Research Notices*, page arXiv:0805.1679, 2010. 15

[LL77] L. D. Landau and E. M. Lifshitz. *Quantum mechanics*. Pergamon Press, Oxford, 1977. 97, 103, 112

[LL84] L. D. Landau and E. M. Lifshitz. *Mechanics*. Pergamon Press, Oxford, New York, 1984. 97

[Mar09] A. P. Markeev. On the theory of motion of a rigid body with a vibrating suspension. *Doklady Physics*, 54(8):392–396, 2009. 11, 98

[Mar12] A. P. Markeev. On the motion of a heavy dynamically symmetric rigid body with vibrating suspension point. *Mechanics of Solids*, 47(4):373–379, 2012. 11, 98

[Mar18] N. Martynchuk. *On monodromy in integrable Hamiltonian systems*. Phd thesis, University of Groningen, 2018. 21, 22, 38

[Mat96] V. S. Matveev. Integrable Hamiltonian systems with two degrees of freedom. Topological structure of saturated neighborhoods of saddle-saddle and focus-focus types. *Matem. Sbornik*, 187(4):29–58, 1996. 21, 41

[MDEW19] N. Martynchuk, H. R. Dullin, K. Efstathiou, and H. Waalkens. Scattering invariants in Euler's two-center problem. *Nonlinearity*, 32:1296–1326, 2019. 21, 22

[MF53] P. Morse and H. Feshbach. *Methods of Theoretical Physics*. McGraw-Hill, New York, 1953. 29

[MJ77] W. Miller Jr. *Symmetry and separation of variables*. Addison-Wesley Publishing Co., Inc., Reading, MA, 1977. 20

[Mos80a] J. Moser. Various aspects of integrable Hamiltonian systems. In S. H. J. Coates, editor, *Dynamical Systems*, C.I.M.E. Lectures, Bressanone 1978, pages 233–290. Birkhäuser, Boston, 2 edition, 1980. 36

[Mos80b] J. Moser. Geometry of quadrics and spectral theory. In W.-Y. Hsiang et al., editors, *The Chern Symposium 1979*, pages 147–188. Springer, Berlin, 1980. 36

[Mos81] J. Moser. *Various Aspects of Integrable Hamiltonia Systems*. Lezioni Fermiane. Accademia Nazionale dei Lincei, Pisa, 1981. 53, 59

[MPW81] W. Miller, J. Patera, and P. Winternitz. Subgroups of Lie groups and separation of variables. *Journal of Mathematical Physics*, 22(2):251–260, 1981. 10, 26, 53

[MR94] J. E. Marsden and T. S. Ratiu. *Introduction to Mechanics and Symmetry*. Springer, New York, 1994. 11, 15, 16, 17, 97

[MS54] J. Meixner and F. W. Schäfke. *Mathieusche Funktionen und Sphäroidfunktionen*. Springer-Verlag, 1954. 20, 28, 31

[Mül63] H. J. W. Müller. Asymptotic expansions of prolate spheroidal wave functions and their characteristic numbers. *J. Reine Angew. Math.*, 212:26–48, 1963. 31

[MW74] J. Marsden and A. Weinstein. Reduction of symplectic manifolds with symmetry. *Reports on Mathematical Physics*, 5(1):121–130, February 1974. 16

[NDD23] D. M. H. Nguyen, H. R. Dullin, and S. R. Dawson. Integrable systems arising from separation of variables on S^3. *arXiv preprint, arXiv:2302.13270*, 2023. 1, 11

[Neu59] C. Neumann. De problemate quodam mechanico, quod ad primam integralium ultraellipticorum classem revocatur (Diss. Regiomonti 1856). *J. Reine Angew. Math.*, 56:46–63, 1859. 36

[Ngọ07] S. V. Ngọc. Moment polytopes for symplectic manifolds with monodromy. *Advances in Mathematics*, 208(2):909–934, 2007. 9, 21, 53

[Osh10] A. A. Oshemkov. The topology of the set of singularities for an integrable Hamiltonian system. *Doklady Mathematics*, 82(2):777–779, oct 2010. 17

[PFTV88] W. H. Press, B. P. Flannery, S. A. Teukolsky, and W. T. Vetterling. *Numerical Recipes in C. The Art of Scientific Computing.* Cambridge University Press, Cambridge, 1988. 26, 28

[PN09] A. Pelayo and S. V. Ngọc. Semitoric integrable systems on symplectic 4-manifolds. *Inventiones mathematicae*, 177(3):571–597, 2009. 9, 21, 53, 79, 97

[PPN14] A. Pelayo, L. Polterovich, and S. V. Ngọc. Semiclassical quantization and spectral limits of $\hbar$-pseudodifferential and berezin-toeplitz operators. *Proceedings of the London Mathematical Society*, 109(3):676–696, 2014. 30

[PR+17] Á. Pelayo, T. S. Ratiu, et al. The affine invariant of generalized semitoric systems. *Nonlinearity*, 30(11):3993–4028, 2017. 21, 50

[PT73] W. H. Press and S. A. Teukolsky. Perturbations of a rotating black hole. II. Dynamical stability of the Kerr metric. *The Astrophysical Journal*, 185:649–674, 1973. 98

[RA95] A. Ronveaux and F. Arscott. *Heun's differential equations*. Oxford University Press, 1995. 22, 28, 98

[Raţ81] T. Raţiu. The C. Neumann problem as a completely integrable system on an adjoint orbit. *Trans. Amer. Math. Soc.*, 264(2):321–329, 1981. 36

[Rei26] F. Reiche. Die Quantelung des symmetrischen Kreisels nach Schrödingers Undulationsmechanik. *Zeitschrift für Physik*, 39(5-6):444–464, 1926. 97

[Res] W. Research. Mathematica, Version 12.0. Champaign, IL, 2019. 30

[RS21] P. E. Ryabov and S. V. Sokolov. Bifurcation diagram of one model of a Lagrange top with a vibrating suspension point. Slides of a presentation at IV International Conference Topological methods in dynamics and related topics, Nizhny Novgorod,, 10 2021. 98

[Sak02] P. Saksida. Neumann system, spherical pendulum and magnetic fields. *Journal of Physics A: Mathematical and General*, 35(25):5237, 2002. 11, 97

[Sch55] C. Schlier. Der Stark-effekt des symmetrischen Kreiselmoleküls bei hohen Feldstärken. *Zeitschrift für Physik*, 141(1):16–18, 1955. 97

[Sch14] K. Schöbel. The variety of integrable Killing tensors on the 3-Sphere. *Symmetry, Integrability and Geometry: Methods and Applications (SIGMA)*, 10:080, 2014. 10, 53, 55, 56, 58, 74

[Sch16] K. Schöbel. Are orthogonal separable coordinates really classified? *Symmetry, Integrability and Geometry: Methods and Applications (SIGMA)*, 12:No 041, 16, 2016. 10, 53, 56

[Sei89] E. Seidel. A comment on the eigenvalues of spin-weighted spheroidal functions. *Classical and Quantum Gravity*, 6(7):1057, 1989. 98

[Shi63] J. H. Shirley. Stark energy levels of symmetric-top molecules. *The Journal of Chemical Physics*, 38(12):2896–2913, 1963. 97, 115

[SL00] S. Slavyanov and W. Lay. *Special functions: a unified theory based on singularities*. Oxford University Press, 2000. 22, 98

[Sle83] D. Slepian. Some comments on fourier analysis, uncertainty and modeling. *SIAM review*, 25(3):379–393, 1983. 28

[SMC+59] J. A. Stratton, P. Morse, L. Chu, J. Little, and F. Corbato. *Spheroidal wave functions*. MIT Press, 1959. 20, 28, 29

[SN17] D. Sepe and S. V. Ngọc. Integrable systems, symmetries, and quantization. *Letters in Mathematical Physics*, 108(3):499–571, 2017. 79

[SV15] K. Schöbel and A. P. Veselov. Separation coordinates, moduli spaces and Stasheff polytopes. *Communications in Mathematical Physics*, 337(3):1255–1274, 2015. 10, 53, 55, 56

[SZ07a] D. Sadovskií and B. Zhilinskií. Hamiltonian systems with detuned 1:1:2 resonance: Manifestation of bidromy. *Annals of Physics*, 322:164 – 200, 2007. 111

[SZ07b] E. Sinitsyn and B. Zhilinskii. Qualitative analysis of the classical and quantum Manakov top. *Symmetry, Integrability and Geometry: Methods and Applications (SIGMA)*, 3:046, 2007. 19, 53

[Teu73] S. A. Teukolsky. Perturbations of a rotating black hole. I. Fundamental equations for gravitational, electromagnetic, and neutrino-field perturbations. *The Astrophysical Journal*, 185:635–648, 1973. 98, 115

[Tot93] J. A. Toth. The quantum c. neumann problem. *International Mathematics Research Notices*, 1993(5):137–139, 1993. 36

[Tsi08] A. V. Tsiganov. On bi-Hamiltonian geometry of the Lagrange top. *Journal of Physics A: Mathematical and Theoretical*, 41(31):315212, 2008. 97

[Ves80] A. P. Veselov. Finite-gap potentials and integrable systems on the sphere with quadratic potentials (in Russian). *Func. Anal. Appl.*, 14(1):48–50, 1980. 36

[Viv03] O. Vivolo. The monodromy of the Lagrange top and the Picard–Lefschetz formula. *Journal of Geometry and Physics*, 46(2):99–124, 2003. 97

[VN99] S. Vũ Ngọc. Quantum monodromy in integrable systems. *Comm. Math. Phys.*, 203(2):465–479, 1999. 21, 36, 41

[Vol03] H. Volkmer. Error estimates for rayleigh–ritz approximations of eigenvalues and eigenfunctions of the mathieu and spheroidal wave equation. *Constructive approximation*, 20(1):39–54, 2003. 28

[Vuk08] M. Vuk. Algebraic integrability of the confluent neumann system. *Journal of Physics A: Mathematical and Theoretical*, 41(39):395201, 2008. 36

[WD02] H. Waalkens and H. R. Dullin. Quantum monodromy in prolate ellipsoidal billiards. *Ann. Physics*, 295:81–112, 2002. 22

[Whi37] E. T. Whittaker. *A Treatise on the Analytical Dynamics of Particles and Rigid Bodies*. Cambridge University Press, Cambridge, 4 edition, 1937. 97, 99

[WW65] E. T. Whittaker and G. N. Watson. *A Course of Modern Analysis*. Cambridge University Press, Cambridge, 4th edition, 1965. 20

[XRY01] H. Xiao, V. Rokhlin, and N. Yarvin. Prolate spheroidal wavefunctions, quadrature and interpolation. *Inverse problems*, 17(4):805, 2001. 28

[Zha17] L. Zhao. *Spherical and Spheroidal Harmonics: Examples and Computations*. Phd thesis, The Ohio State University, 2017. 28

[Zou92] M. Zou. Kolmogorov's condition for the square potential spherical pendulum. *Physics Letters A*, 166(5-6):321–329, 1992. 11, 97

[Zun97] N. T. Zung. A note on focus-focus singularities. *Differential Geom. Appl.*, 7(2):123–130, 1997. 21, 41

[Zun00] N. T. Zung. Symplectic topology of integrable hamiltonian systems, ii: Topological classification. *Compositio Mathematica*, 138(2):125–156, 2000. 17